Synthesis of Nanoparticles and Surface Modifications

Self-Assembly

- Static assembly
- Dynamic assembly
  - RT = 8.314 J/mol x 300 = 2.4 kJ/mol
- Driving forces
  - Chemisorption
  - Surface effect
  - Hydrophobic-hydrophilic
  - Intermolecular forces
  - Capillary force

Langmuir-Blodgett Films

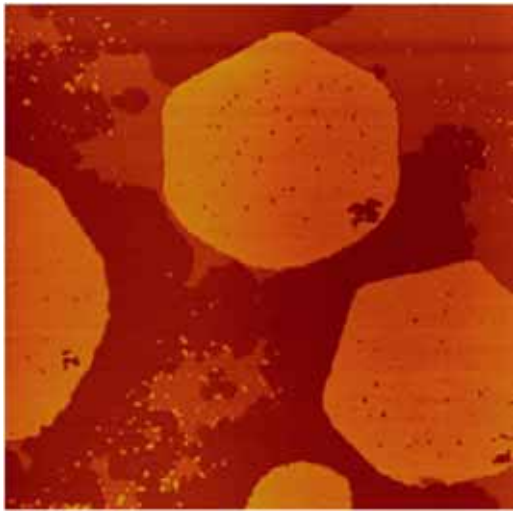

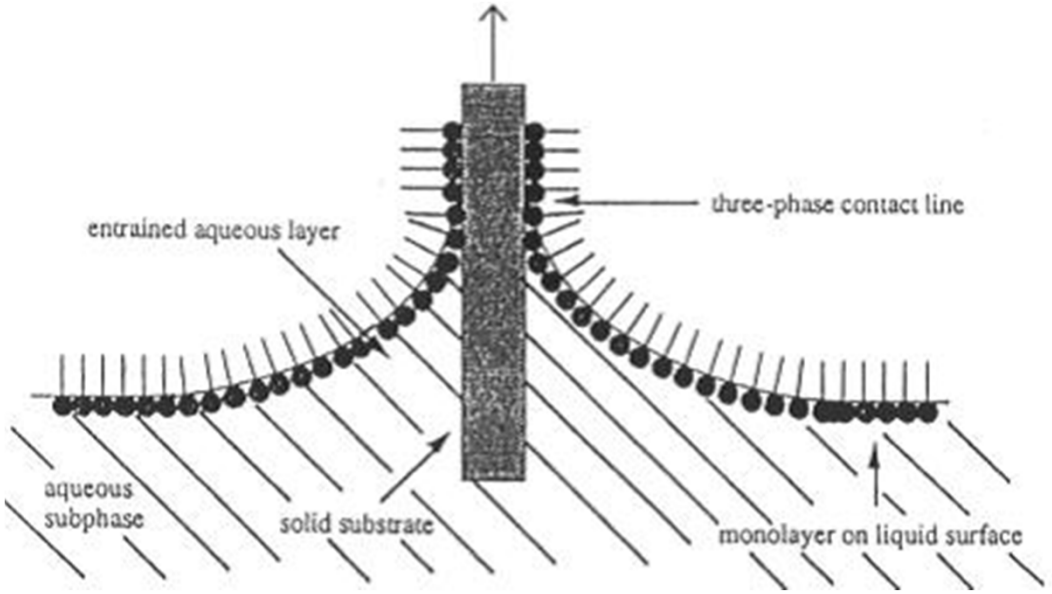

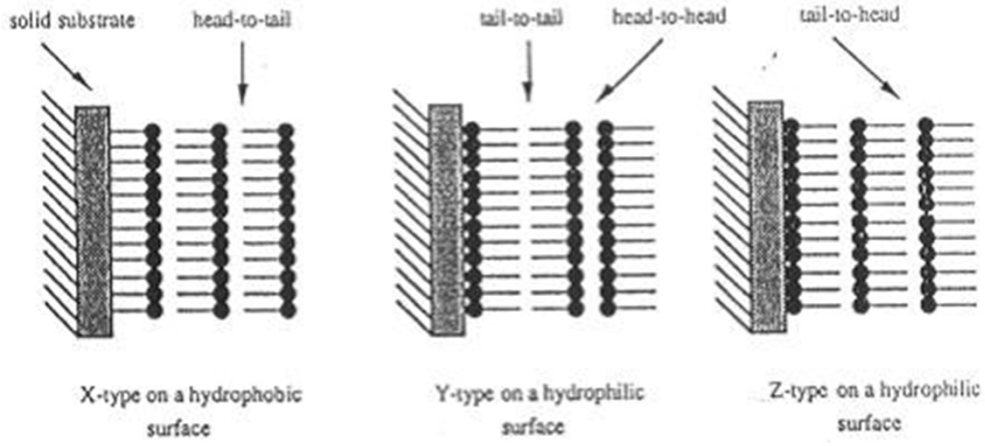

Langmuir-Blodgett Films

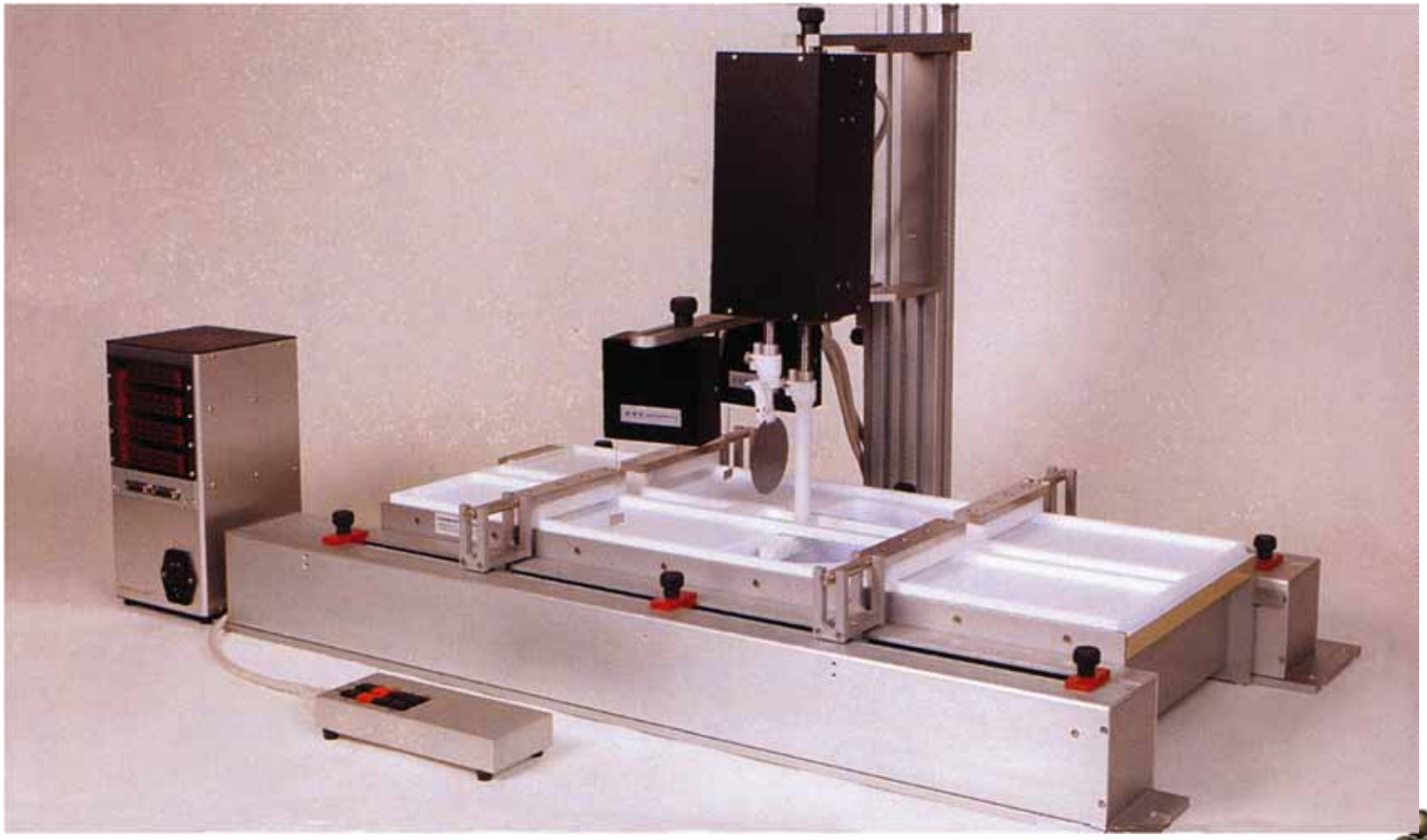

Isotherm

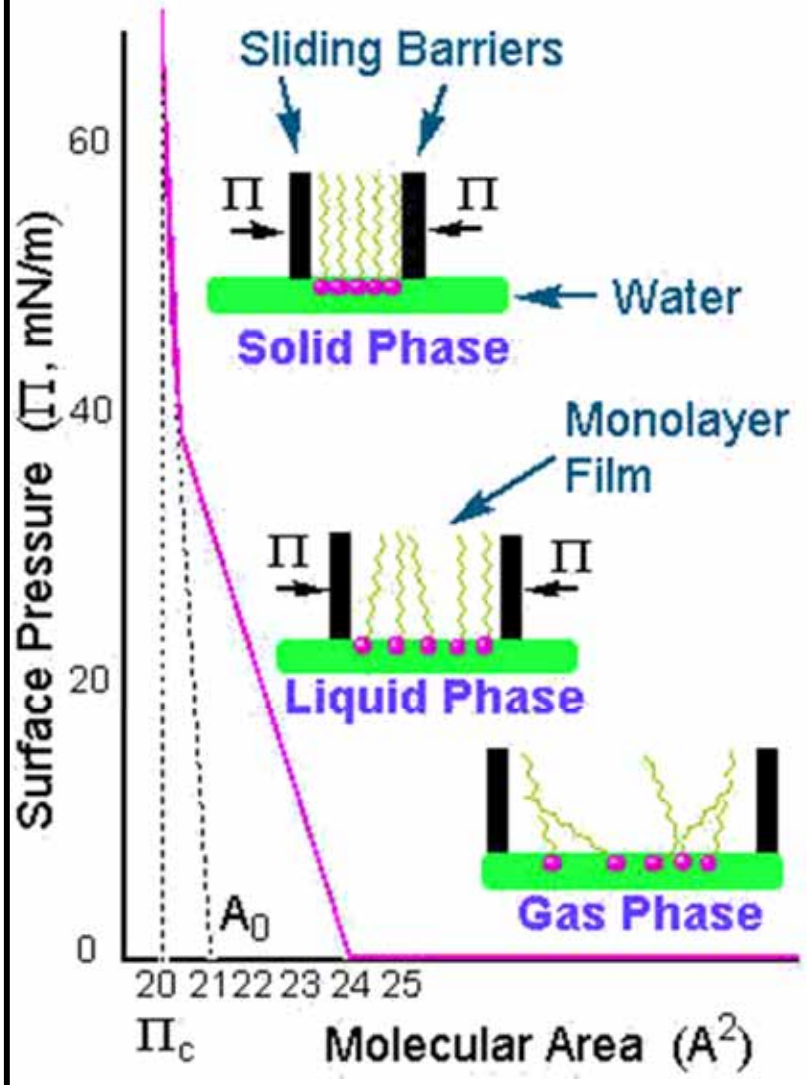
Sliding Barriers
Π
Π
Water
Solid Phase
Monolayer
Film
Liquid Phase
Gas Phase
A0
Surface Pressure (Π, mN/m)
60
40
20
0
20 21 22 23 24 25
Πc
Molecular Area (A2)

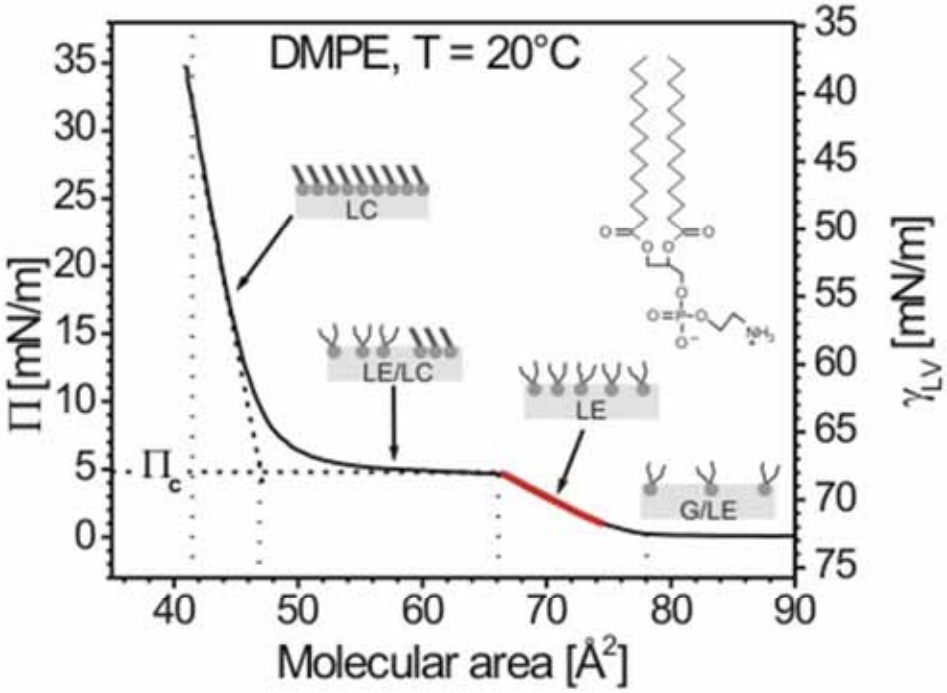
DMPE, T = 20°C
LC
LE/LC
LE
G/LE
Πc
Π [mN/m]
35
30
25
20
15
10
5
0
40
50
60
70
80
90
Molecular area [Å2]
γLV [mN/m]
35
40
45
50
55
60
65
70
75

Self-Assemble Monolayer (SAM)

Chem. Rev. **2005**, *105*, 1103–1169

Ligand	Substrates	Morphology of Substrate: Thin Films or Bulk Material	Morphology of Substrate: Nanoparticles or Other Nanostructures
ROH	Fe_xO_y		35
	Si-H	36	
	Si	37	
RCOO-/RCOOH	α-Al_2O_3	38,39	
	Fe_xO_y		40
	Ni		41,42
	Ti/TiO_2	43	
RCOO-OOCR	Si(111):H	44	
	Si(100):H		
Ene-diol	Fe_2O_3		45
RNH_2	FeS_2	46	
	Mica	47	
	Stainless Steel 316L	48	
	$YBa_2Cu_3O_{7-\delta}$	49	
	CdSe		50
RCsN	Ag	51	
	Au		
R-NwN$^+$(BF_4^-)	GaAs(100)	52	
	Pd	52	
	Si(111):H	52	
RSH	Ag	26	53,54
	Ag_xNi_{1-x}	55	
	AgS		56
	Au	26	57
	AuAg		58
	AuCu		58
	Au_xPd_{1-x}		58
	CdTe		59
	CdSe		60
	CdS		61,62
	Cu	26	58
	FePt		63-66
	GaAs	67	
	Ge	68	
	Hg	69-71	
	HgTe		72
	InP	73	
	Ir		74
	Ni	75	
	PbS		76-78
	Pd	30	74,79
	PdAg		58
	Pt	32	80
	Ru		81
	Stainless Steel 316L	48	
	$YBa_2Cu_3O_{7-\delta}$	82	
	Zn	83	
	ZnSe	84	
	ZnS		85
RSAc	Au	86	
	Au		87
RSR'	Au	88	

Ligand	Substrates	Morphology of Substrate: Thin Films or Bulk Material	Morphology of Substrate: Nanoparticles or Other Nanostructures
RSSR'	Ag	89	90
	Au	20	90-92
	CdS		61
	Pd	30	
	Au	93	
RCSSH	Au	94	
	CdSe		95
$RS_2O_3Na^+$	Au	96	98
	Cu	97	
RSeH	Ag	99	
	Au	100,101	
	CdS		60
	CdSe		102
RSeSeR'	Au	101	
R_3P	Au		103
	FeS_2	46	
	CdS		104
	CdSe		104
	CdTe		104
$R_3P{=}O$	Co		105,106
	CdS		104
	CdSe		104
	CdTe		104
RPO_3^{2-}/$RP(O)(OH)_2$	Al	107	
	Al-OH	108	
	$Ca_{10}(PO_4CO_3)_6(OH)_2$	109	
	GaAs	110	
	GaN	110	
	Indium tin oxide (ITO)	111	
	Mica	112	
	TiO_2	113,114	
	ZrO_2	114,115	
	CdSe		116-118
	CdTe		118,119
RPO_4^{2-}	Al_2O_3	120	
	Nb_2O_5	120	
	Ta_2O_5	121	
	TiO_2	120,122	
RNuC	Pt	123	124
$R1RC{=}CH_2$	Si	37	
RC≡CH	Si(111):H	125	
$RSiX_3$ X = H, Cl, OCH_2CH_3	HfO_2	126	
	ITO	127	
	PtO	128	
	TiO_2	113,126,129	
	ZrO_2	126,129	

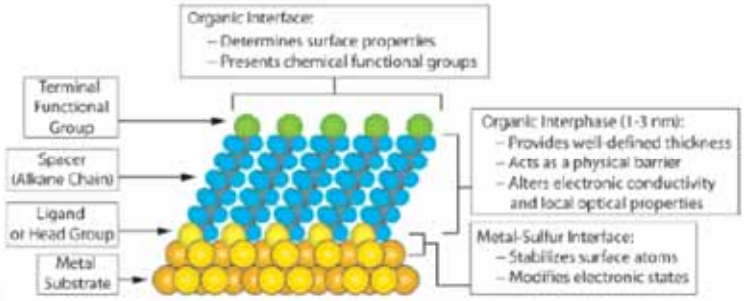

S-Au 25-30 Kcal/mole

Si-O 190 kcal/mole

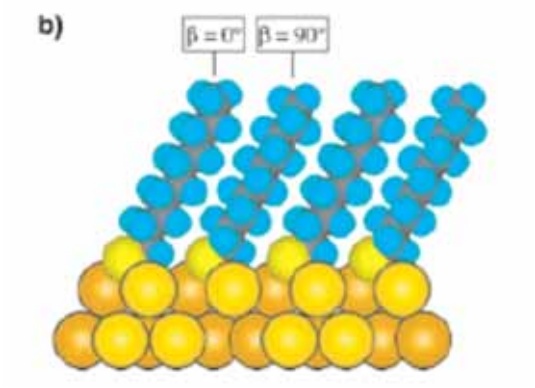

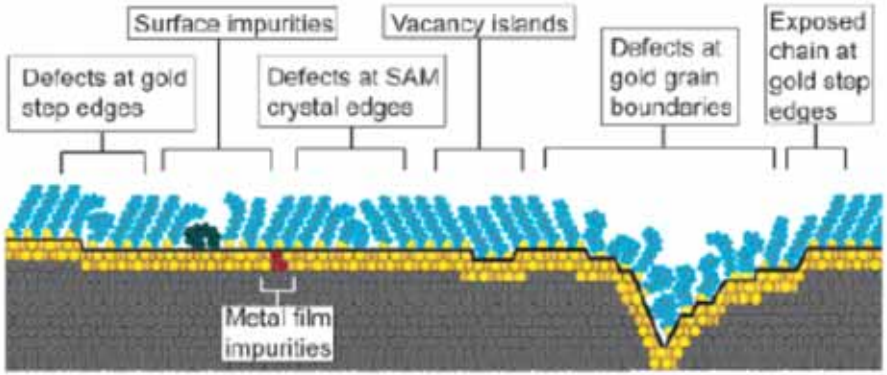

Figure 7. Schematic illustration of some of the intrinsic and extrinsic defects found in SAMs formed on polycrystalline substrates. The dark line at the metal–sulfur interface is a visual guide for the reader and indicates the changing topography of the substrate itself.

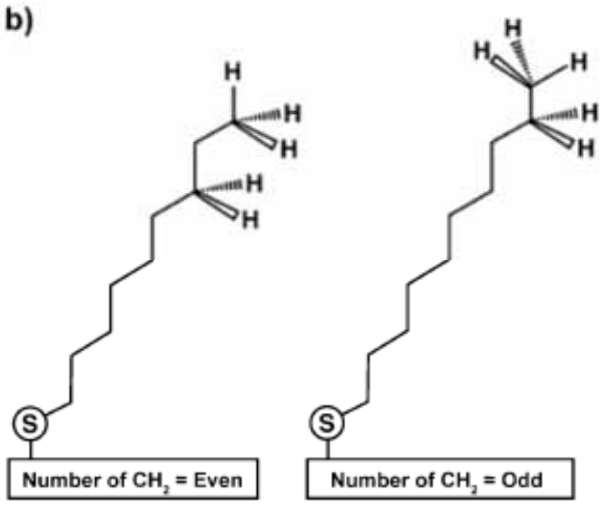

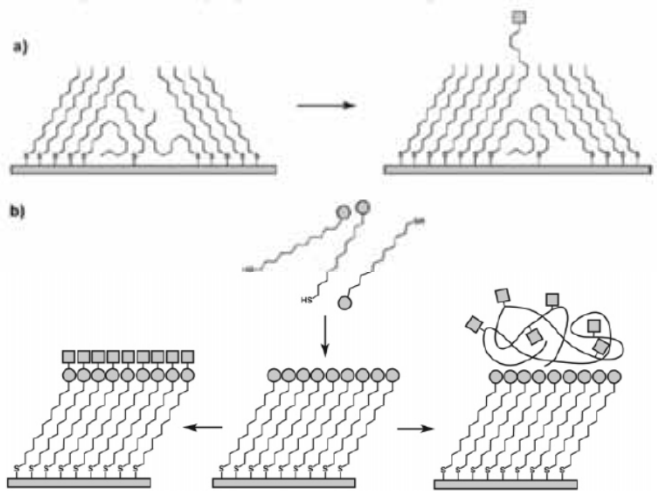

[a] (a) Insertion of a functional adsorbate at a defect site in a preformed SAM. (b) Transformation of a SAM with exposed functional groups (circles) by either chemical reaction or adsorption of another material.

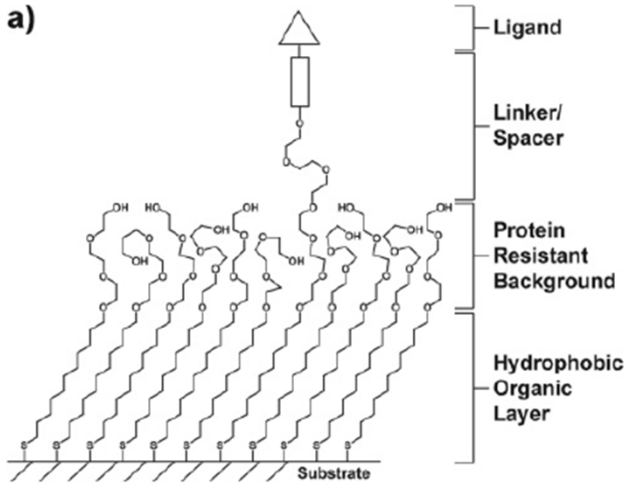

Figure 21. Schematic illustrations of (a) a mixed SAM and (b) a patterned SAM. Both types are used for applications in biology and biochemistry.

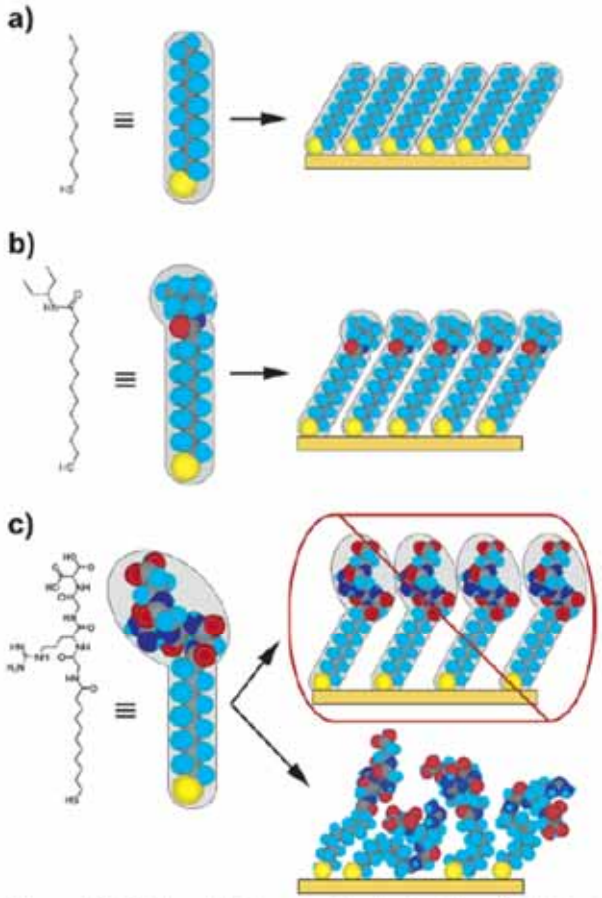

Figure 22. Schematic diagram illustrating the effects that large terminal groups have on the packing density and organization of SAMs. (a) Small terminal groups such as $-CH_3$, $-CN$, etc., do not distort the secondary organization of the organic layer and have no effect on the sulfur arrangement. (b) Slightly larger groups (like the branched amide shown here) begin to distort the organization of the organic layer, but the strongly favorable energetics of metal−sulfur binding drive a highly dense arrangement of adsorbates. (c) Large terminal groups (peptides, proteins, antibodies) sterically are unable to adopt a secondary organization similar to that for alkanethiols with small terminal groups. The resulting structures probably are more disordered and less dense than those formed with the types of molecules in a and b.

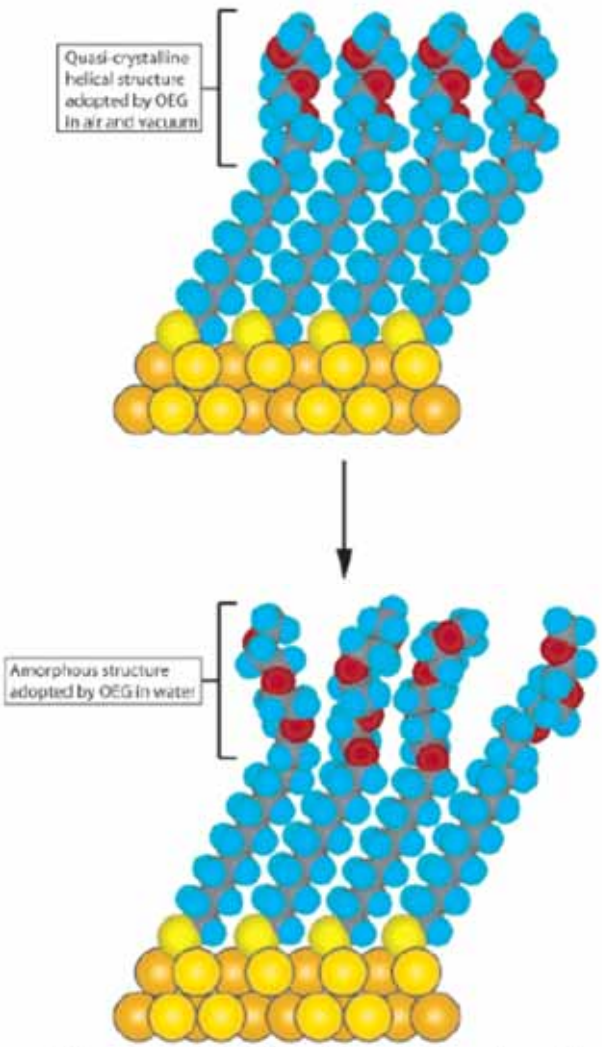

Figure 23. Schematic illustration of the order–disorder transition evidenced by SAMs of alkanethiolates terminated with triethylene glycol. The EG_3 group loses conformational ordering upon solvation in water.

Temperature Programmed Desorption

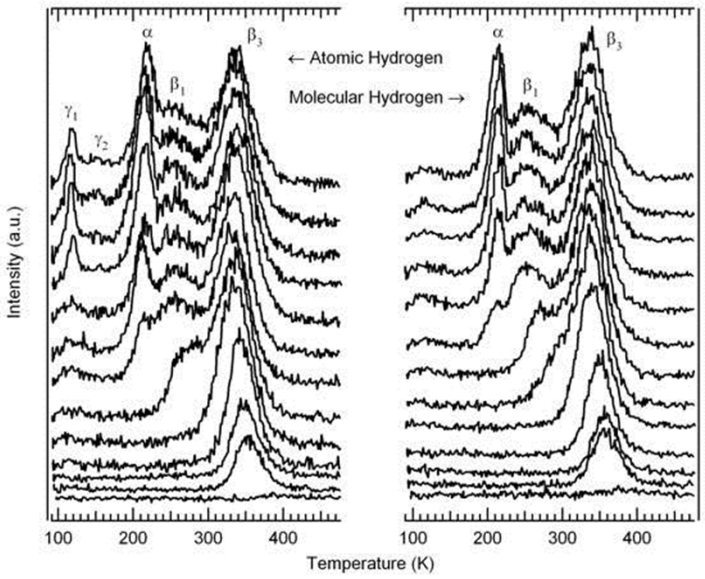

Self-Assembly

- Substrates
- Interstitial adhesion layer
- Noble metal layer
- Organo-sulfur

Organosilanes

Self-assembled monolayers

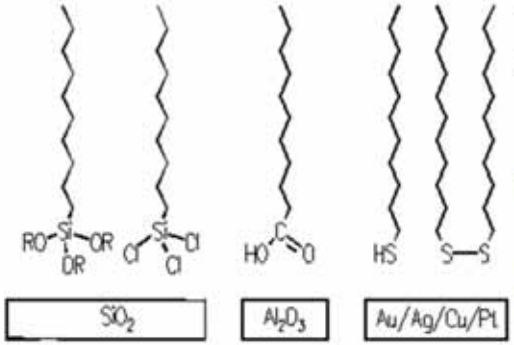

- Surface
- silicon oxide: silanisation
- aluminum oxide: fatty acids
- metals: thiols and sulfides

Immersion of substrate in a solution containing the adequate molecules for 12 - 24 hours yields an ordered monolayer

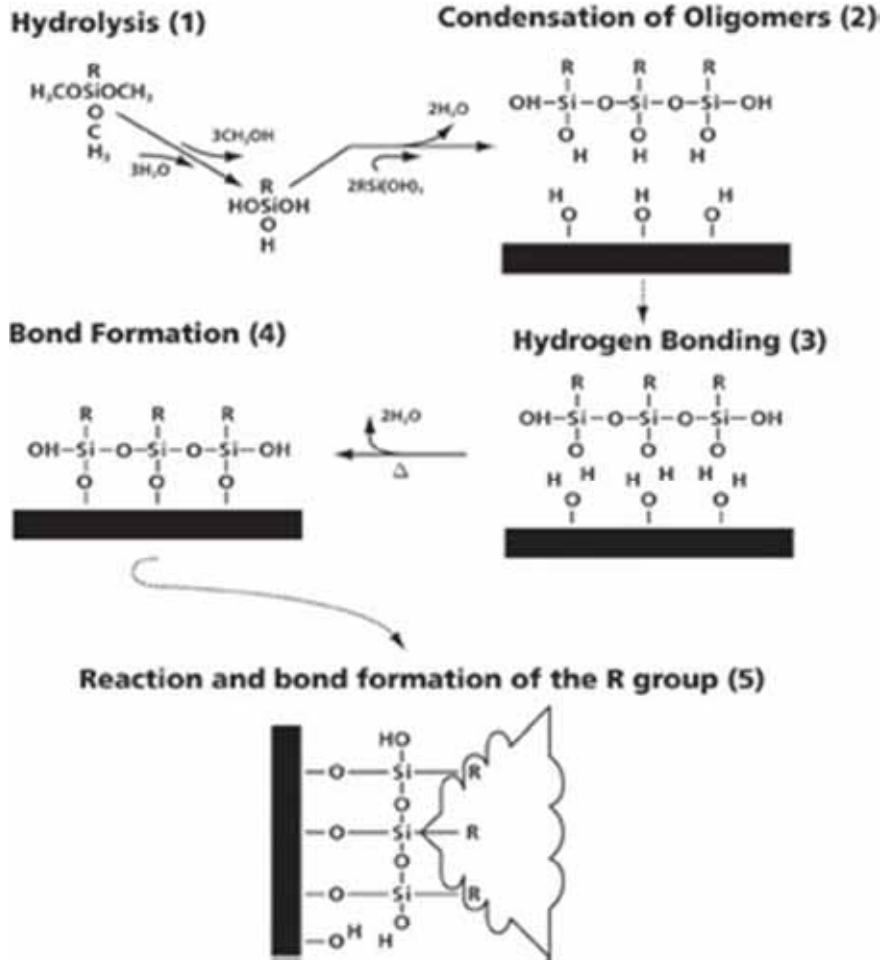

Metal Reduction

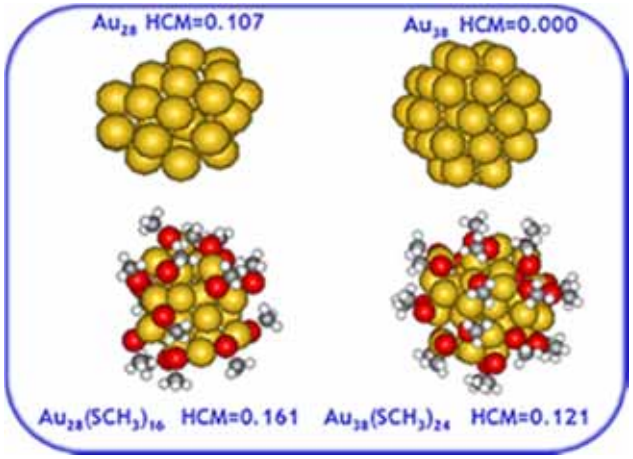

Synthesis of Silver Nanoparticles

1. ***A solution of $AgNO_3$ (1.0×10^{-3} M) in deionized water was heated until it began to boil.***
2. ***Sodium citrate solution was added dropwise to the silver nitrate solution as soon as the boiling commenced. The color of the solution slowly turned into grayish yellow, indicating the reduction of the Ag+ ions.***
3. ***Heating was continued for an additional 15 min, and then the solution was cooled to room temperature before employing for further experimentation.***

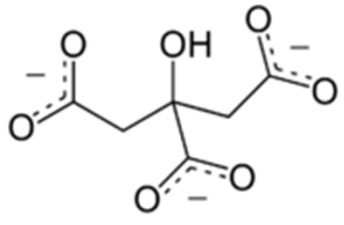

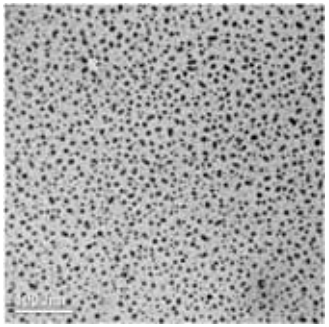

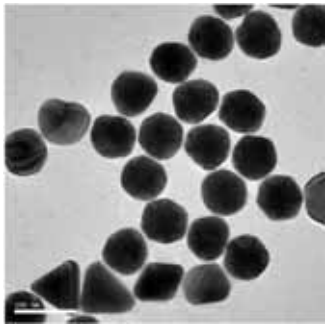

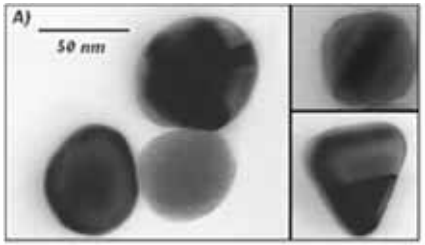

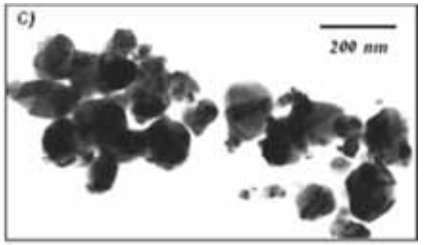

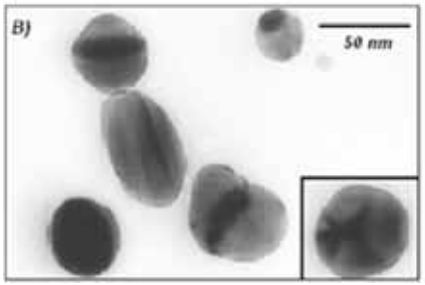

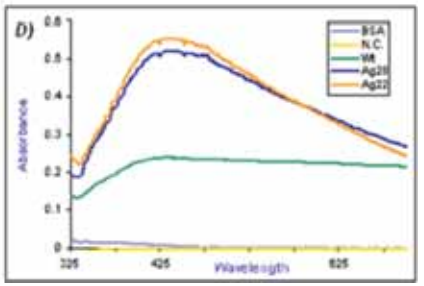

Synthesis of Gold Nanoparticles

1. ***Add 20 mL of 1.0 mM $HAuCl_4$ to a 50 mL round bottom flask on a stirring hot plate.***
2. ***Add a magnetic stir bar and bring the solution to a boil.***
3. ***To the boiling solution, add 2 mL of a 1% solution of trisodium citrate dihydrate***
4. ***The gold sol gradually forms as the citrate reduces the gold(III). Stop heating when a deep red color is obtained.***

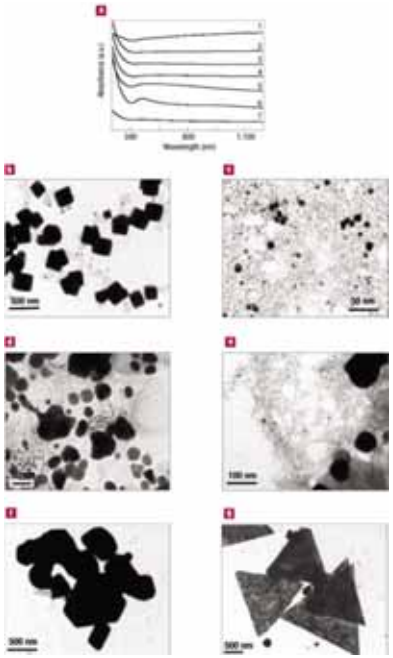

(1) $M_xO_y \xrightarrow[(\text{medium})\ \Delta_T]{\text{Reducing Agent}} M_n + H_2O$

(Reducing Agent = R - COH)

(2) $M(L)_x \xrightarrow[(\text{medium})\ \Delta_T]{\text{Reducing Agent}} M_n + L^-$

($L=NO_3^-, C_2H_5O^-$)

(Reducing Agent = R - COH)

Construction of Core Shell Ag/Au@SiO_2 Nanoparticles

1. *Under vigorous stirring, 1 ml of the silver/ gold colloids solution was mixed with 250 mL of isopropanol and 25 mL of deionized water.*
2. *Immediately after the addition of 4 mL of 30% ammonium hydroxide, different amounts of tetraethoxysilane (TEOS) were added to the reaction mixture.*
3. *To obtain different silica layer thicknesses, TEOS solutions with a concentration between 50% and 100% was added to the suspension. The reaction was stirred at room temperature for 30 minutes and then was allowed to age without agitation at 4℃ overnight.*
4. *Each suspension of silica-coated silver/gold nanoparticles was washed and centrifuged, followed by re-suspension in water. The thickness of the silica layers was determined from TEM images .*

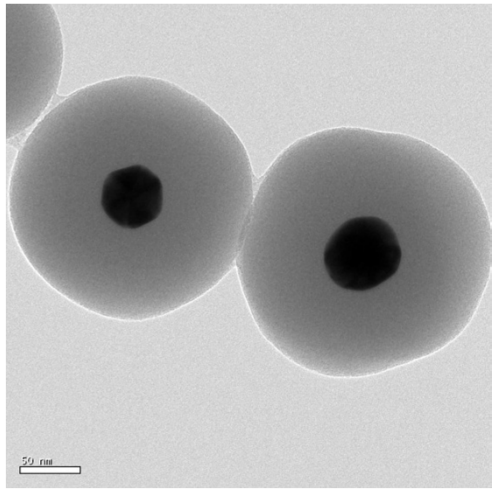

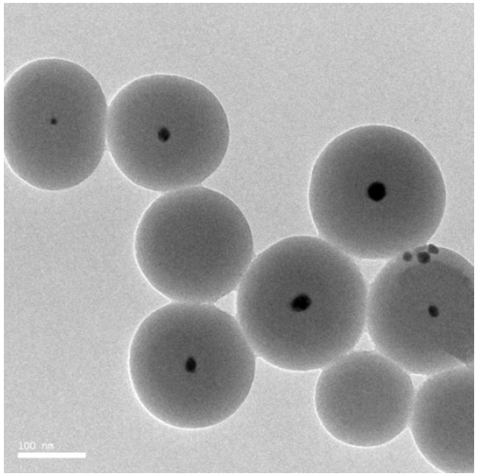

Core-Shell Nanoparticles

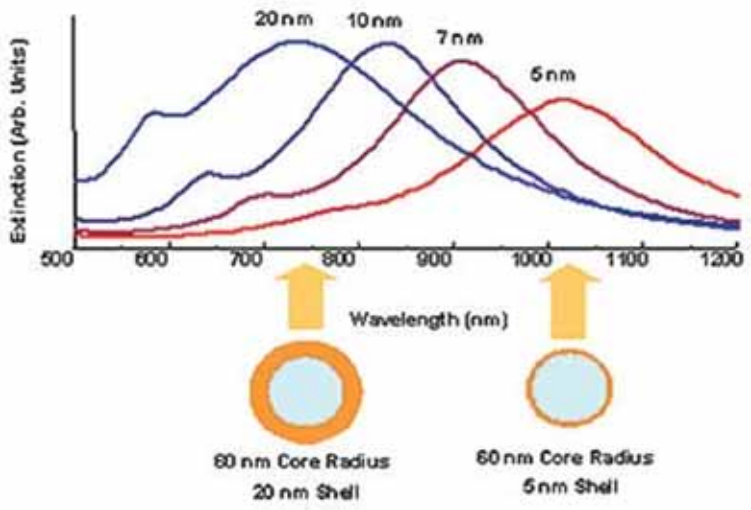

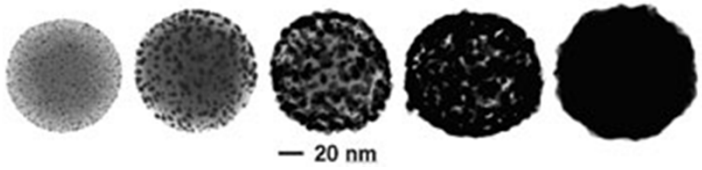

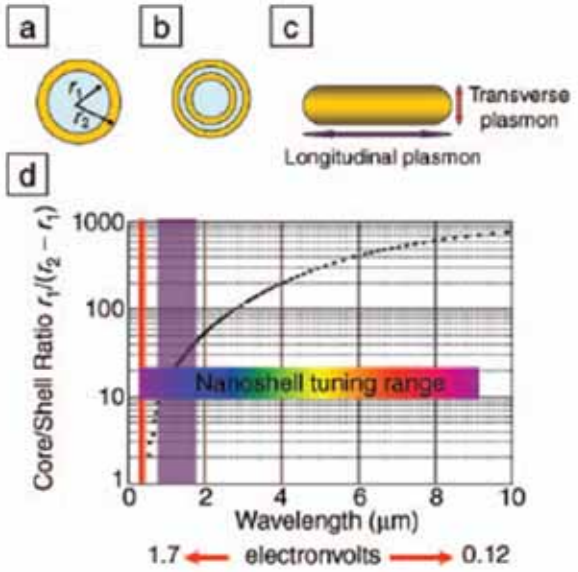

Figure 1. (a) Schematic illustration of a silica-core, gold-shell nanoshell, indicating inner (r_1) and outer (r_2) radii of the shell layers. (b) Depiction of a four-layer, concentric nanoshell. (c) Schematic illustration of a metallic nanorod. (d) Plot of nanoshell resonance as a function of core and shell dimensions, overlaid with reported spectral ranges of nanorod resonances (red, transverse plasmon; purple, longitudinal plasmon), and reported nanoshell and concentric nanoshell combined spectral range of plasmon response.

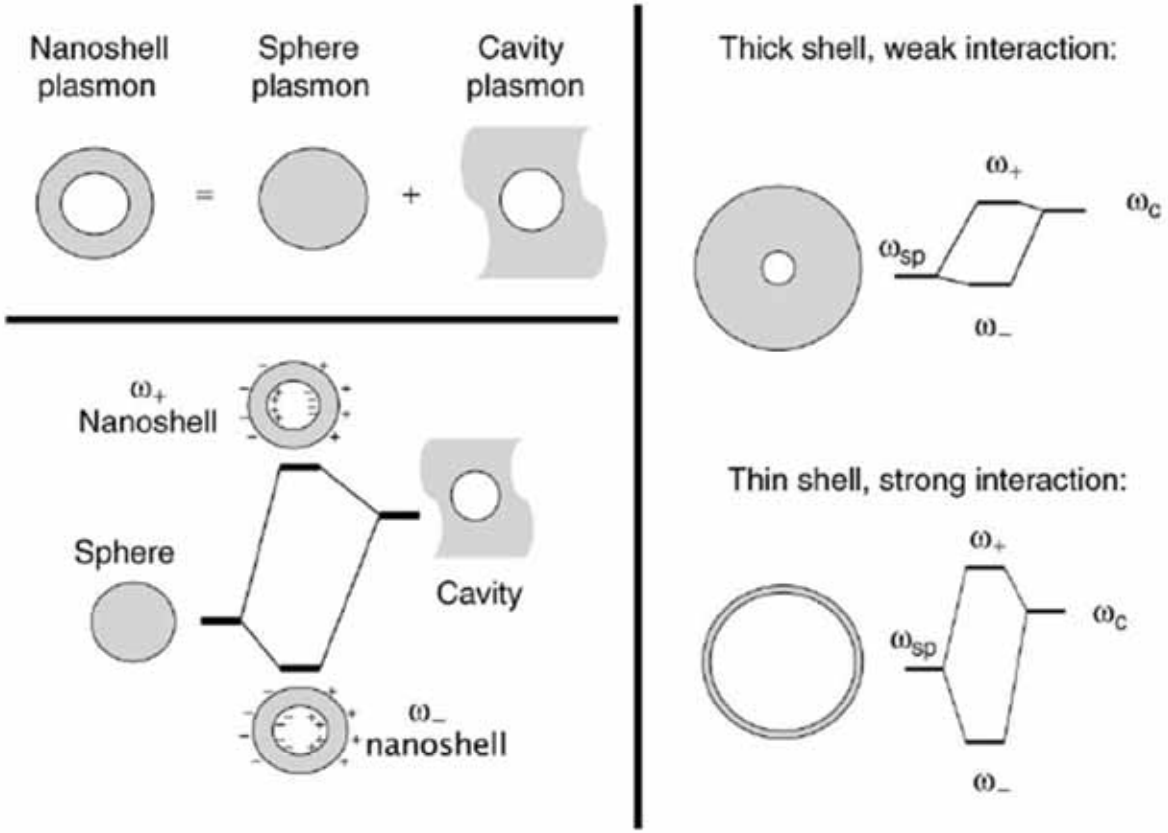

Figure 2. Plasmon hybridization and the sphere–cavity model for nanoshells: the interaction between a sphere (resonance frequency, ω_{sp}) and a cavity plasmon (resonance frequency, ω_c) is tuned by varying the thickness of the shell layer of the nanoparticle. Two hybrid plasmon resonances, the ω_- "bright," or "bonding," plasmon and the ω_+ "dark," or "anti-bonding," plasmon resonances are formed. The lower-energy plasmon couples most strongly to the optical field.

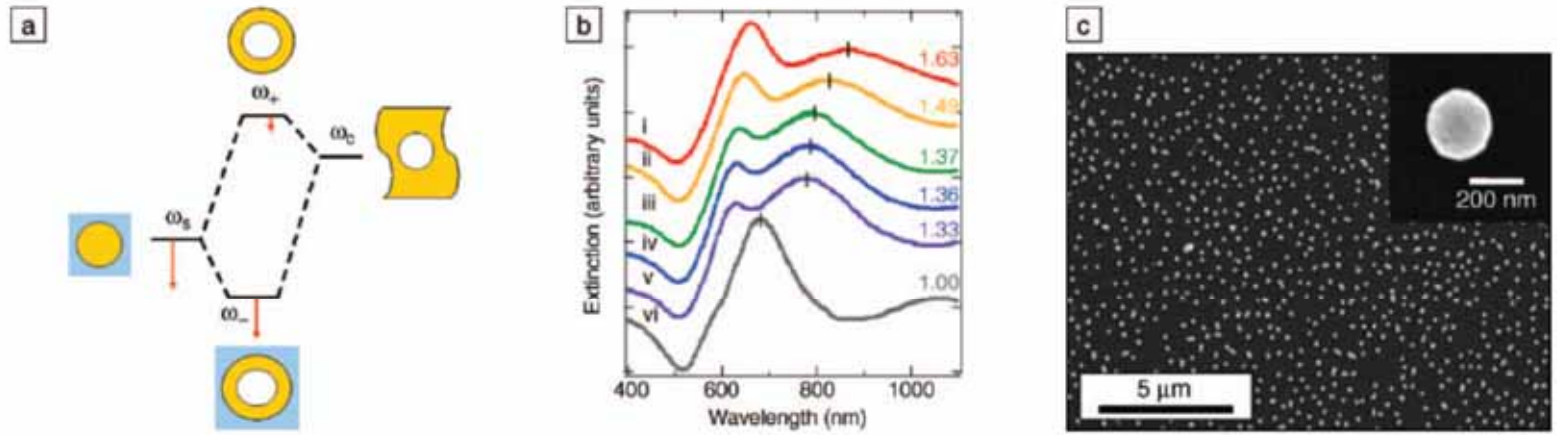

Figure 5. (a) Plasmon hybridization picture applied to surface plasmon resonance sensing with nanoshells: the low-energy "bonding" plasmon, ω_-, is sensitized to changes in its dielectric environment. The blue background schematically denotes the embedding medium for the nanoparticle. (b) Experimental curves showing plasmon resonance shifts for nanoshell-coated films in various media: (i) carbon disulfide, (ii) toluene, (iii) hexane, (iv) ethanol, (v) H_2O, and (vi) air. The index of refraction for each embedding medium is noted on the far right of the spectra. Spectra are offset for clarity. (c) Scanning electron micrograph of nanoshells deposited onto a poly(vinyl pyridine) functionalized glass surface, as used to acquire data in (b). Inset: individual nanoshell.

Preparation of Fe_3O_4@Ag/Au

1. *To the magnetic nanoparticle suspension obtained from commercial company, add 50 ml of a solution of Au (III) salt or Ag (I) salt at concentration of 0.01–1% mmol/L , shaking for 30 minutes, allowing Au (III) or Ag (I) ion to absorb on the surface of magnetic nanoparticle sufficiently,*
2. *Then adding 15–40 ml of reducing agent, such as hydroxylamine hydrochloride at concentration of 40 mmol/L, reacting for 5–40 minutes.*
3. *Further adding 1–10 ml of a solution of Au (III) salt or Ag (I) salt at concentration of 0.01–1%, shaking for 10 minutes, coating a reduced layer of gold or silver on the surface of the magnetic nanoparticle, forming super-paramagnetic composite particles having core/shell structure, separating magnetically, washing repeatedly with distilled water.*

.

Synthesis of Quantum Dots

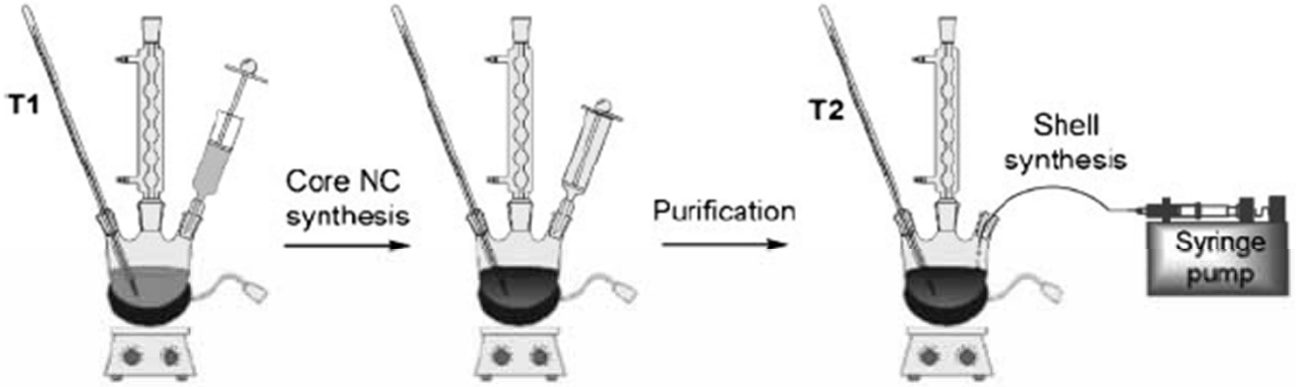

Figure 2. Two–step synthesis of core/shell nanocrystals.

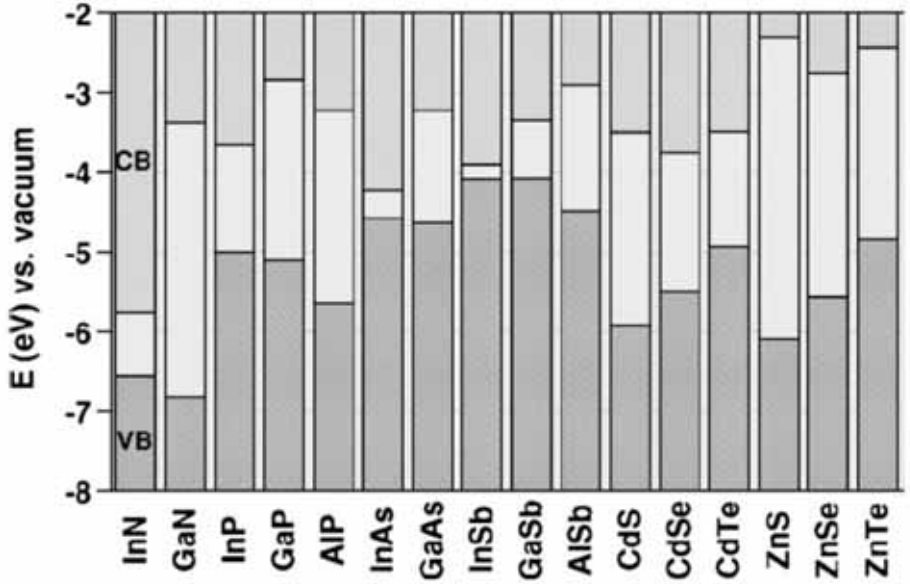

Scheme 1. Electronic energy levels of selected III–V and II–VI semiconductors using the valence-band offsets from Reference [12] (VB: valence band, CB: conduction band).

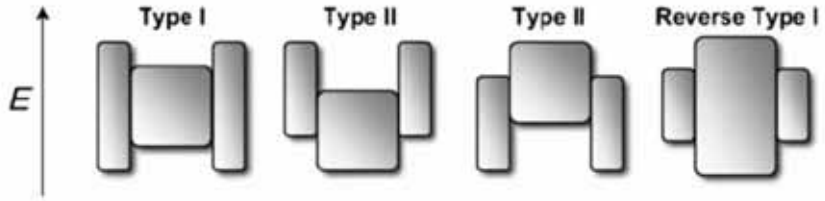

Figure 1. Schematic representation of the energy-level alignment in different core/shell systems realized with semiconductor NCs to date. The upper and lower edges of the rectangles correspond to the positions of the conduction- and valence-band edge of the core (center) and shell materials, respectively.

Successive Ion Layer Adsorption and Reaction

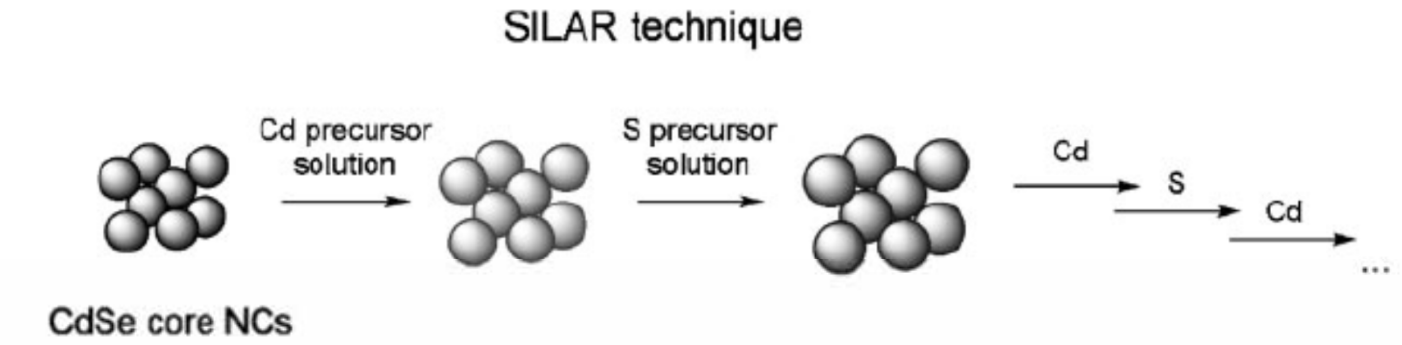

Figure 3. Shell synthesis using the SILAR method, schematically illustrated for the CdSe/CdS core/shell system.

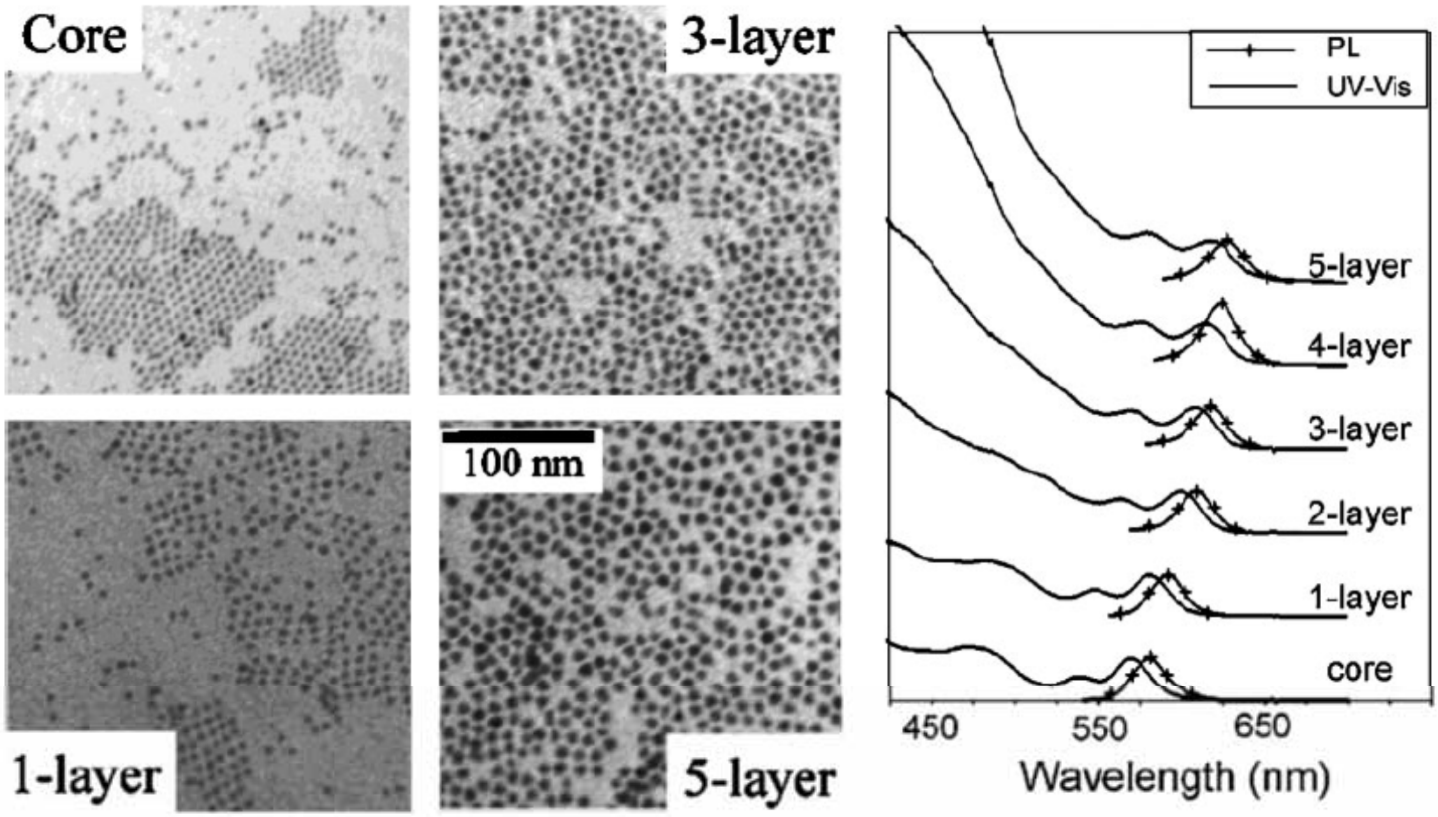

Figure 4. Left panel: TEM images of CdSe NCs depicting the increase in diameter upon growth of several monolayers of a CdS shell by means of the SILAR technique. Right panel: UV/Vis and PL spectra of samples with different shell thicknesses. Reprinted with permission from Reference [25]. Copyright 2001, American Chemical Society.

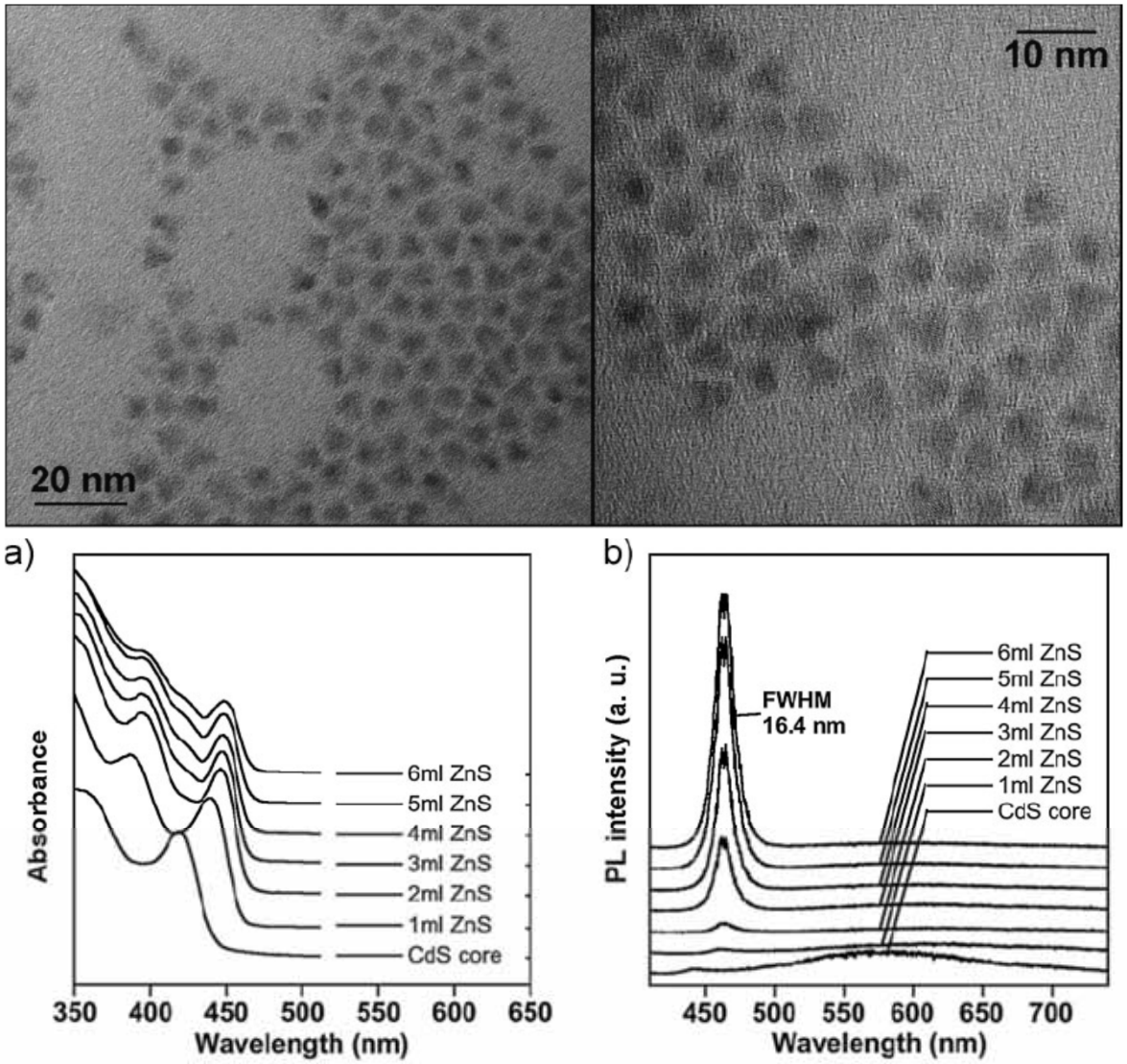

Figure 6. Top: TEM images at different magnifications of CdS/ZnS NCs. [63] Bottom: a) UV/Vis absorption spectra; b) PL spectra recorded during the addition of 6 mL of the ZnS precursor solution corresponding to the growth of a 5-monolayer-thick ZnS shell on 4-nm CdS core NCs.

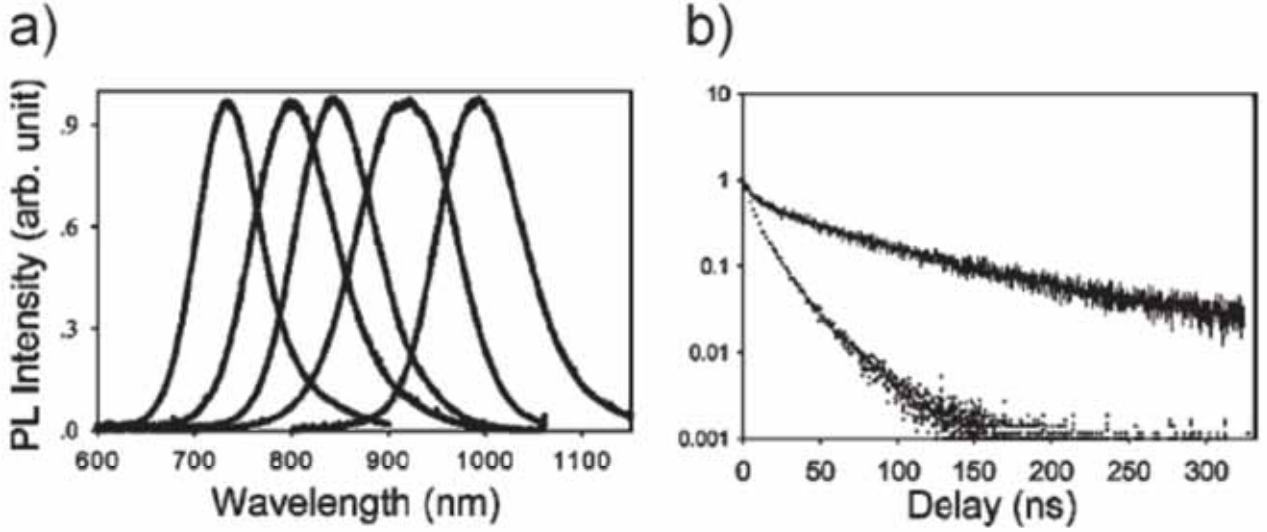

Figure 9. a) Normalized PL spectra of CdTe/CdSe CS NCs having a core/shell radii of 1.6/1.9 nm, 1.6/3.2 nm, 3.2/1.1 nm, 3.2/2.4 nm, 5.6/1.9 nm (from left to right, respectively). b) Normalized PL decays of 3.2/1.1-nm CdTe/CdSe CS NCs and of the corresponding 3.2-nm CdTe core NCs (dotted line). Reprinted with permission from Reference [37]. Copyright 2003, American Chemical Society.

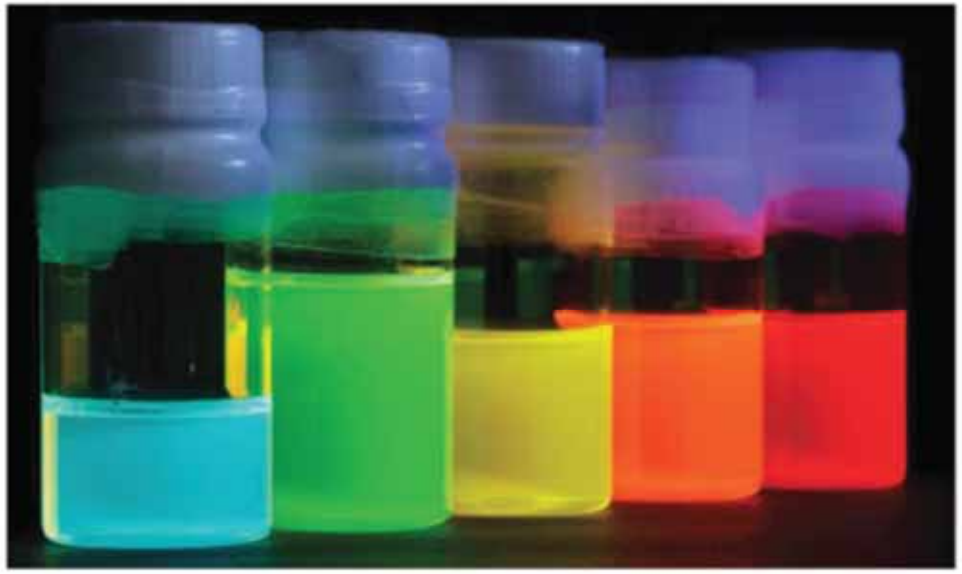

Fig. 1 Suspensions of colloidal CdSe NCs of different sizes (1.7 to 4.5 nm diameter, from left to right) under UV excitation. This iconic image of colloidal nanoscience provides a beautiful visual demonstration of two fundamental nanoscale effects: quantum confinement (size dependent luminescence colours) and large surface to volume ratio (colloidal stability).

Synthesis of CdSe/ZnS Quantum Dots

20mL (31mg, 0.16 mmol) colloidal solution of CdSe QDs from stock solution (54mg dissolved in 35mL toluene) was placed in a two-neck flask. TOPO (6g) and HAD (6g) were added and then toluene was removed through vacuum, flask refilled with nitrogen. The reaction mixture was heated at 350 ^{0}C for two hours. In another flask zinc acetate in 1:3 ratio with respect of CdSe and was dissolved in 4mL of oleic acid stirred at 120 ^{0}C for 2 hours obtained a light yellow coloured solution and temperature reduced to 60-70 ^{0}C. After cooling to room temperature, TOPSe was mixed with Zn salt solution. And the mixture was injected slowly through syringe in to reaction solution of CdSe-TOPO at 180-200 ^{0}C. The stirring was done for another an hour. The similar procedure was followed for work up of reaction as avobe experiment. The final product was re-dispersed in toluene.

Light emission from CdSe/ZnSe Quantum dots

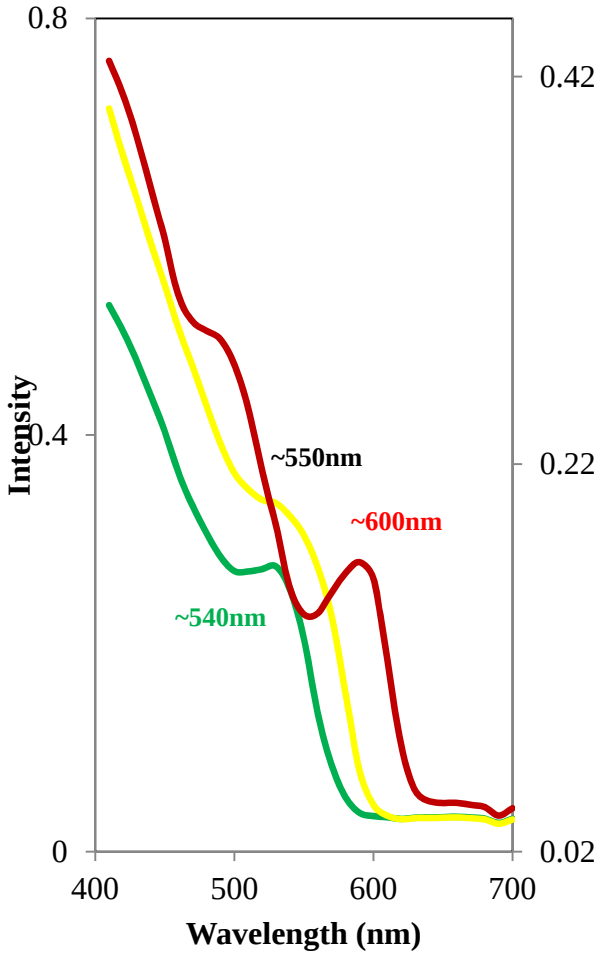

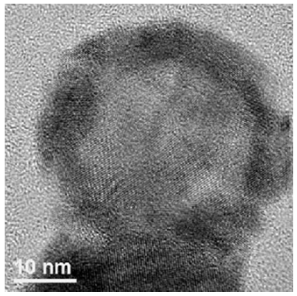

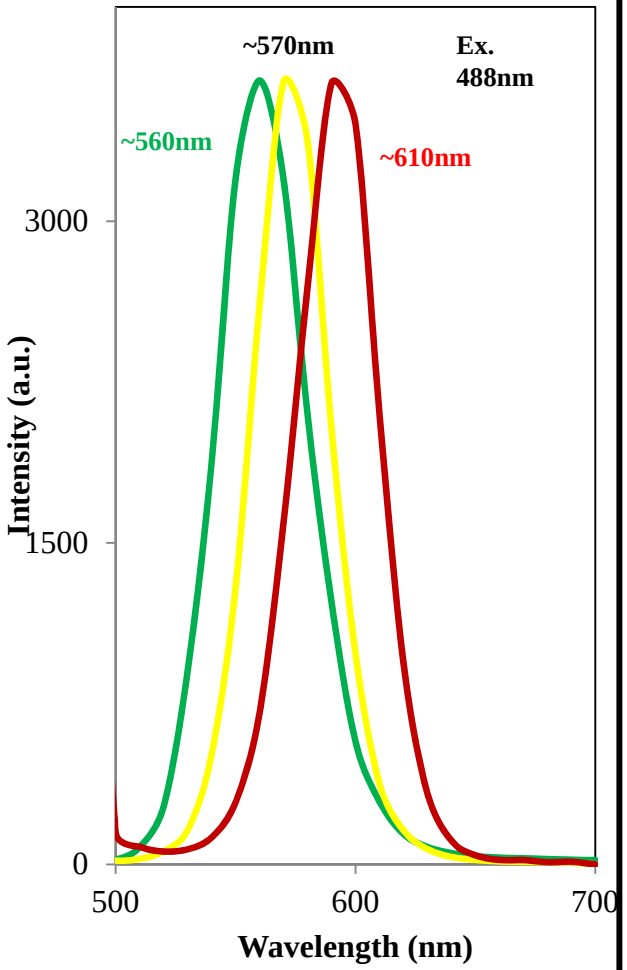

UV-Visible and PL spectra of CdSe/ZnSe re-dispersed in toluene

Template Synthesis

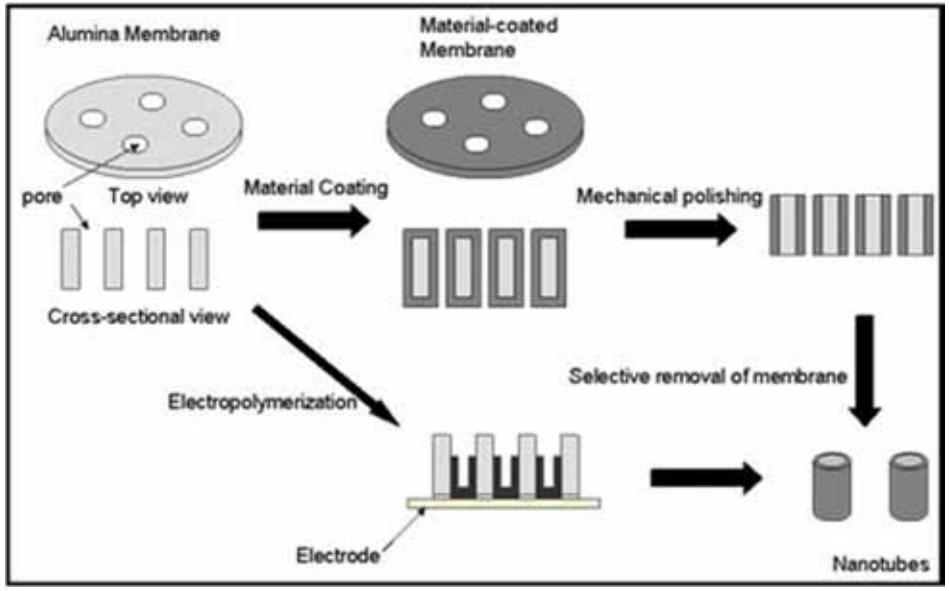

Porous Materials

- AAO
- MCM-41

Mobil Crystalline Materials, or MCM-41

Santa Barbara Amorphous type material, or SBA-15

- Micro: < 2nm
- Meso:
- Macro: > 50nm

AAO

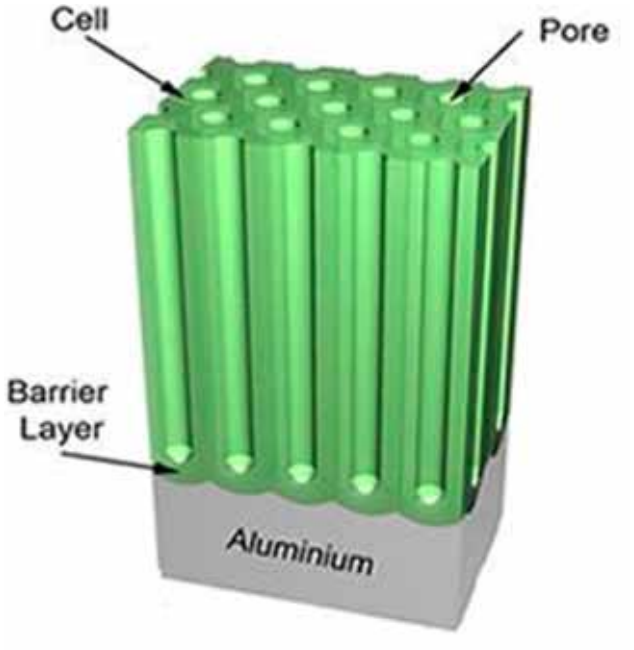

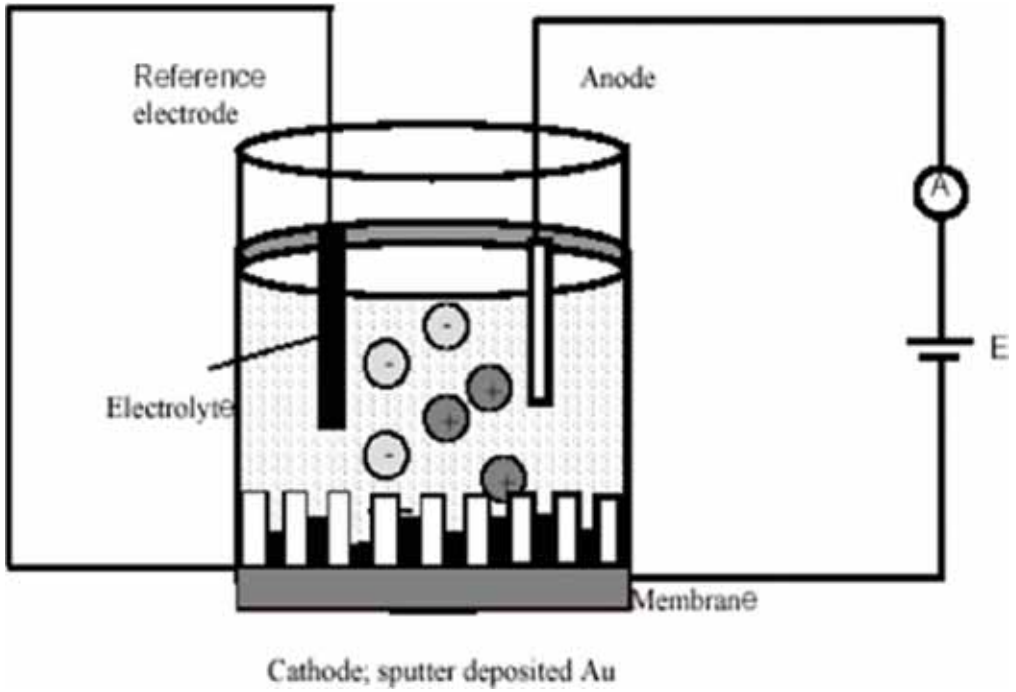

Cathode; sputter deposited Au

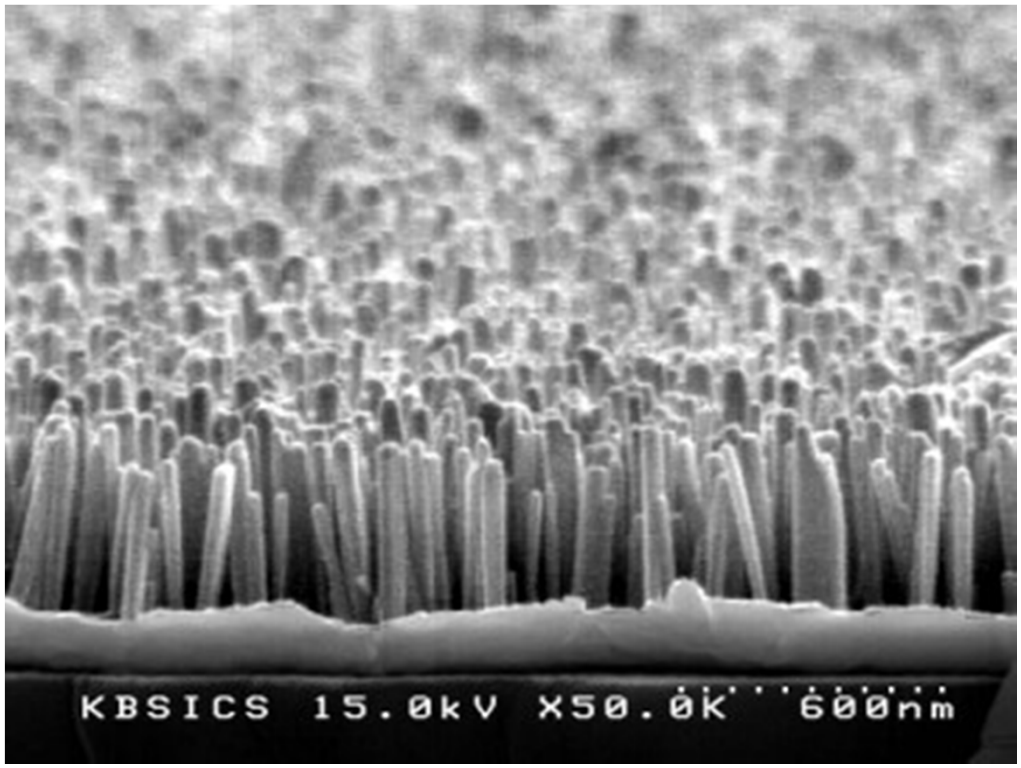
KBSICS 15.0kV X50.0K 600nm

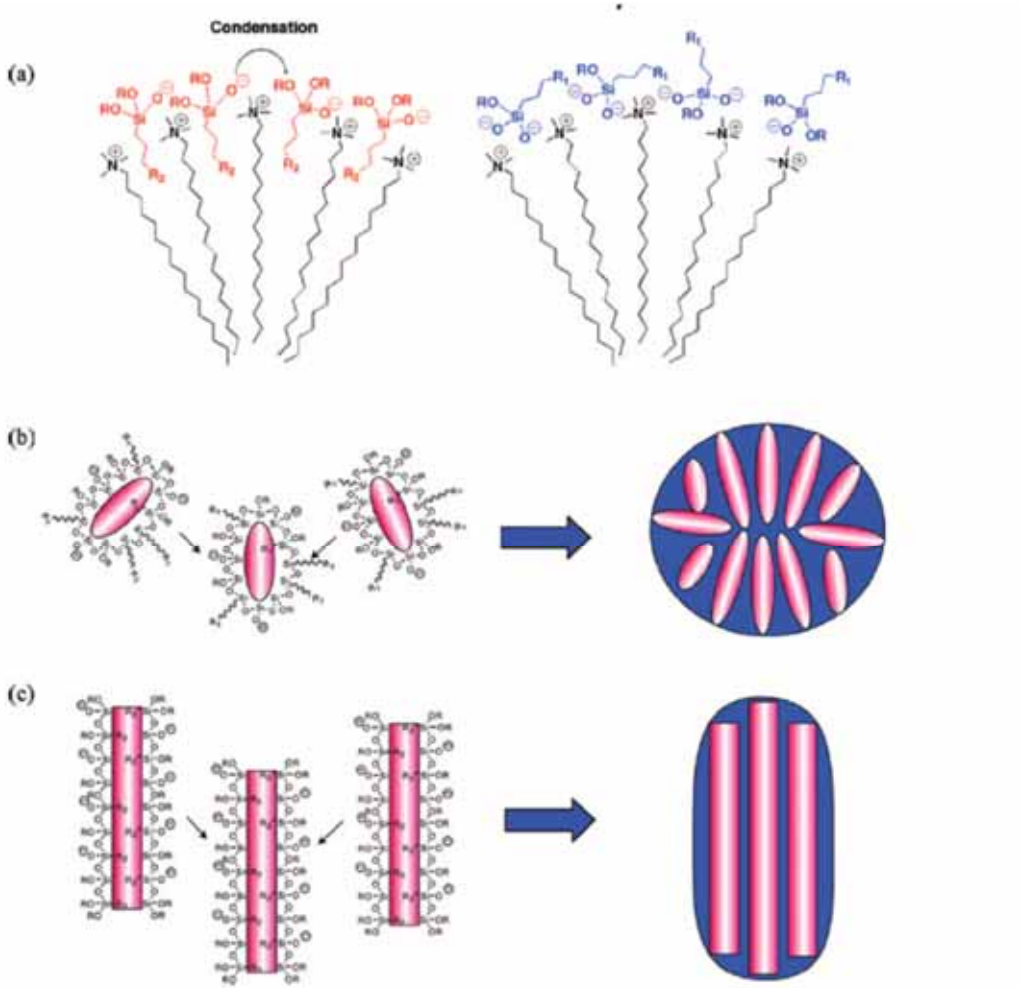

[a] R, methyl or ethyl groups; R_1, hydrophilic functional groups; R_2, hydrophobic functional groups.

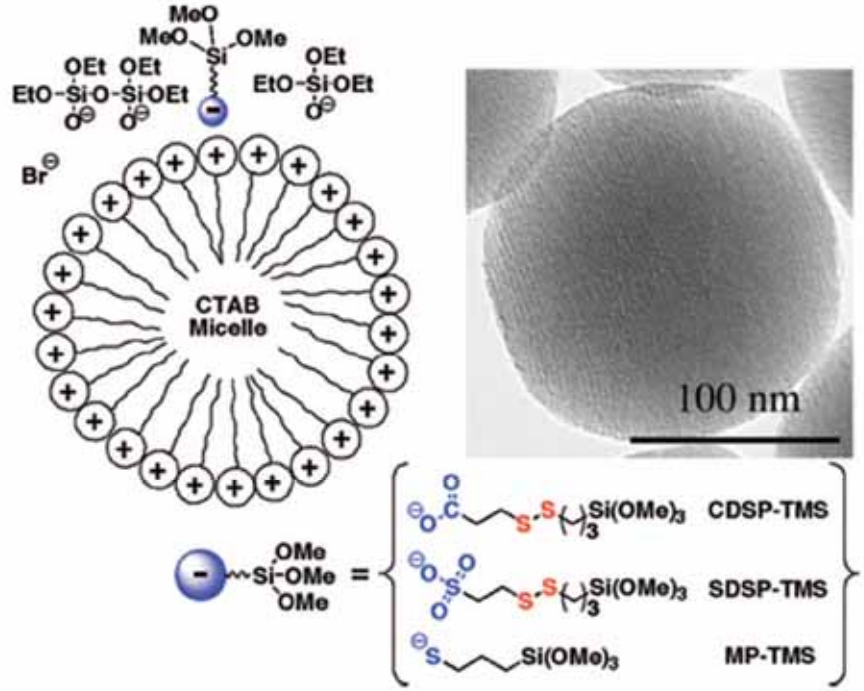

FIGURE 3. Schematic representation of the use of anionic organoalkoxysilanes for controlling the functionalization of the MSN materials. The MCM-41-type mesoporous channels are illustrated by the parallel stripes shown in the transmission electron microscopy (TEM) micrograph of the MSN–SH material. Reproduced with permission from ref 15. Copyright 2005, Royal Society of Chemistry.

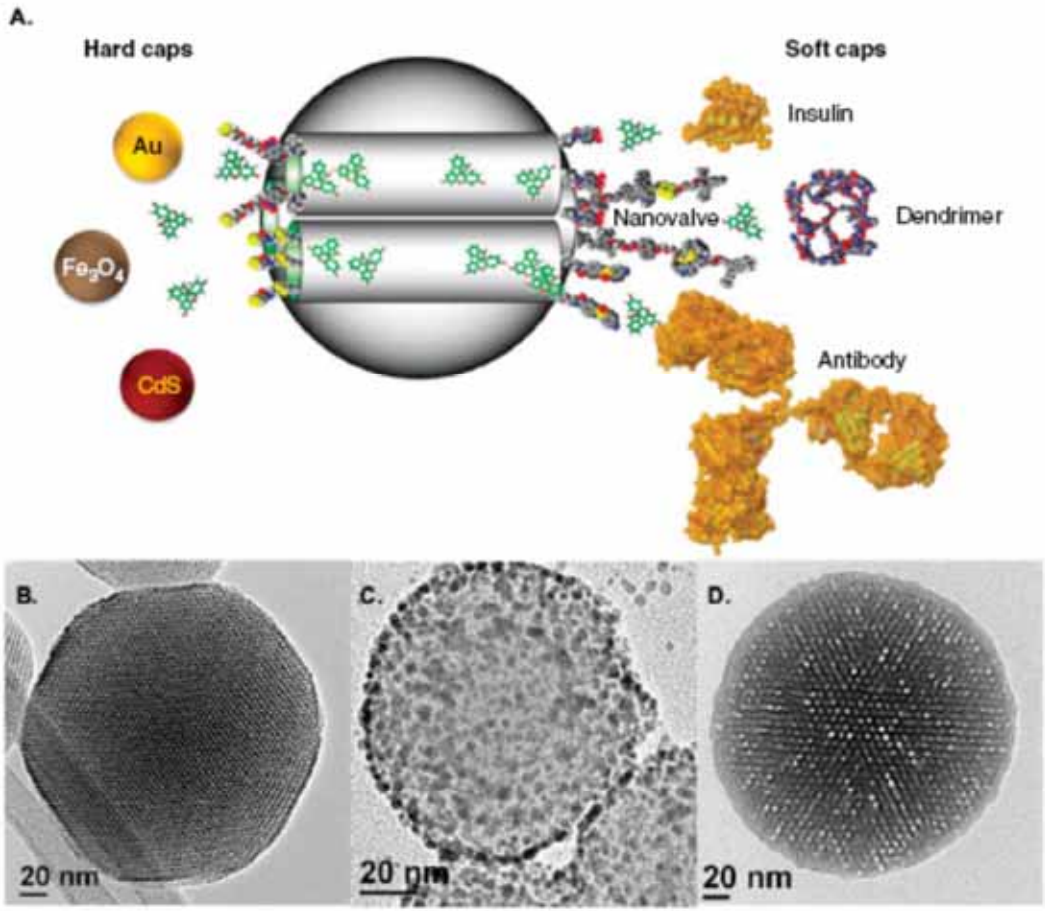

Figure 1. A. Schematic representation of a MSN loaded with drugs and capped with hard caps and soft caps highlighted in this review. Transmission electron microscopy images of (**B**) a MSN along the axis of the mesopores, (**C**) capped with hard (Au NP) and (**D**) with soft (polymer) caps.

MSN: Mesoporous silica nanoparticle.

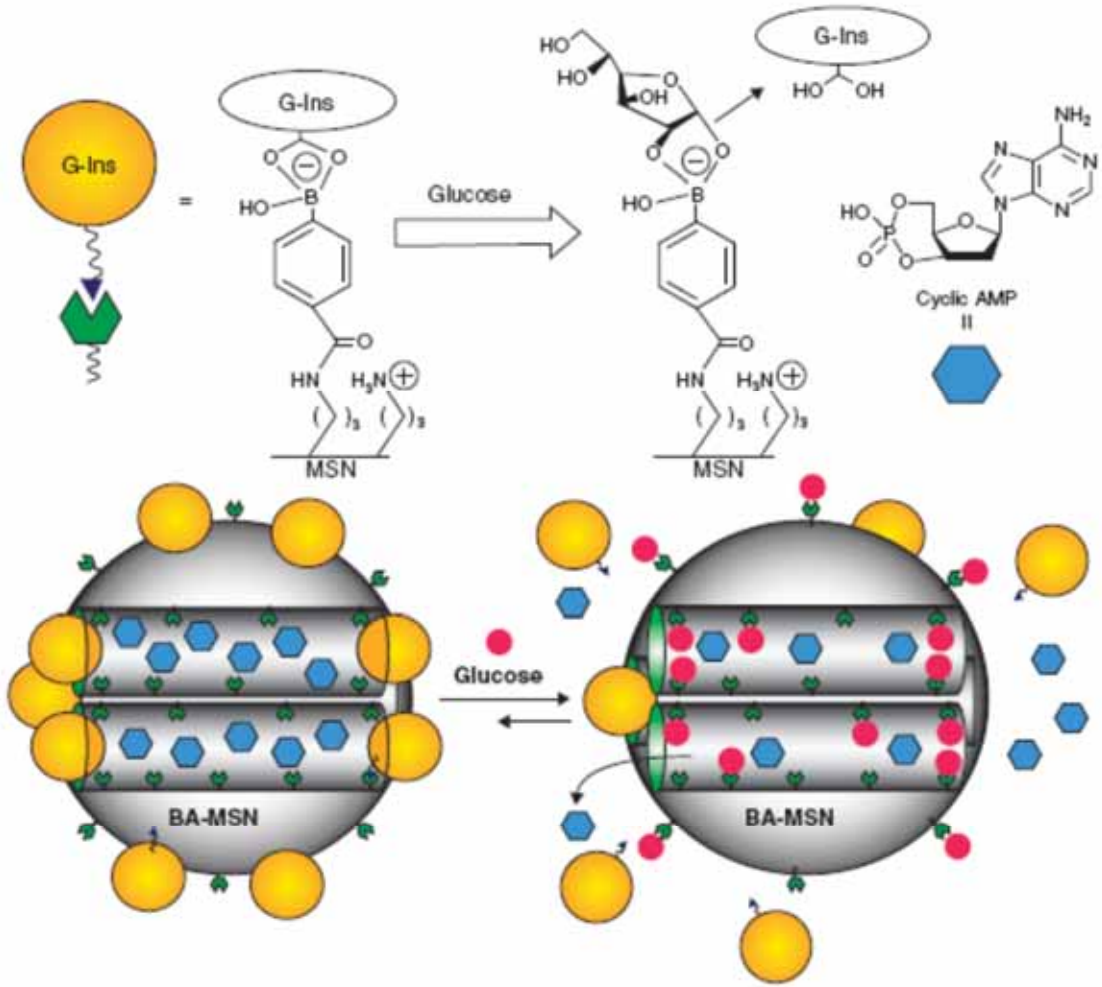

Figure 5. Schematic representation of the glucose-responsive MSN-based double delivery system for controlled release of bioactive G-Ins and cyclic AMP. The controlled release mechanism was achieved by means of the displacement reaction between blood glucose and G-Ins based on reversible boronic acid-diol complexation. High glucose concentration triggers the G-Ins uncapping and the release of cyclic AMP sequentially to diminish the higher than normal level of blood glucose.

Reproduced with permission from [19].

G-Ins: G-insulin; MSN: Mesoporous silica nanoparticle.

Polymer

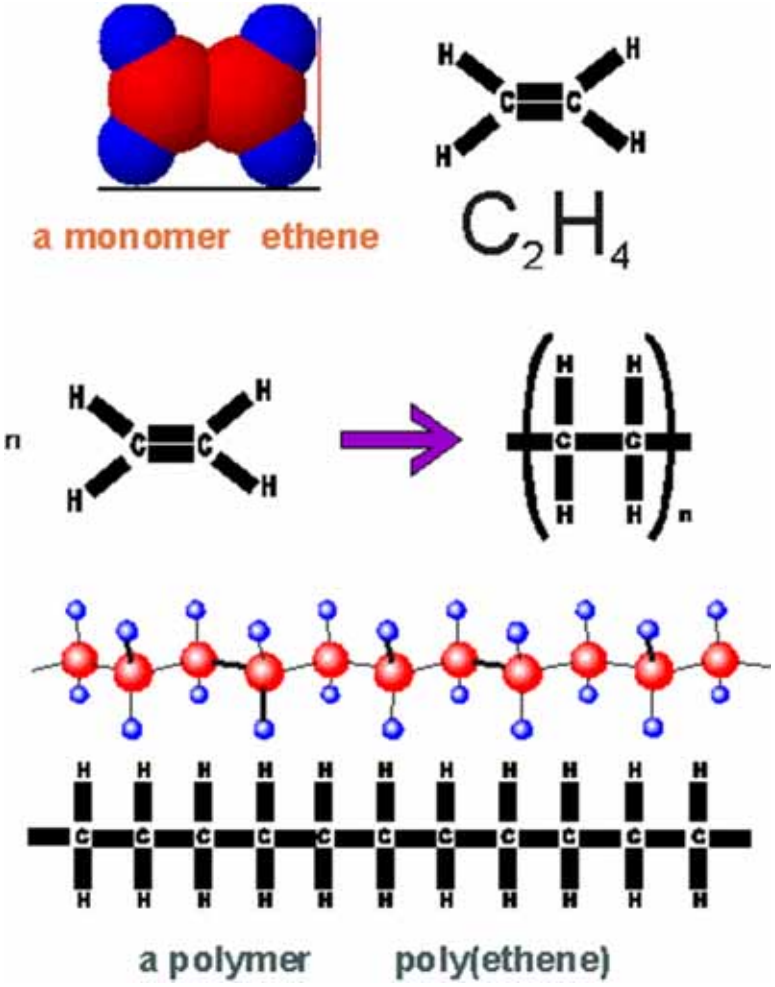

Block copolymer

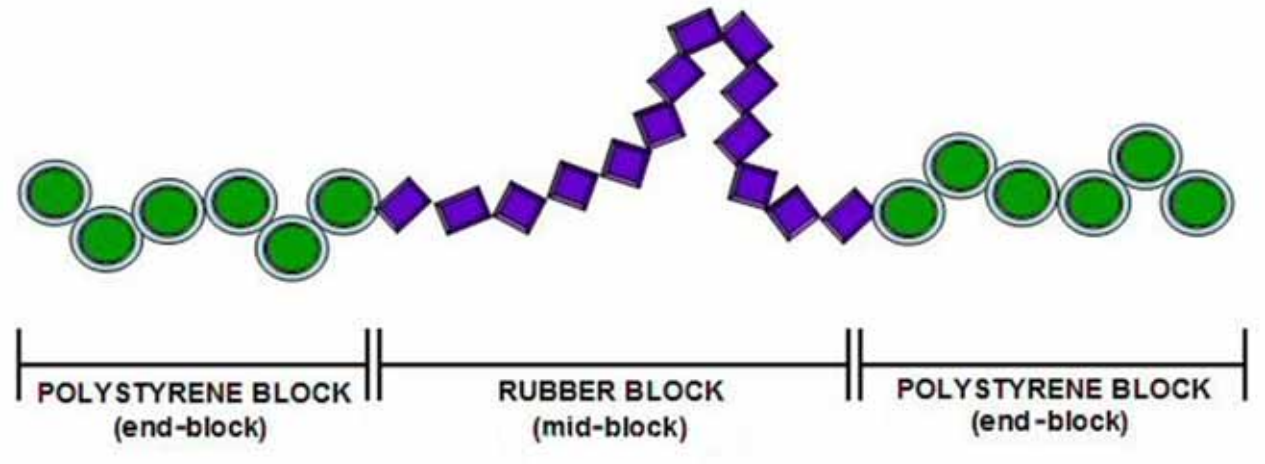

Phase Segregation

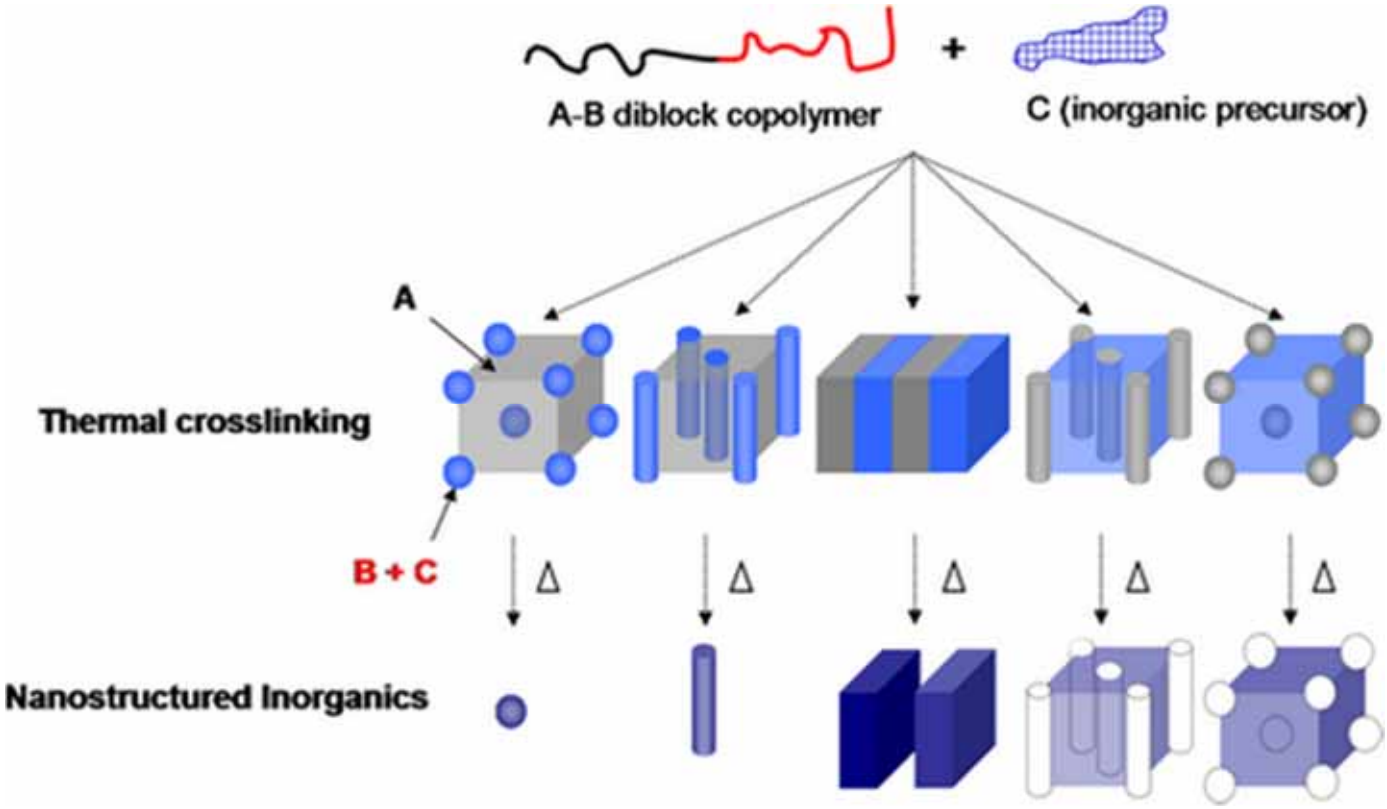

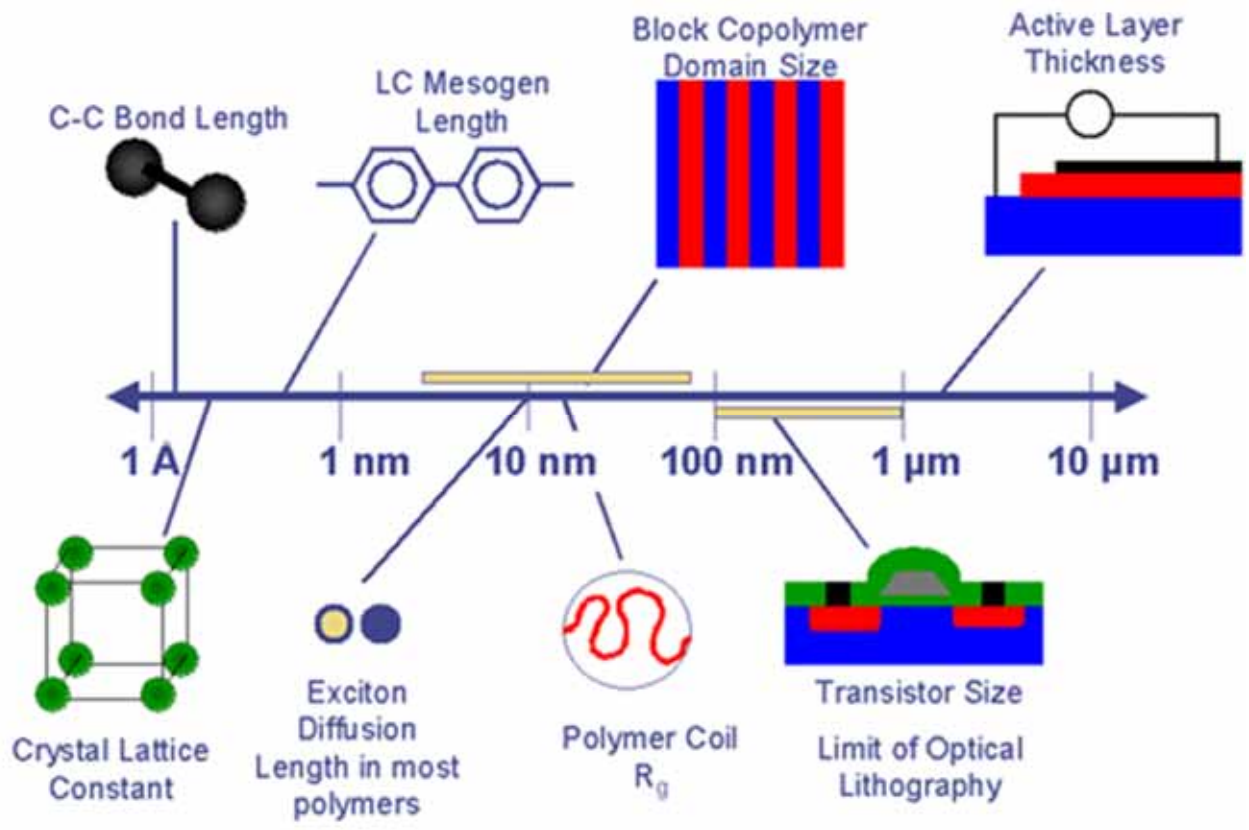
C-C Bond Length
LC Mesogen Length
Block Copolymer Domain Size
Active Layer Thickness
1 A
1 nm
10 nm
100 nm
1 µm
10 µm
Crystal Lattice Constant
Exciton Diffusion Length in most polymers
Polymer Coil R_g
Transistor Size
Limit of Optical Lithography

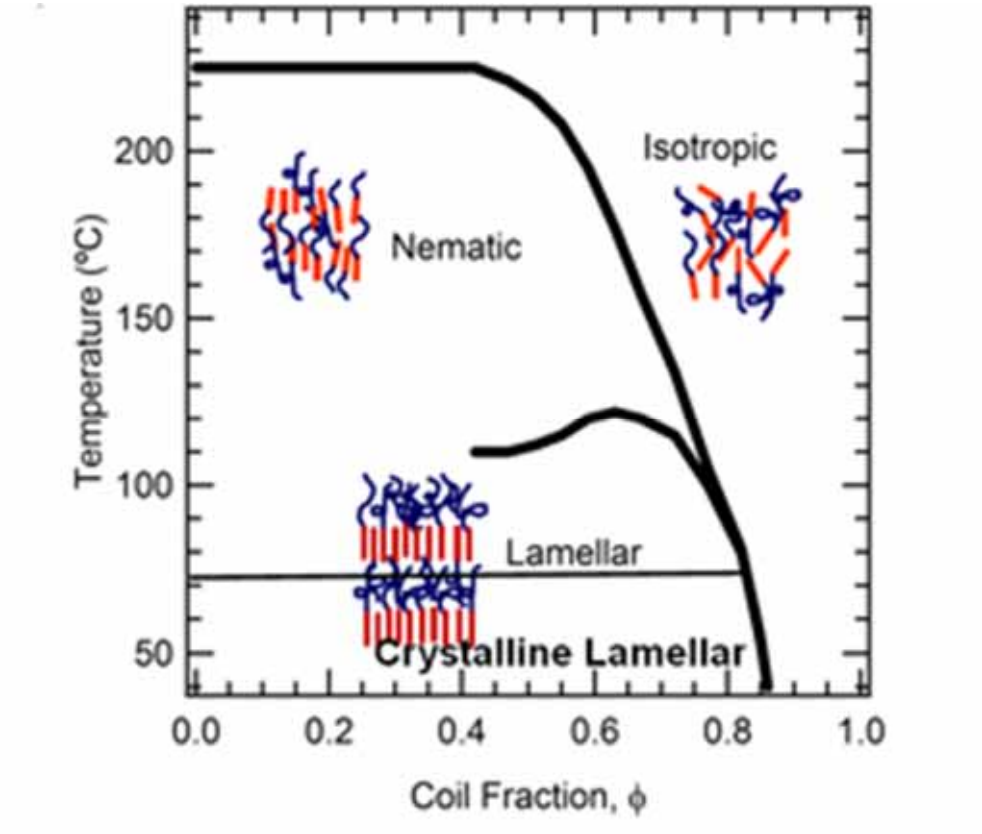
Isotropic
Nematic
Lamellar
Crystalline Lamellar
Temperature (°C)
200
150
100
50
0.0
0.2
0.4
0.6
0.8
1.0
Coil Fraction, ϕ

Self-Assembled Block-copolymer

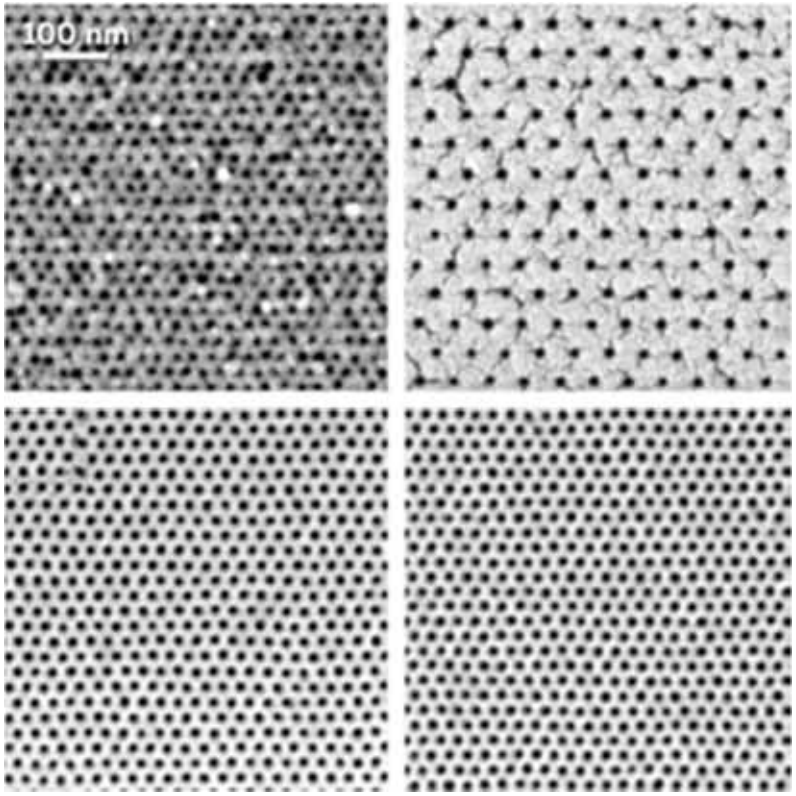

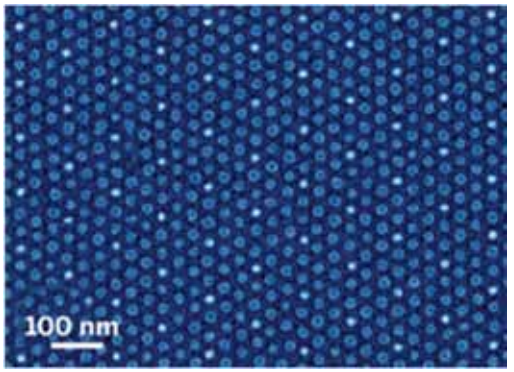

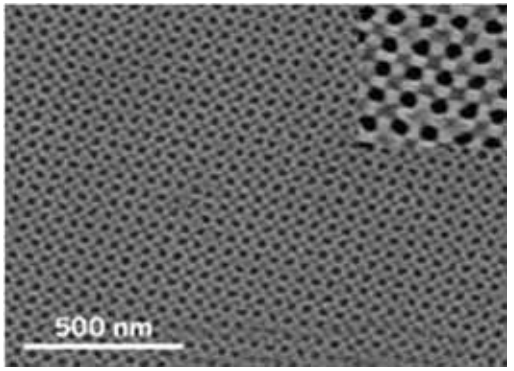

CNT

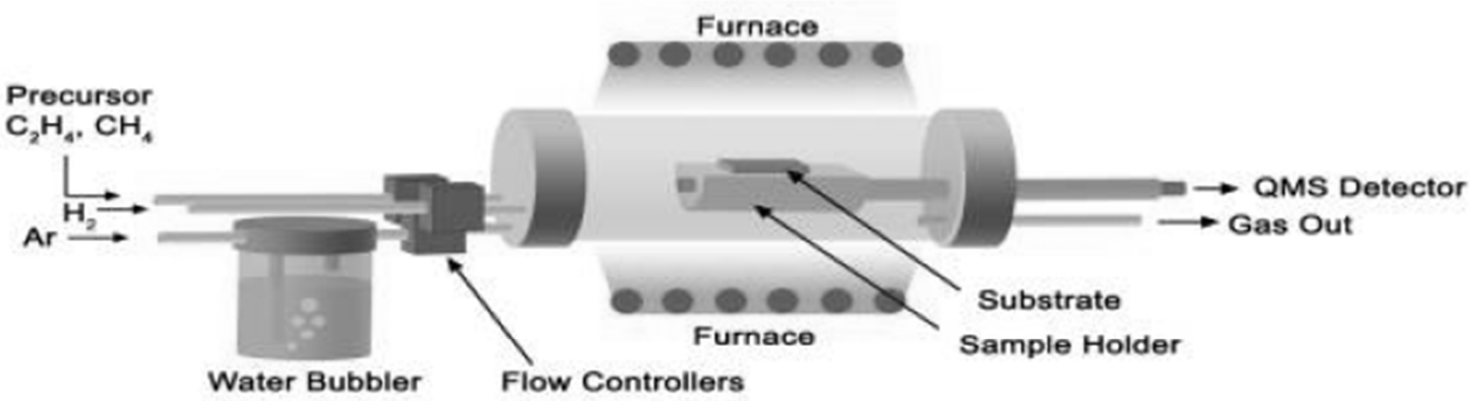

Fig. 1. Schematic of a CVD reactor for carbon nanotube growth. (Sketch by S. Yarmolenko from NCA&T State University)

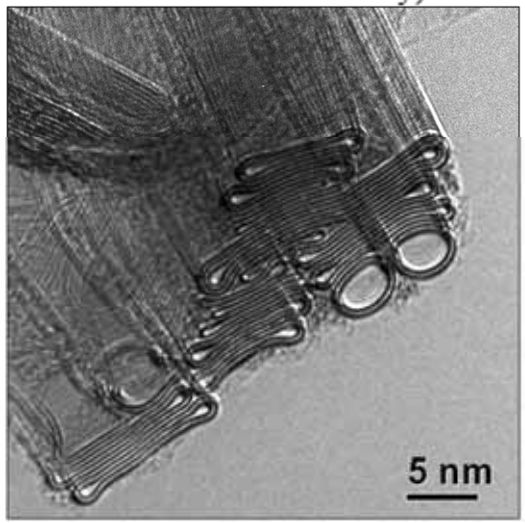

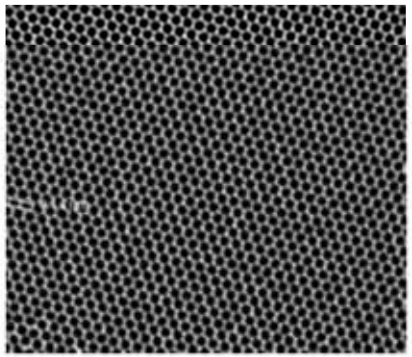

Surface Functionalization

- Recognition
  - Molecular Recognition
    - Protein
    - DNA
    - Saccharide
- Reporting/Detection
  - Dye
  - Quantum dots
  - SPR
  - SERS/LSPR
- Separation
  - Gel/Chromatography
  - Magnetic

- Surfaces
  - Gold and silver
  - Silicon oxide (glass)
  - Quantum dots
  - Polymer

Carboxyl Presenting Surfaces

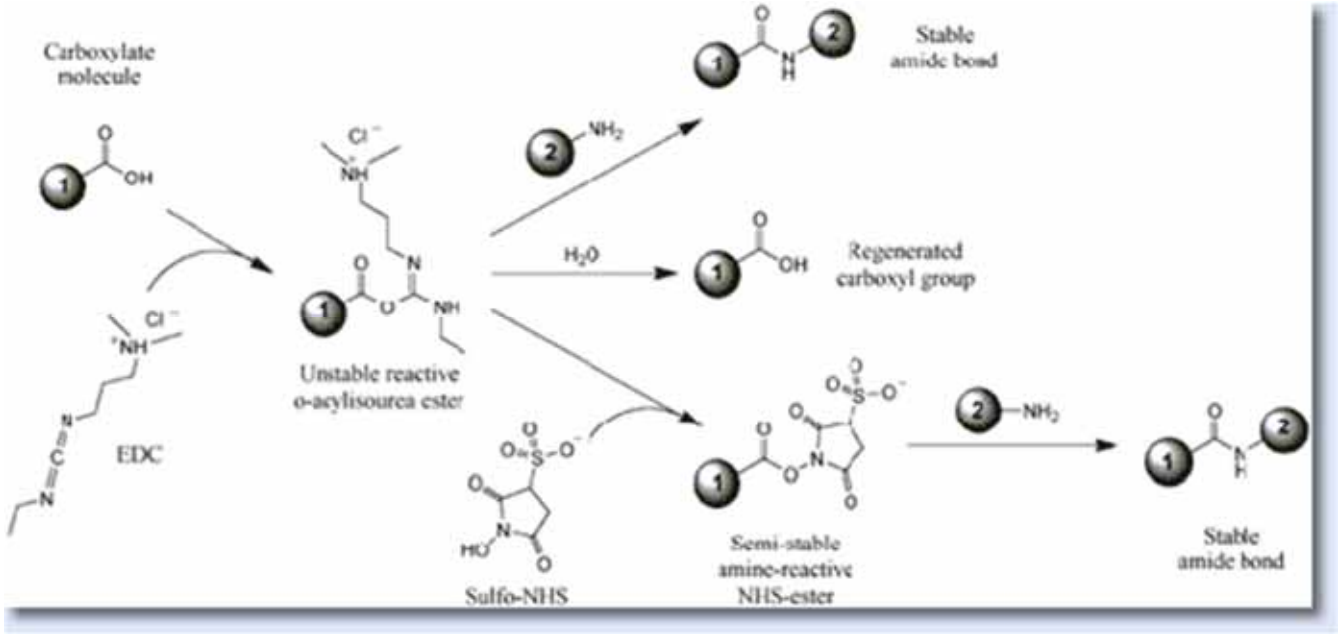

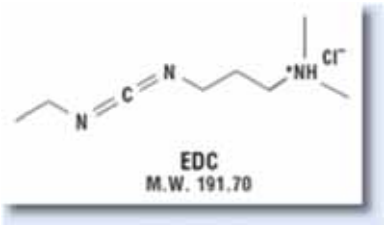

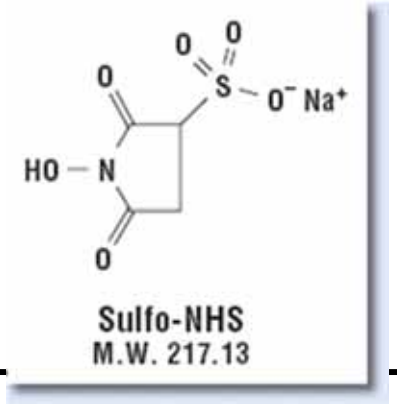

EDC (1-Ethyl-3-[3-dimethylaminopropyl]carbodiimide Hydrochloride)

Amine Presenting Surface

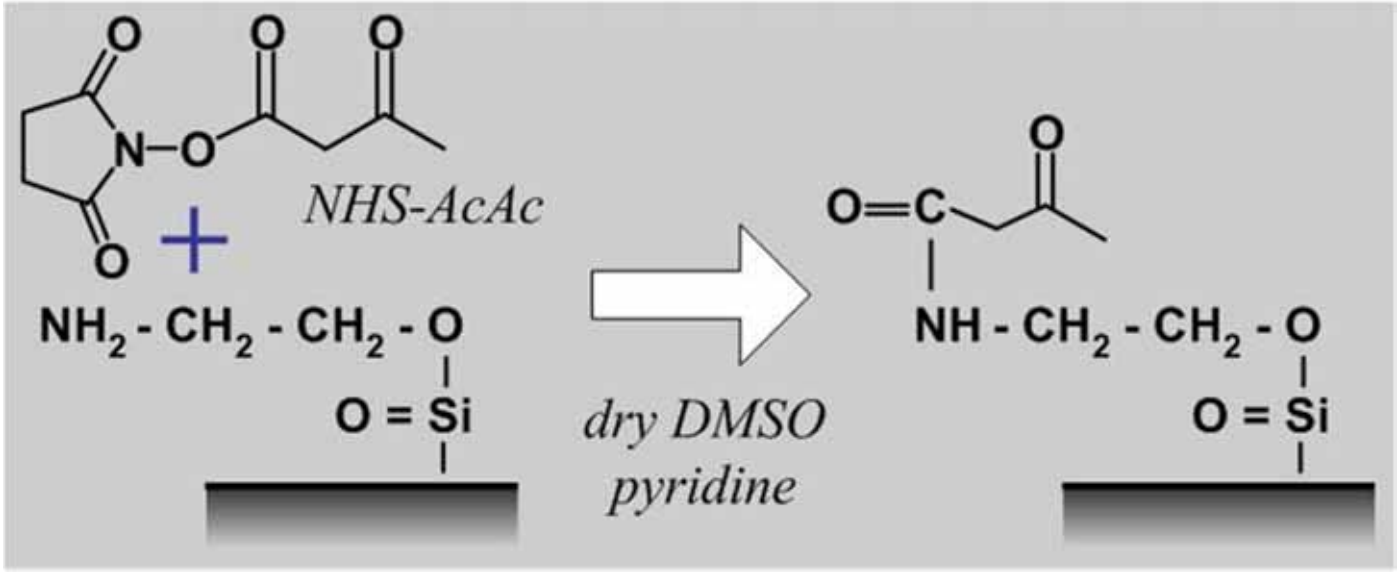

Sulfhydryl Labeling

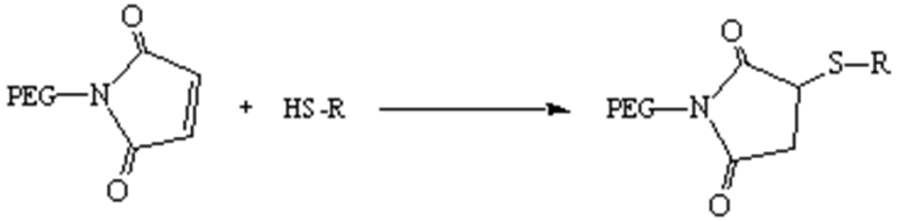

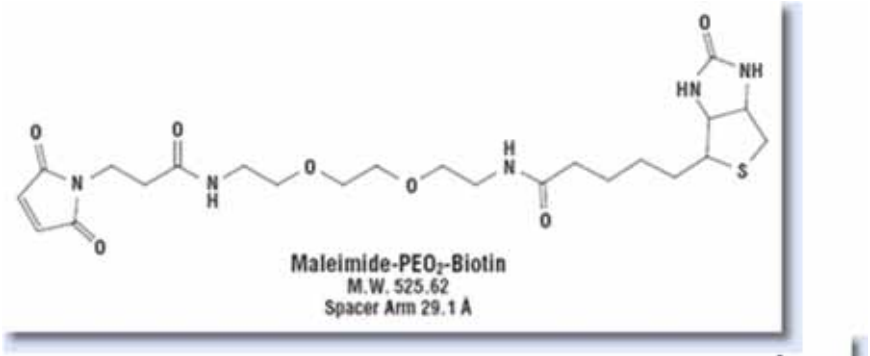

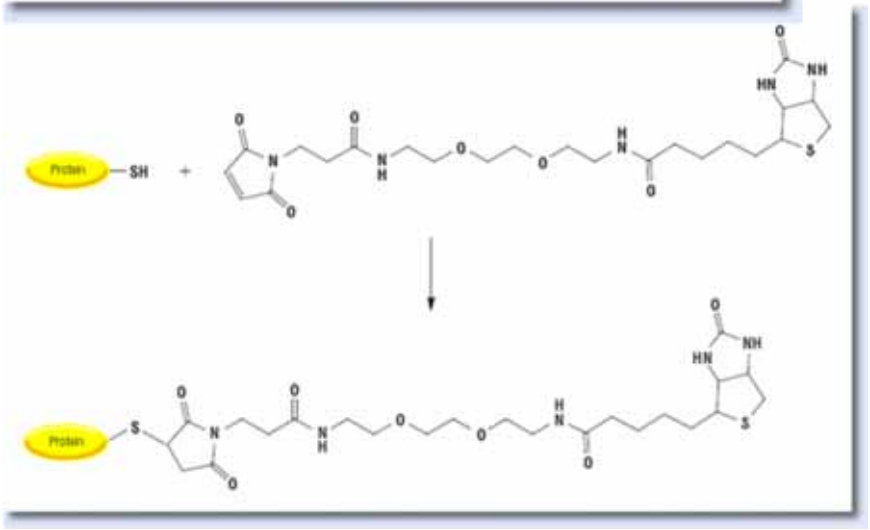

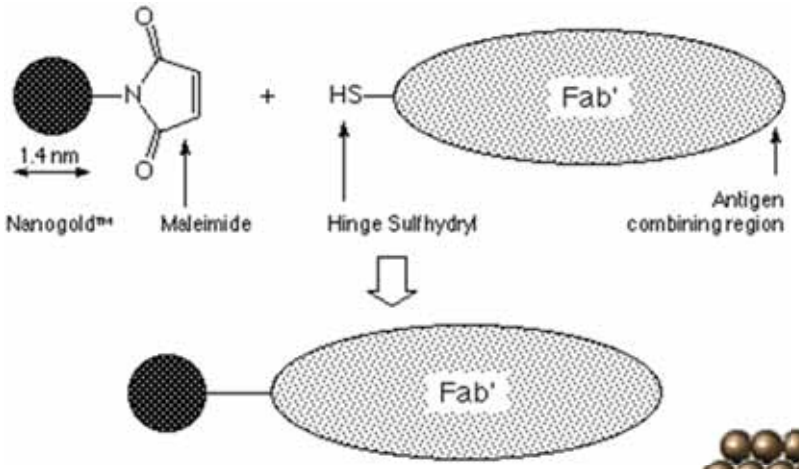

Silica Modification

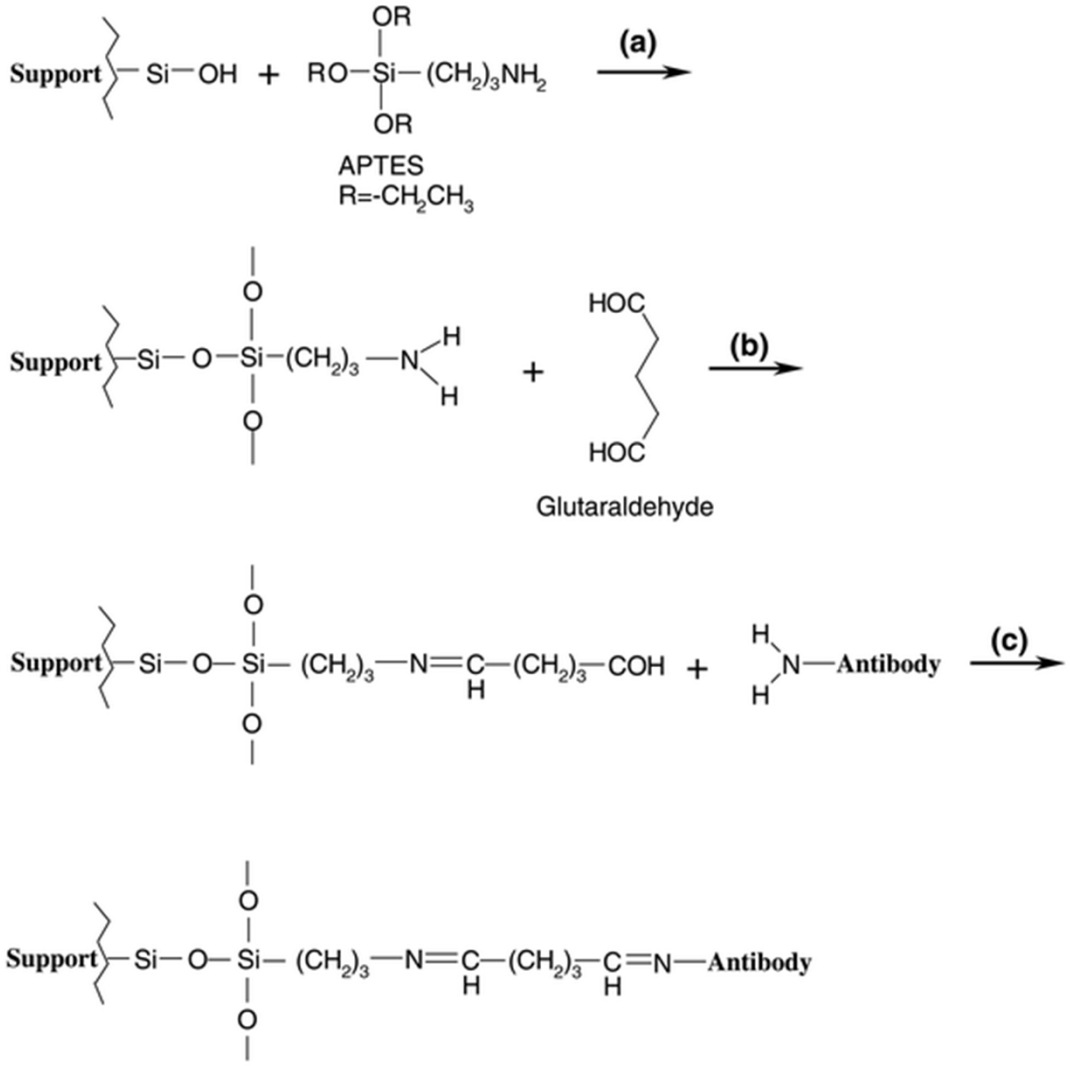

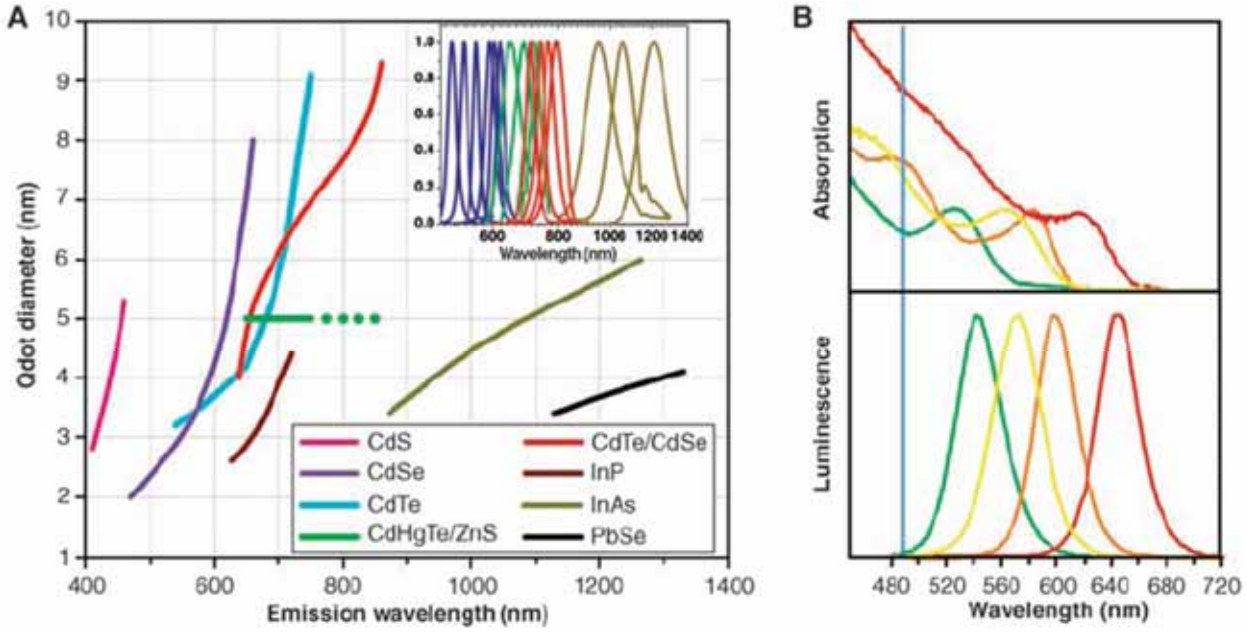

Fig. 1. (A) Emission maxima and sizes of quantum dots of different composition. Quantum dots can be synthesized from various types of semiconductor materials (II-VI: CdS, CdSe, CdTe…; III-V: InP, InAs…; IV-VI: PbSe…) characterized by different bulk band gap energies. The curves represent experimental data from the literature on the dependence of peak emission wavelength on qdot diameter. The range of emission wavelength is 400 to 1350 nm, with size varying from 2 to 9.5 nm (organic passivation/solubilization layer not included). All spectra are typically around 30 to 50 nm (full width at half maximum). Inset: Representative emission spectra for some materials. Data are from (*12*, *18*, *27*, *76*–*82*). Data for CdHgTe/ZnS have been extrapolated to the maximum emission wavelength obtained in our group. (**B**) Absorption (upper curves) and emission (lower curves) spectra of four CdSe/ZnS qdot samples. The blue vertical line indicates the 488-nm line of an argon-ion laser, which can be used to efficiently excite all four types of qdots simultaneously. [Adapted from (*28*)] (**C**) Size comparison of qdots and comparable objects. FITC, fluorescein isothiocyanate; GFP, green fluorescent protein; qdot, green (4 nm, top) and red (6.5 nm, bottom) CdSe/ZnS qdot; qrod, rod-shaped qdot (size from Quantum Dot Corp.'s Web site). Three proteins—streptavidin (SAV), maltose binding protein (MBP), and immunoglobulin G (IgG)—have been used for further functionalization of qdots (see text) and add to the final size of the qdot, in conjunction with the solubilization chemistry (Fig. 2).

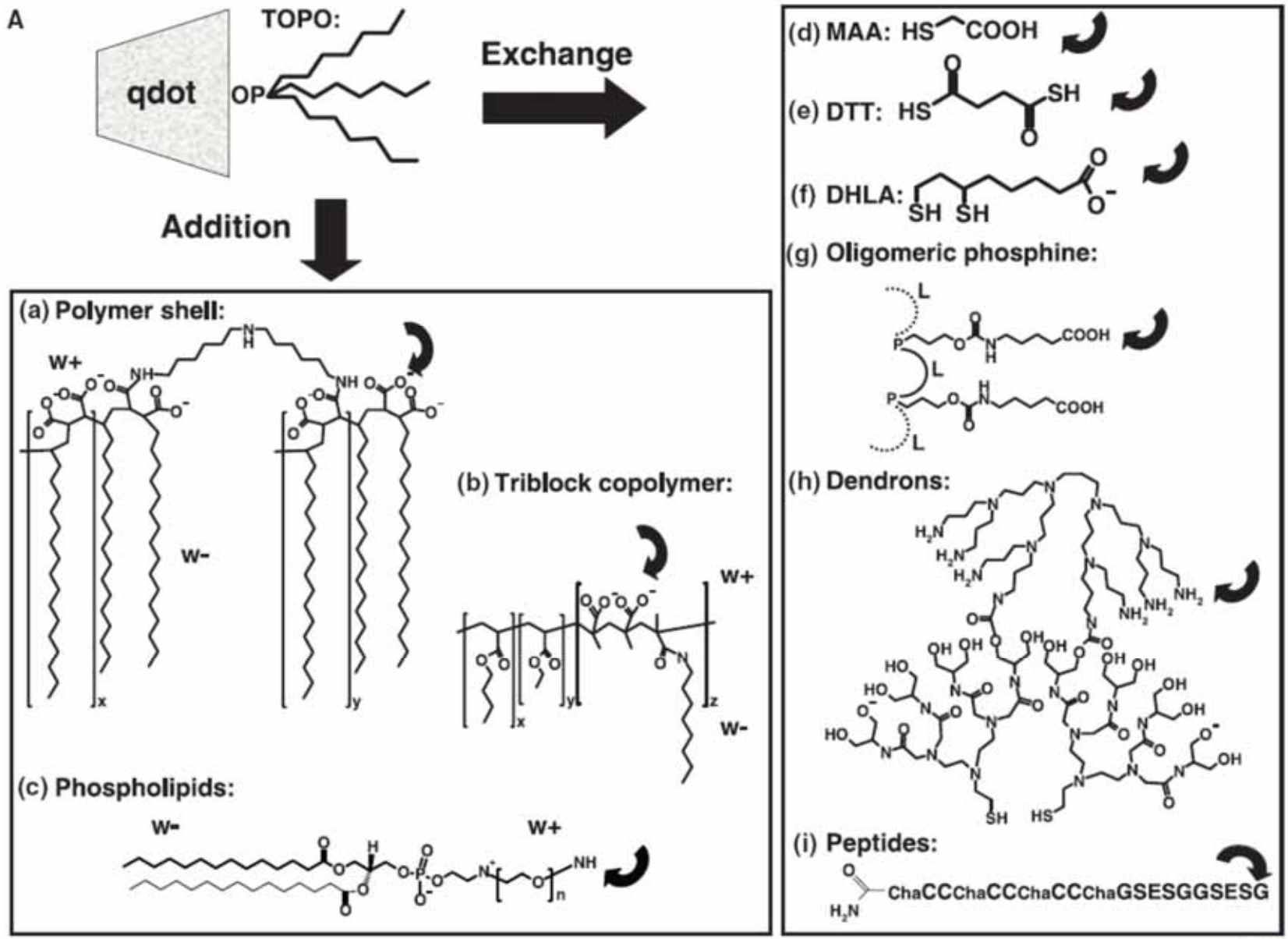
A
TOPO:
qdot
OP
Exchange
Addition
(a) Polymer shell:
W+
W-
(b) Triblock copolymer:
W+
W-
(c) Phospholipids:
W-
W+
(d) MAA: HS COOH
(e) DTT: HS SH
(f) DHLA: SH SH
(g) Oligomeric phosphine:
L
COOH
(h) Dendrons:
(i) Peptides:
ChaCCChaCCChaCCChaGSESGGSESG

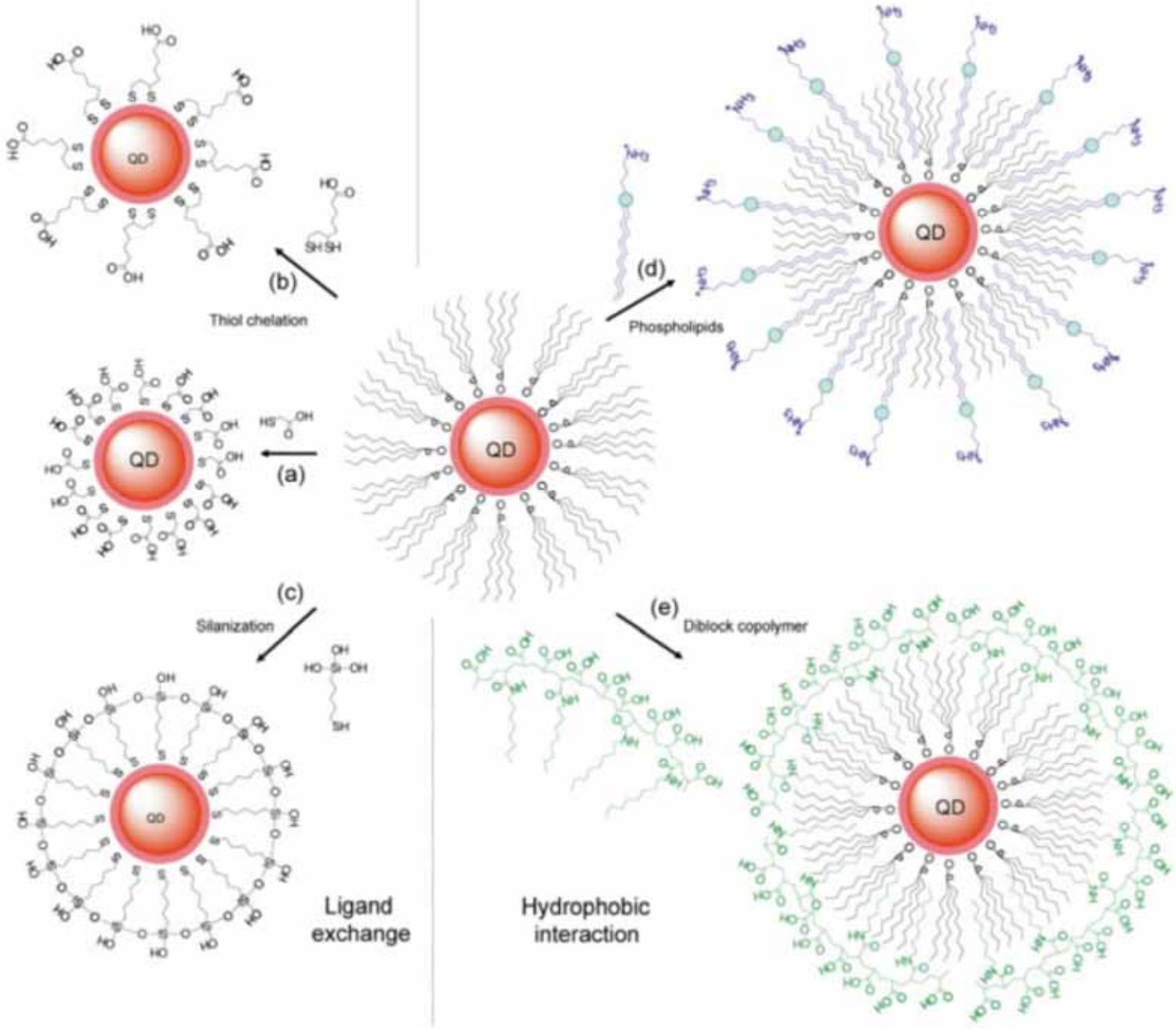
QD
(b)
Thiol chelation
(a)
(d)
Phospholipids
(c)
Silanization
Ligand
exchange
(e)
Diblock copolymer
Hydrophobic
interaction

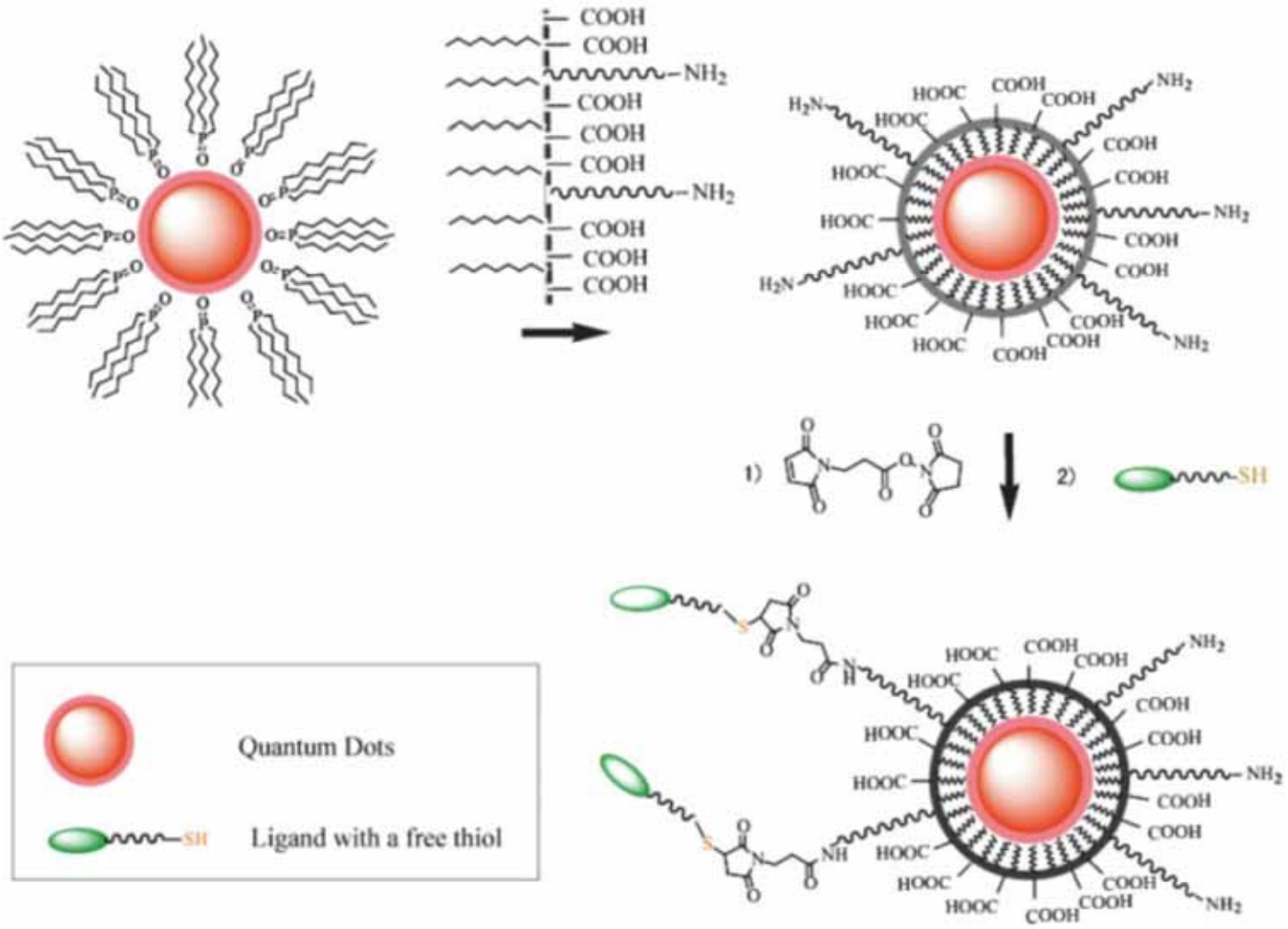

FIGURE 3 Maleimide functionalized QDs for conjugating thiol-containing ligands. TOPO stabilized QDs are coated with a primary amine functionalized tri-block amphiphilic copolymer for producing water-soluble QDs, which facilitate further conjugation to ligands with free thiols through bi-functional cross-linkers.

Cells incubated with tiopronin coated QDs

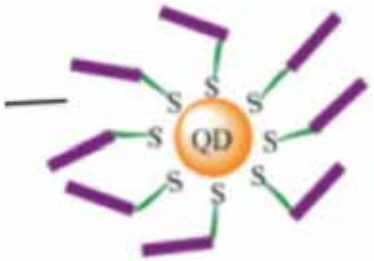

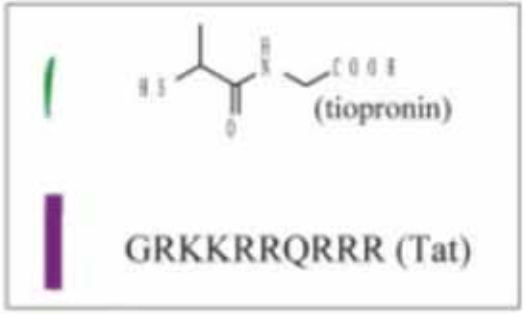

Cells incubated with Tat functionlized QDs

Scheme 1. Modular Design of Hydrophilic Ligands with Terminal Functional Groups Used in This Study

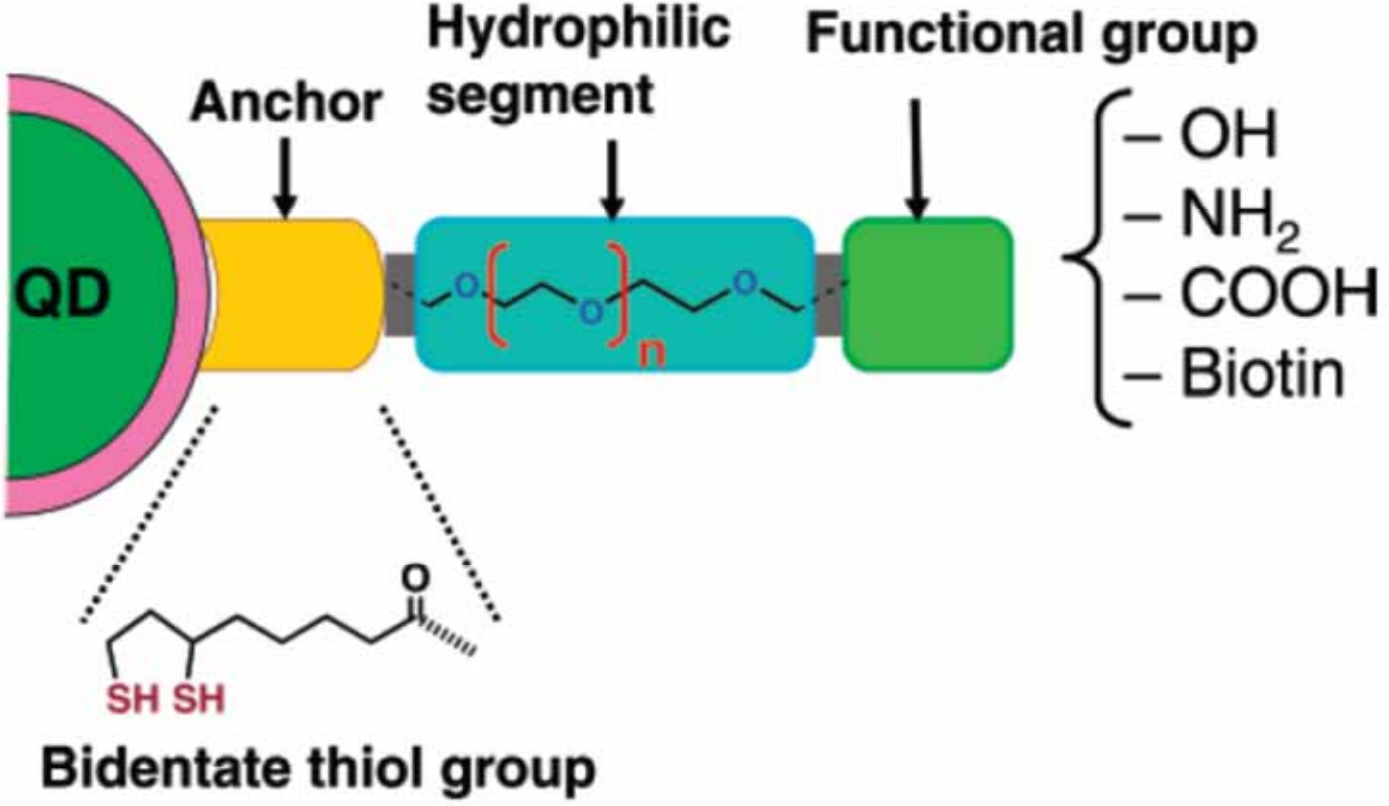

Molecular Recognition

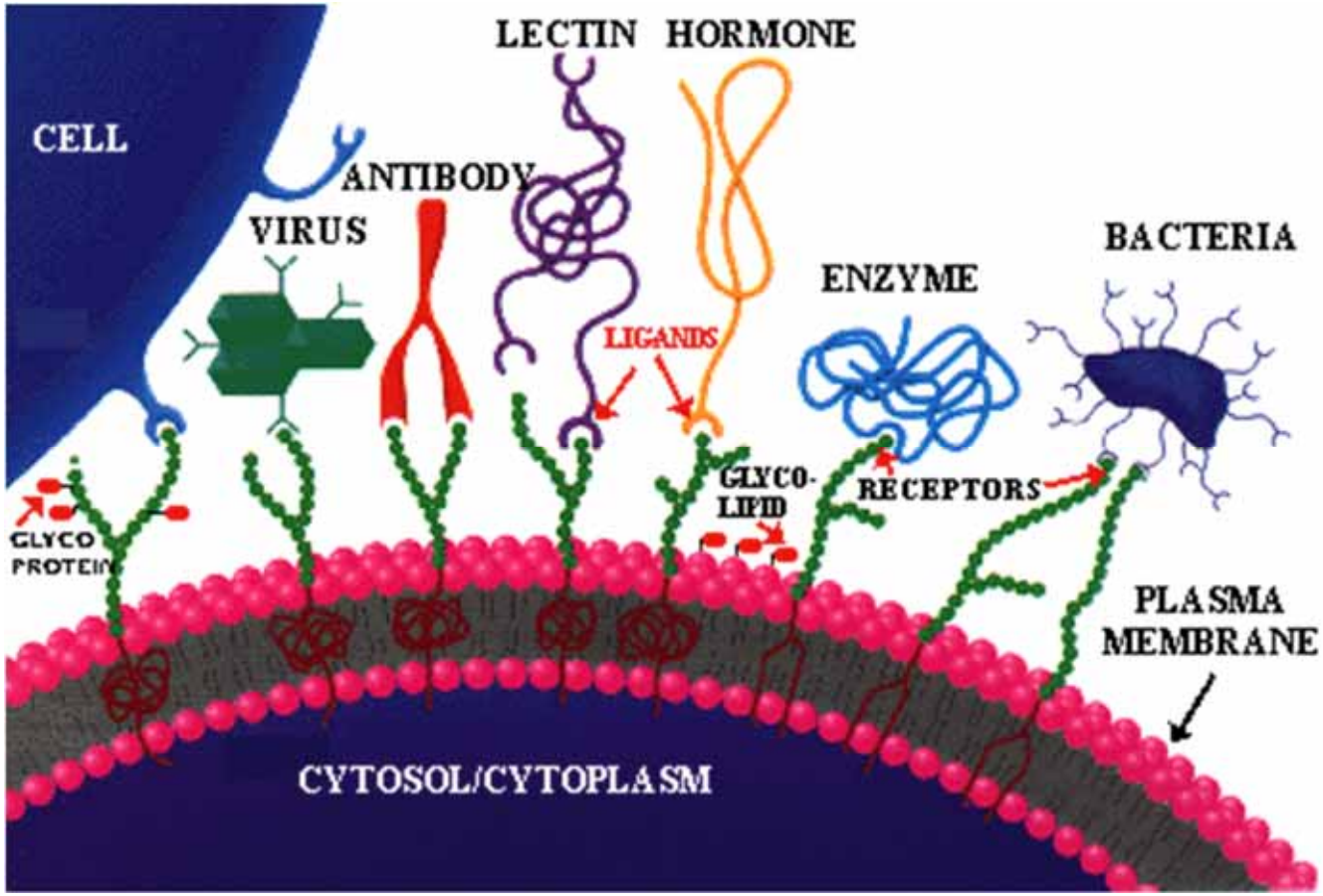

Antibody and Antigen

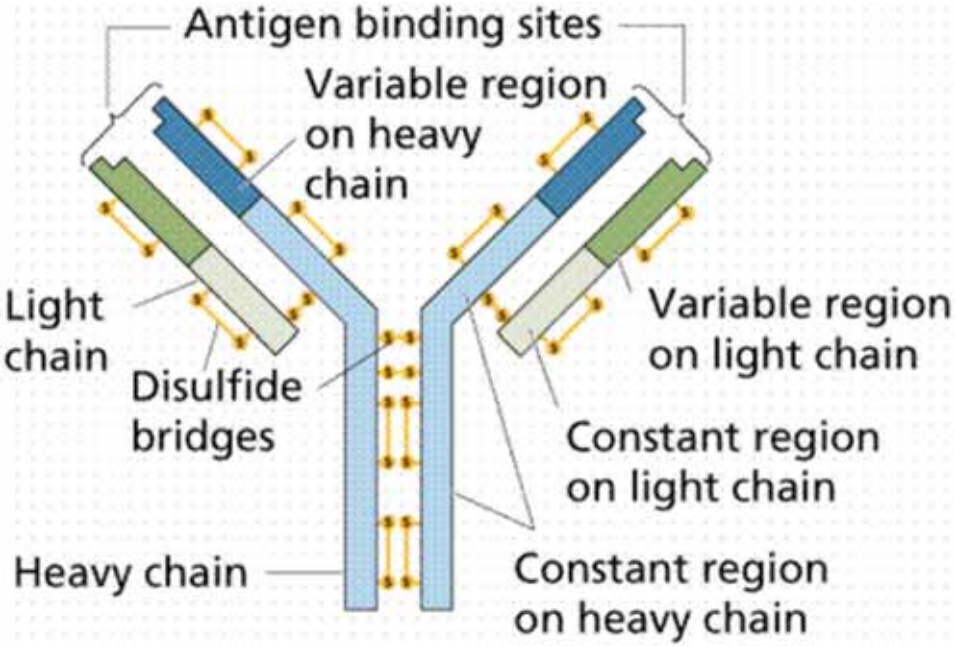

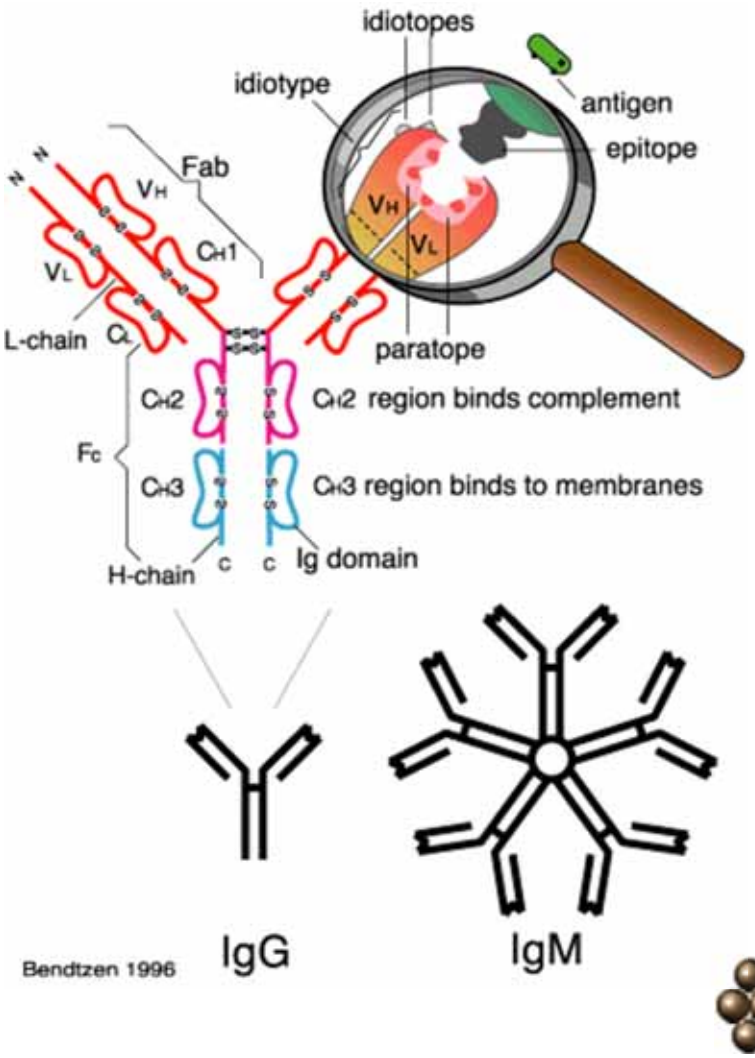

Enzyme-Linked ImmunoSorbent Assay (ELISA)

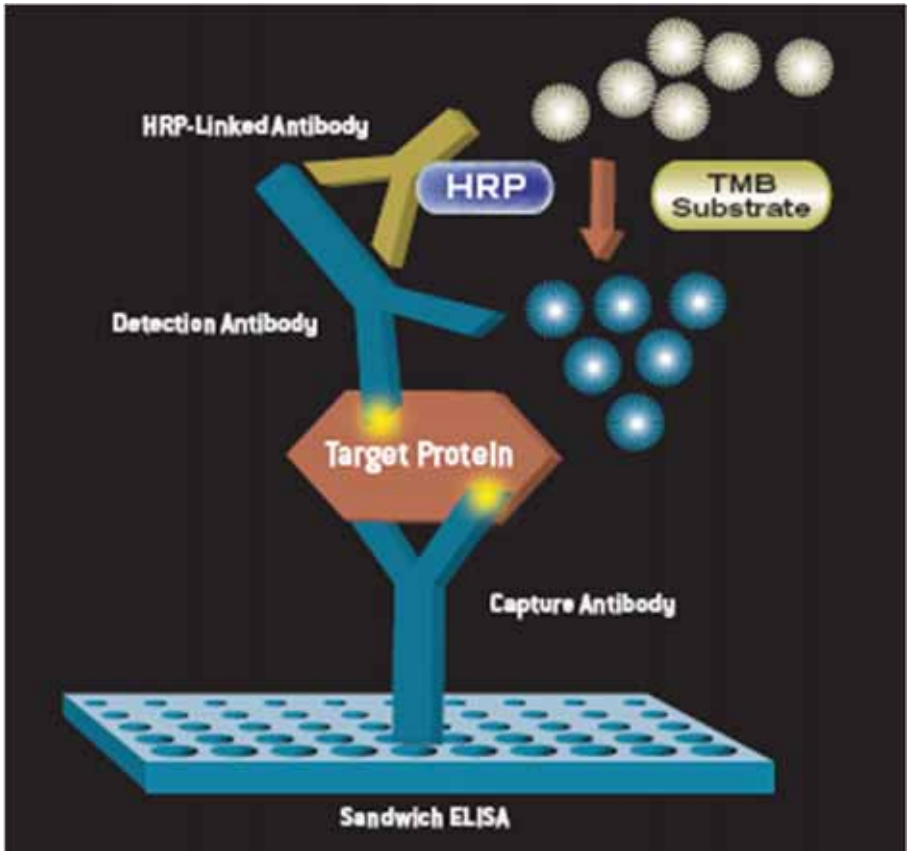

Labeling
BSA/PEG

Microarray

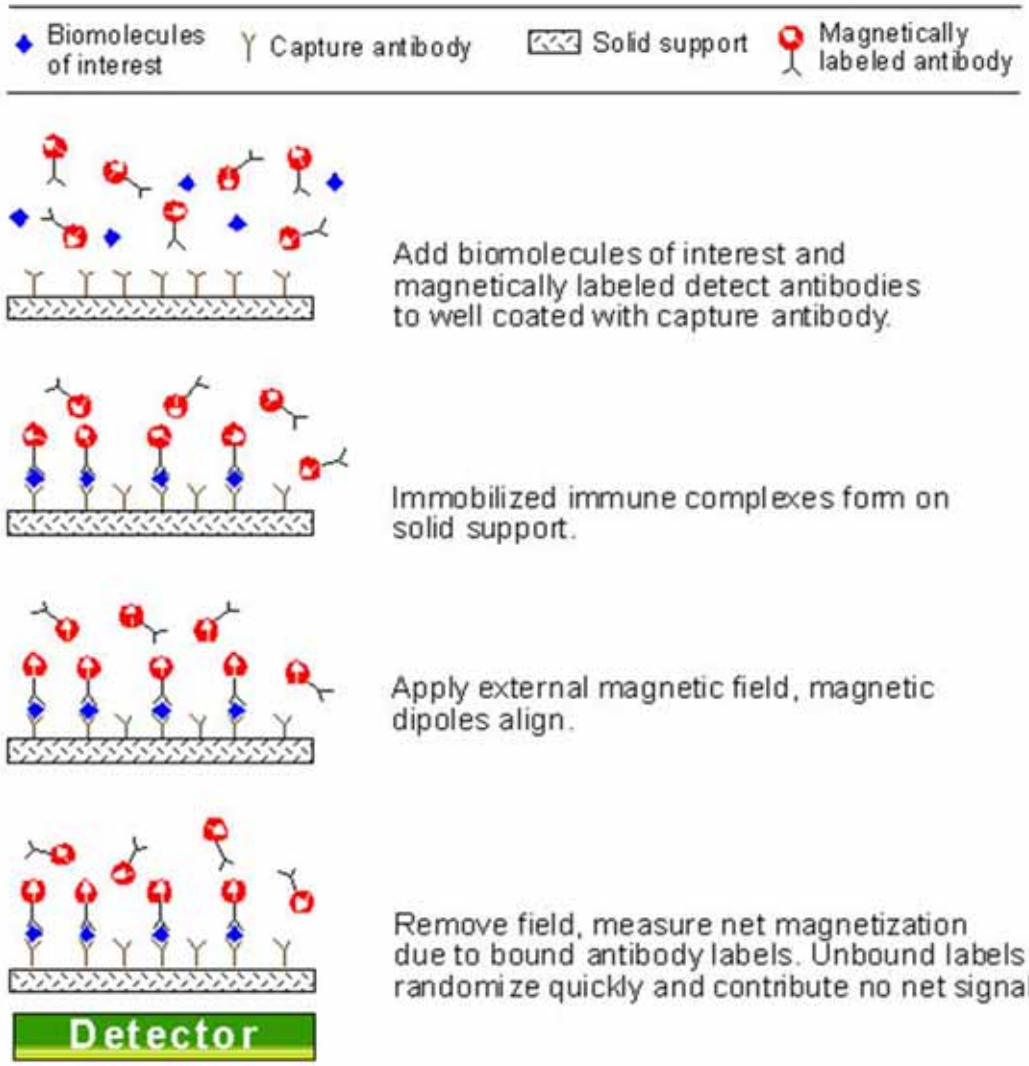
Biomolecules of interest
Capture antibody
Solid support
Magnetically labeled antibody
Add biomolecules of interest and magnetically labeled detect antibodies to well coated with capture antibody.
Immobilized immune complexes form on solid support.
Apply external magnetic field, magnetic dipoles align.
Remove field, measure net magnetization due to bound antibody labels. Unbound labels randomize quickly and contribute no net signal.
Detector

Microarray

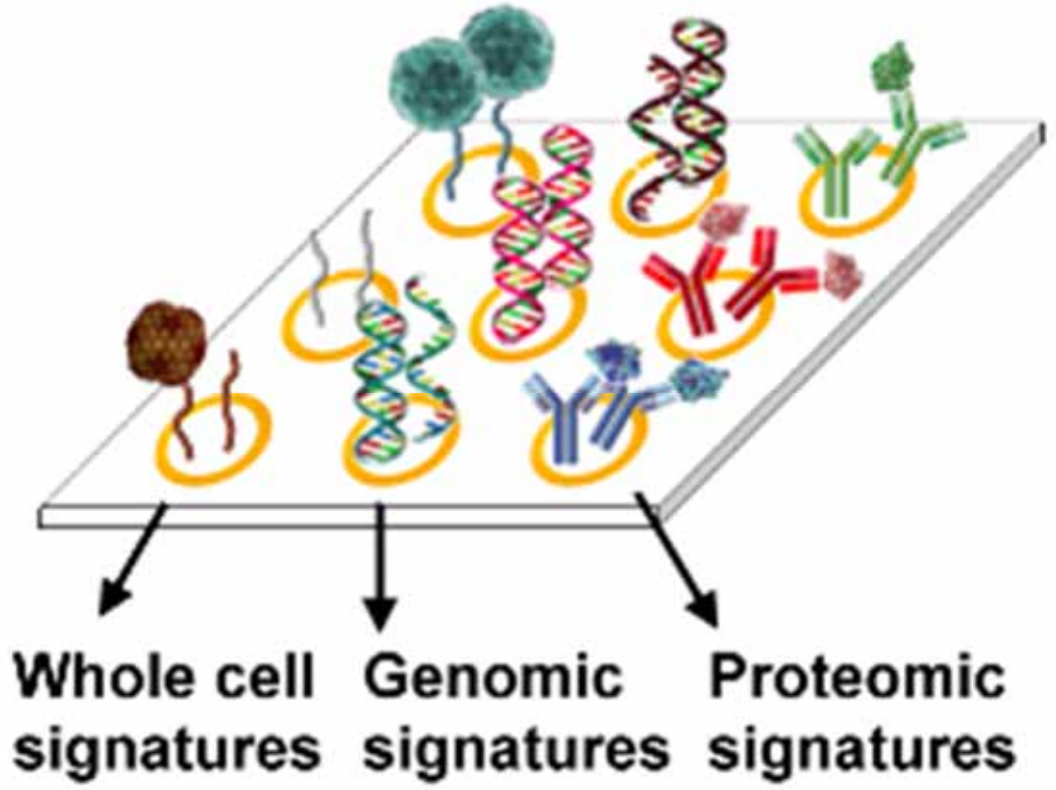
Whole cell signatures
Genomic signatures
Proteomic signatures

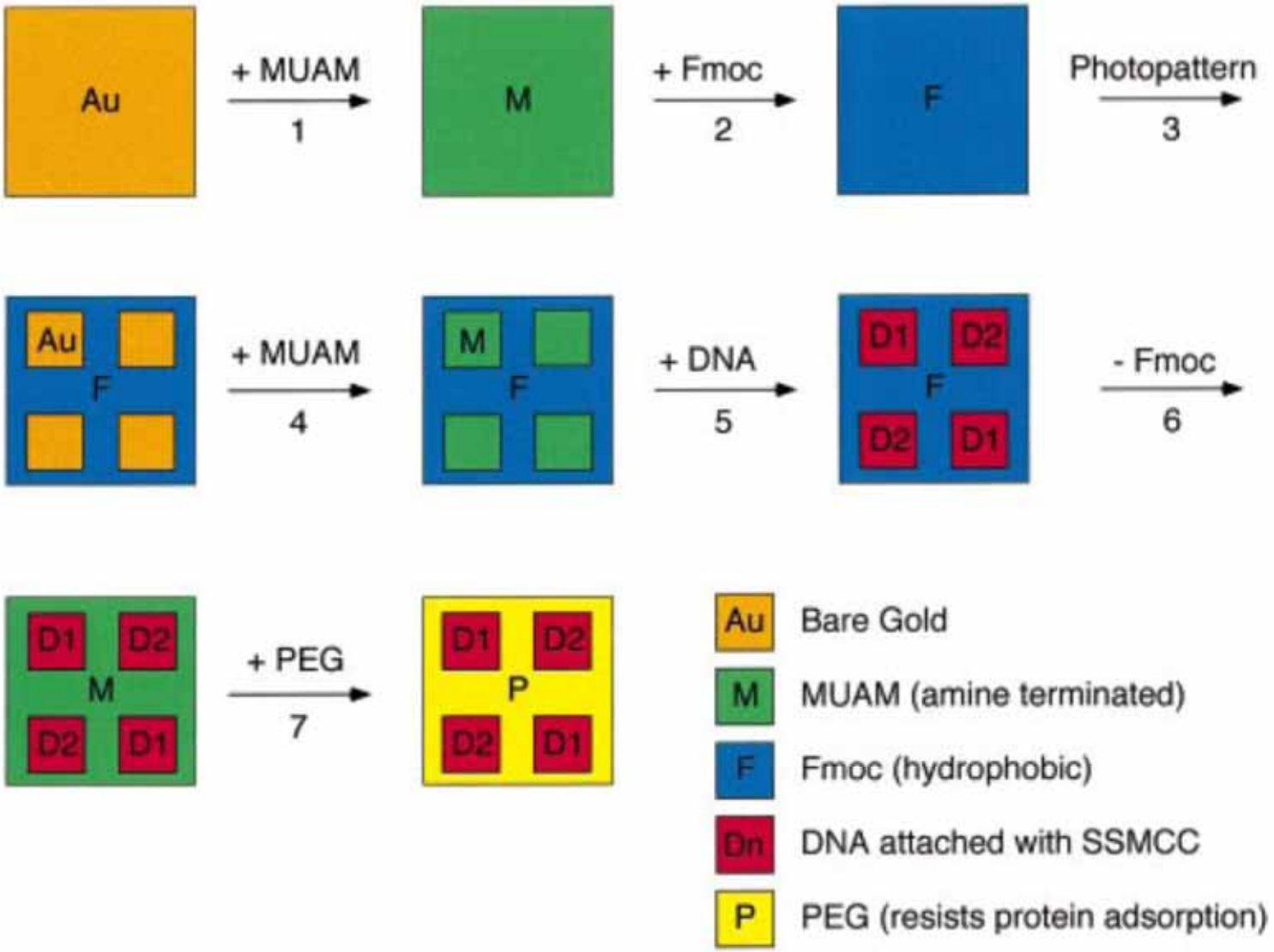

Figure 1. Fabrication scheme for the construction of multi-element DNA arrays. A clean gold surface is reacted with the amine-terminated alkanethiol MUAM, and subsequently reacted with Fmoc-NHS to create a hydrophobic surface. This surface is then exposed to UV radiation through a quartz mask and rinsed with solvent to remove the MUAM+Fmoc from specific areas of the surface, leaving bare gold pads. These bare gold areas on the sample surface are filled in with MUAM, resulting in an array of MUAM pads surrounded by a hydrophobic Fmoc background. Solutions of DNA are then delivered by pipet onto the specific array locations and are covalently bound to the surface via the bifunctional linker SSMCC. In the final two steps, the Fmoc-terminal groups on the array background are removed and replaced by PEG groups which prohibit the nonspecific binding of analyte proteins to the background.

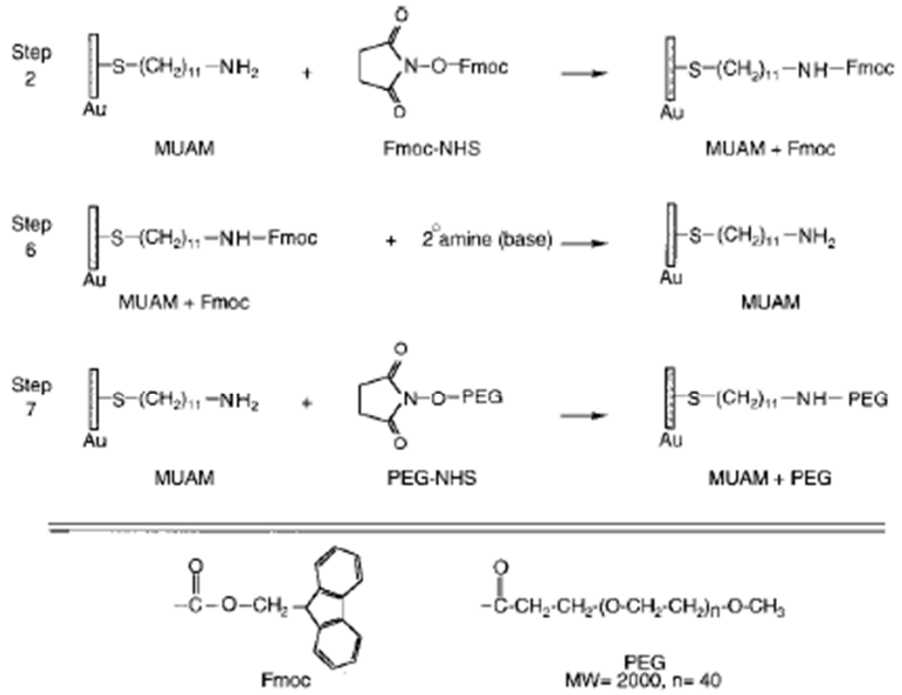

Figure 2. Surface reaction scheme showing the steps involved in the reversible modification of the array background. (Step 2) The starting amine-terminated alkanethiol surface (MUAM) is reacted with the Fmoc-NHS protecting group to form a carbamate linkage thus creating a hydrophobic Fmoc-terminated surface. (Step 6) After DNA immobilization (see Figure 3), the hydrophobic Fmoc group is removed from the surface with a basic secondary amine, resulting in the return of the original MUAM surface. (Step 7) In the final array fabrication step, the deprotected MUAM is reacted with PEG-NHS to form an amide bond that covalently attaches PEG to the array surface.

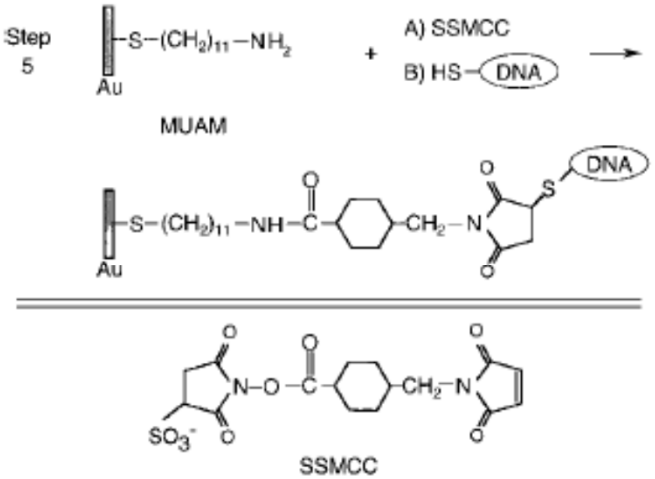

Figure 3. Surface reaction scheme showing the immobilization of thiol-terminated DNA to the array surface. In Step 5 of the DNA array fabrication, the heterobifunctional linker SSMCC is used to attach 5′-thiol modified oligonucleotide sequences to reactive pads of MUAM. This linker contains an NHSS ester functionality (reactive toward amines) and a maleimide functionality (reactive toward thiols). The surface is first exposed to a solution of the linker, whereby the NHSS ester end of the molecule reacts with the MUAM surface. Excess linker is rinsed away and the array surface is then spotted with 5′-thiol-modified DNA that reacts with the maleimide groups forming a covalent bond to the surface monolayer.

Glass Surface Modification

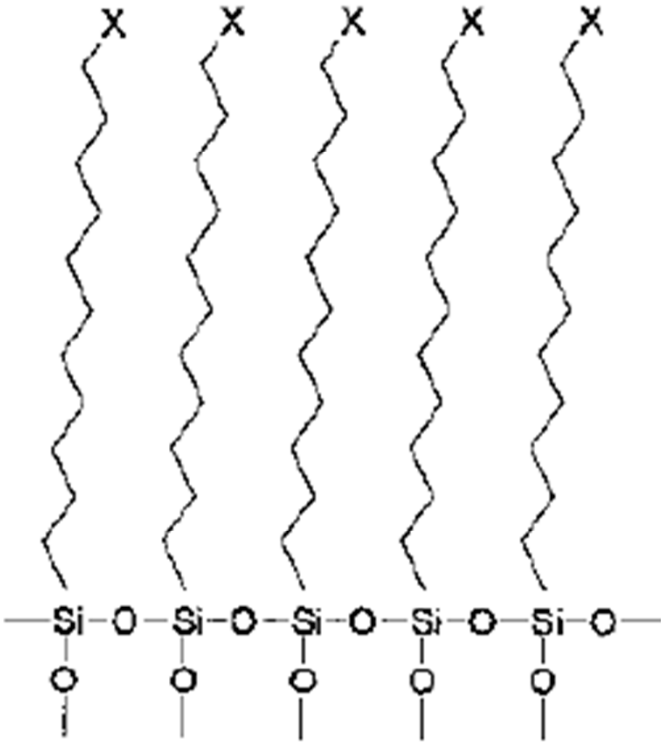

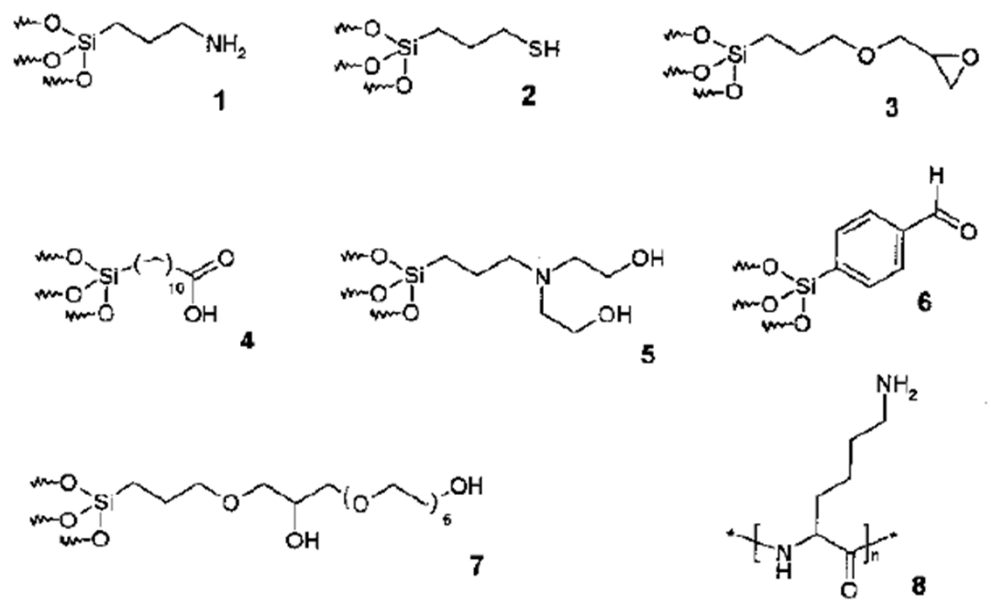

Scheme 2.2 Reagents for derivatization of glass surfaces. 1 APTES = aminopropyltriethoxysilane; **2** MPTS = 3-mercaptopropyltrimethoxysilane; **3** GPTS = glycidoxypropyltrimethoxysilane; **4** TETU = triethoxysilane undecanoic acid; **5** HE-APTS = bis(hydroxyethyl)aminopropyltriethoxysilane); **6** 4-trimethoxysilylbenzaldehyde; **7** GPTS/HEG = glycidoxypropyltrimethoxysilane-hexaethylene glycol; **8** poly(lysine).

Scheme 2.1 2D schematic description of a polysiloxane monolayer on a glass surface (X = terminal functional

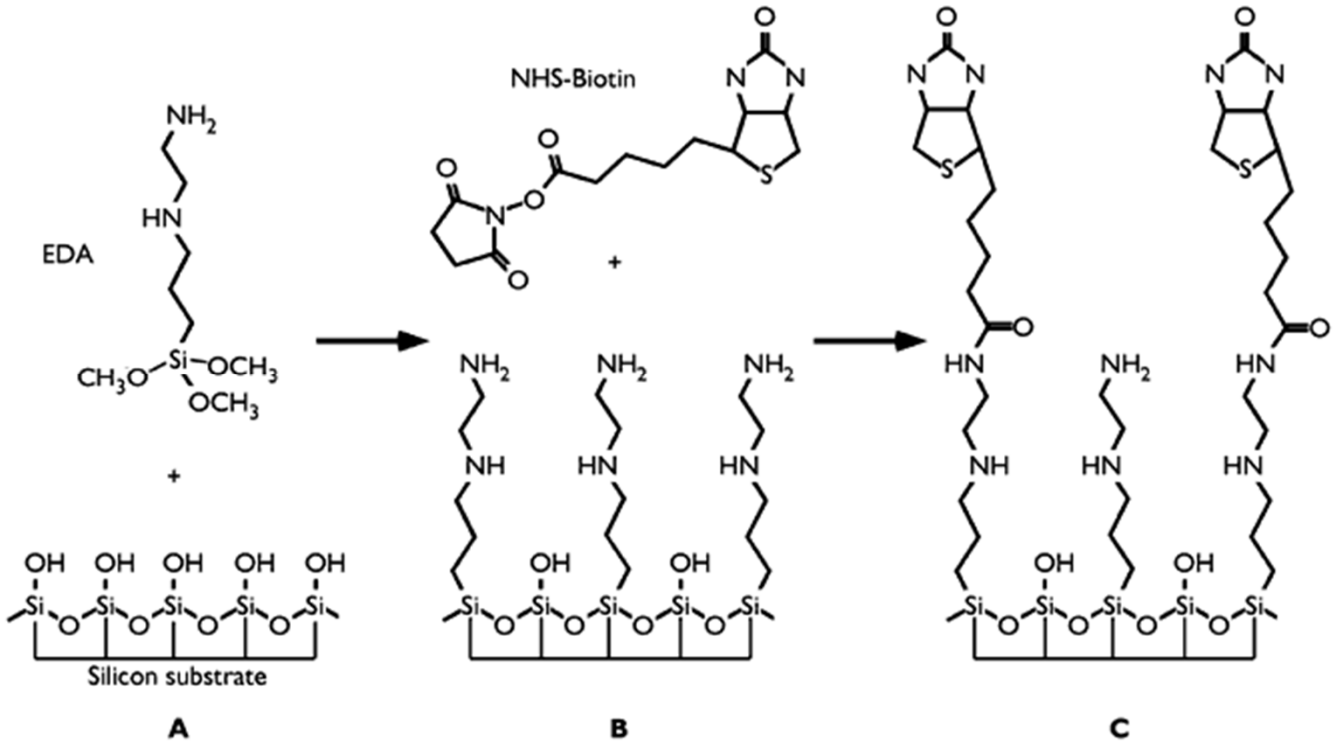
NHS-Biotin
EDA
Silicon substrate
A
B
C

Biotin-Streptavidin

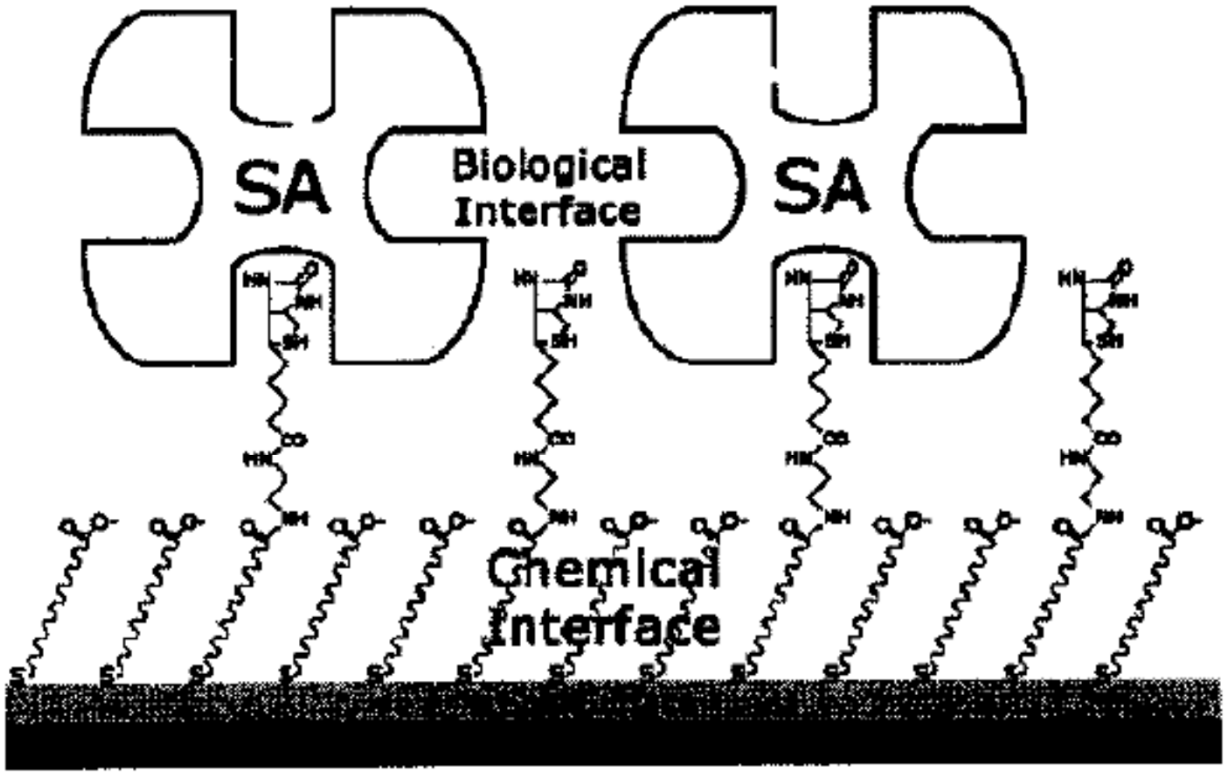

Figure 2.3 Schematic respresentation of a steptavidin sensor surface assembled on a reaction-controlled biotinylated SAM [28].

Biotin

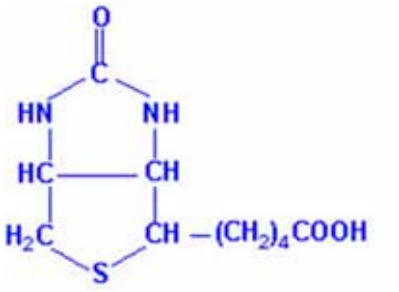

Avidin has a very strong affinity for biotin with a K_D (dissociation constant) of approximately 10^{-15} M^{-1}

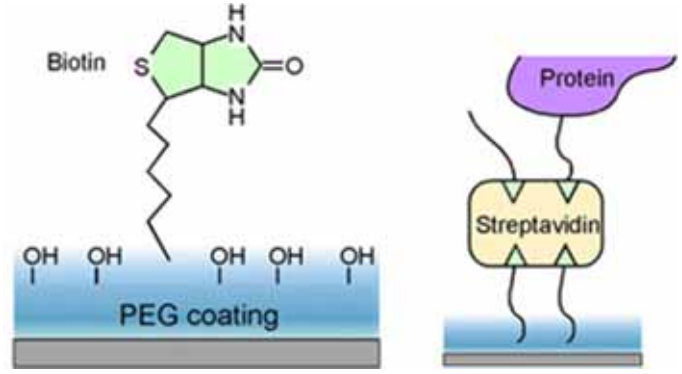

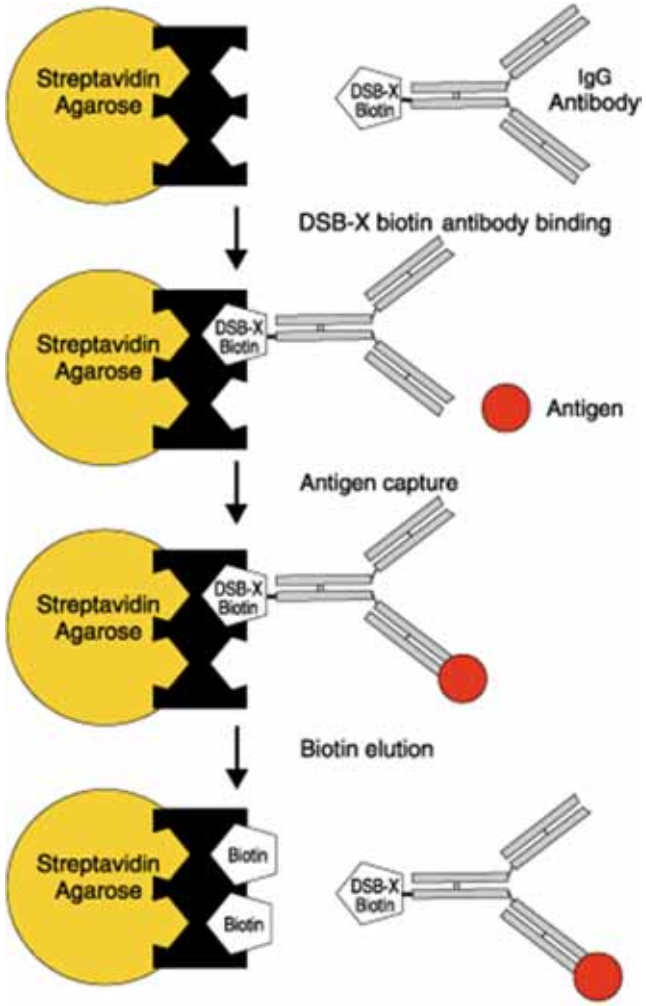
Streptavidin Agarose
DSB-X Biotin
IgG Antibody
DSB-X biotin antibody binding
Antigen
Antigen capture
Biotin elution
Biotin
Biotin

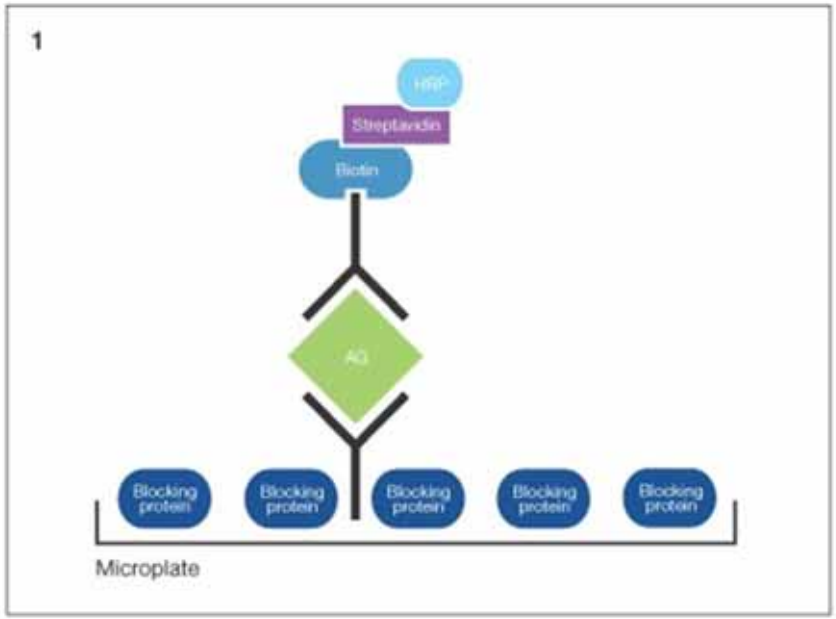
1
HRP
Streptavidin
Biotin
AG
Blocking protein
Blocking protein
Blocking protein
Blocking protein
Blocking protein
Microplate

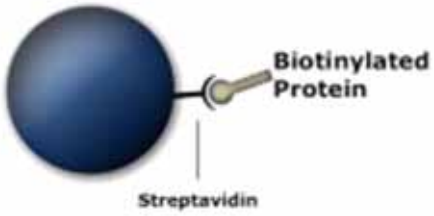
Biotinylated Protein
Streptavidin

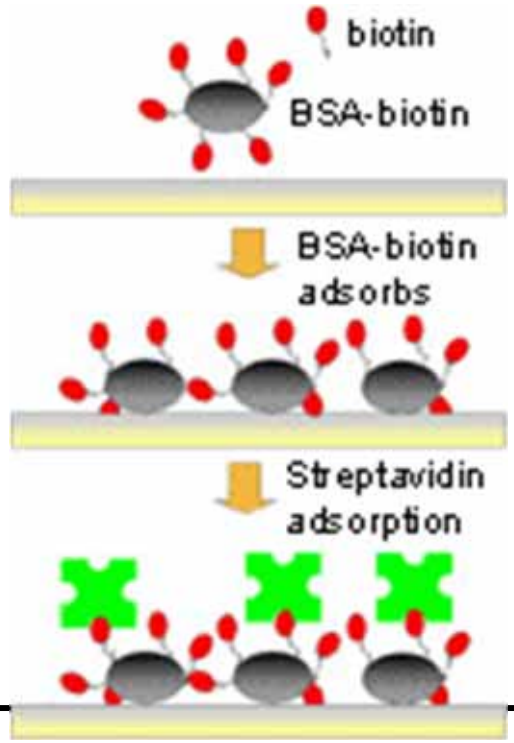
biotin
BSA-biotin
BSA-biotin adsorbs
Streptavidin adsorption

Protein Labeling

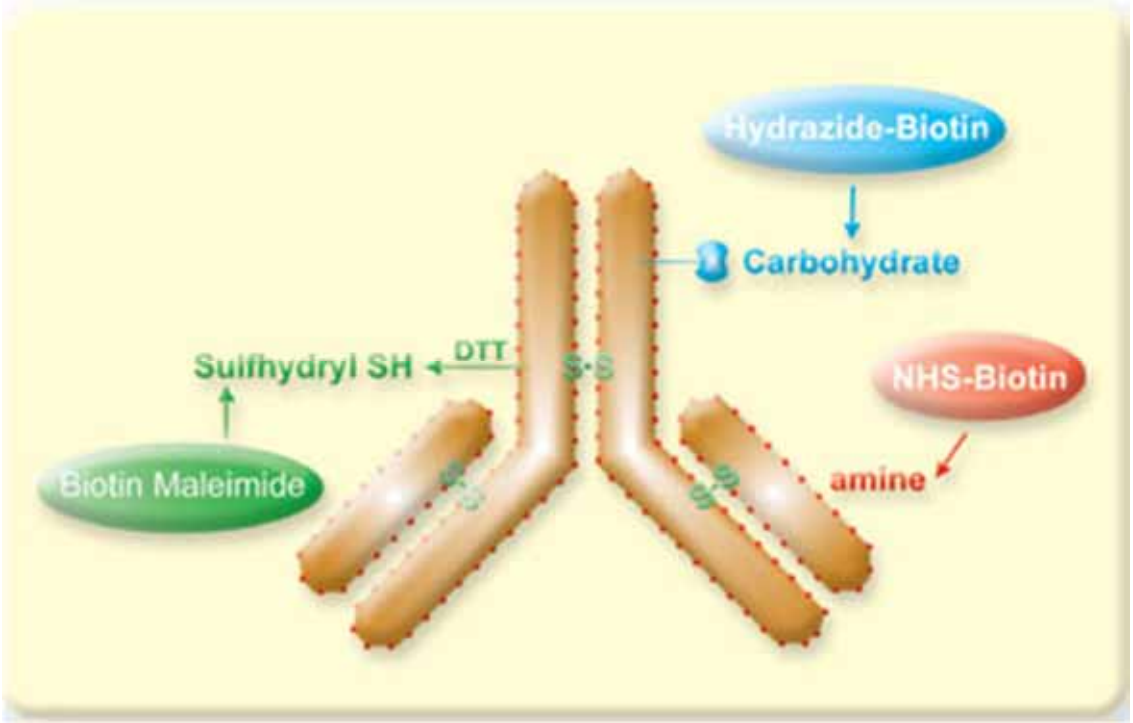

Amine Reactive Labeling

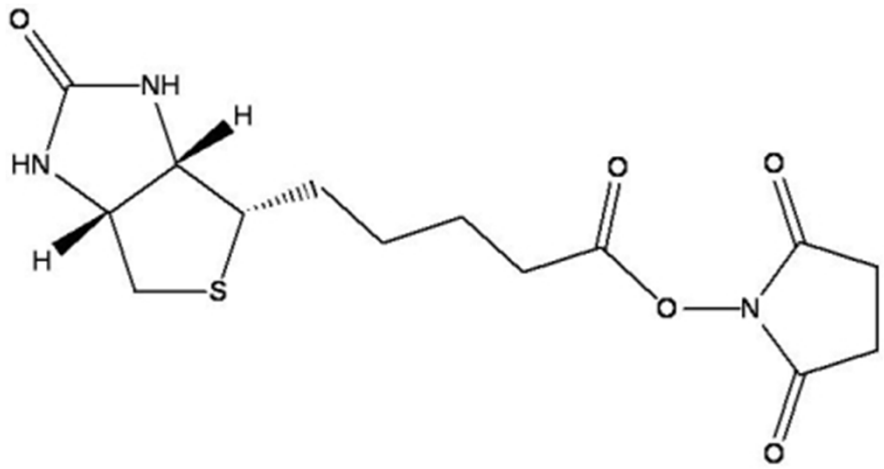

NHS ester

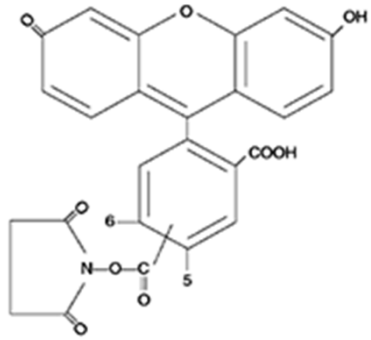

NHS-Fluorescein
MW 473.4

Sulfhydryl Labeling

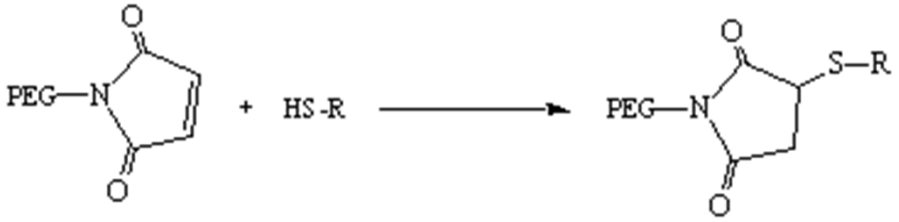

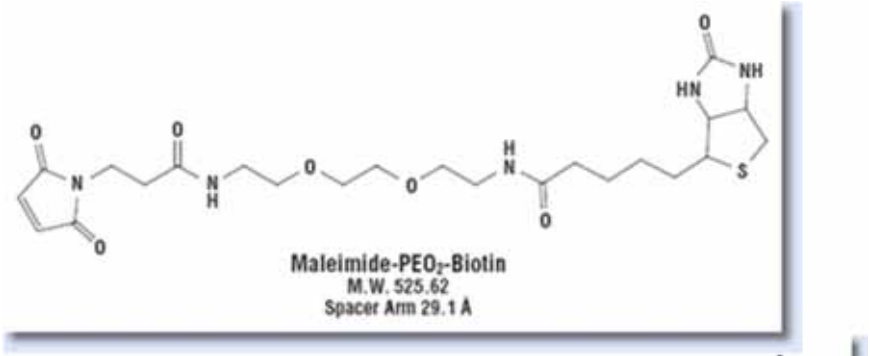

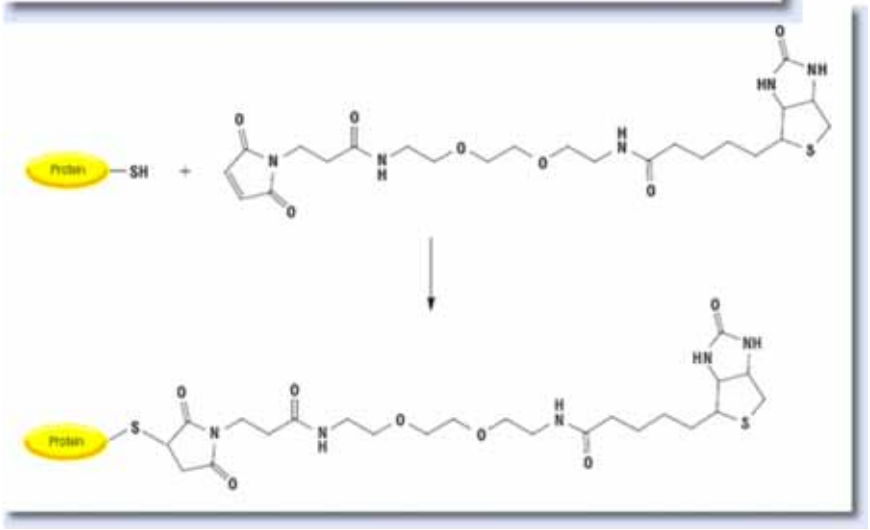

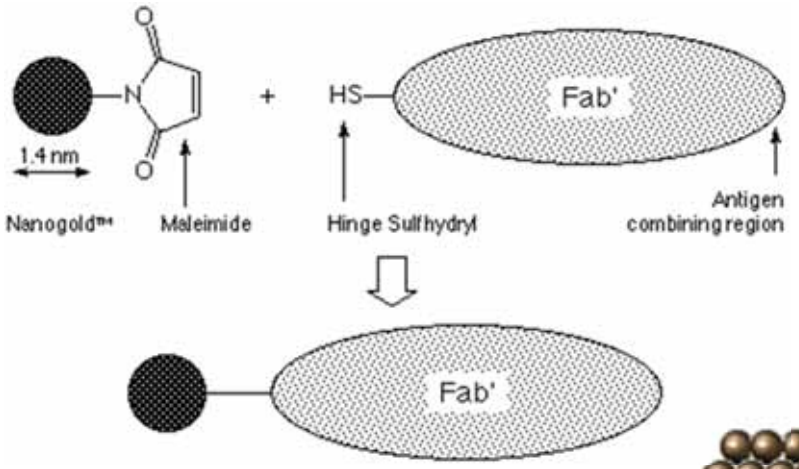

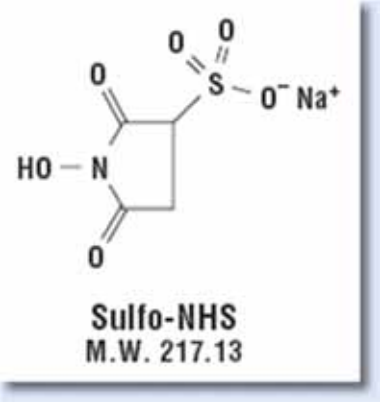

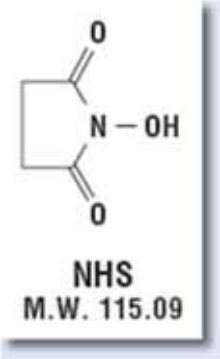

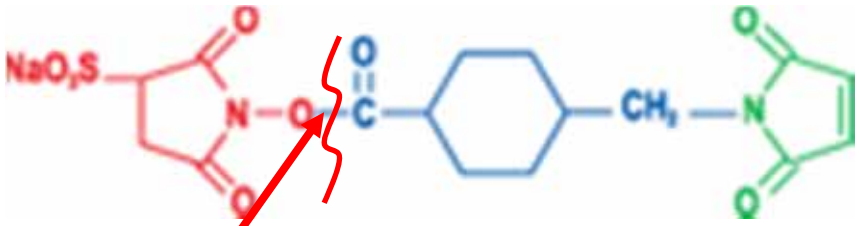

SulfoSuccinimidyl-4-(N-Maleimidomethyl)Cyclohexane-1-Carboxylate
SSMCC

The most popular NH_2- and SH- crosslinker

N-hydroxysuccinimide

NH_2 => amide

$R_1NH_2 + NHS\text{-}R_2 = >R_1NHC=OR_2$

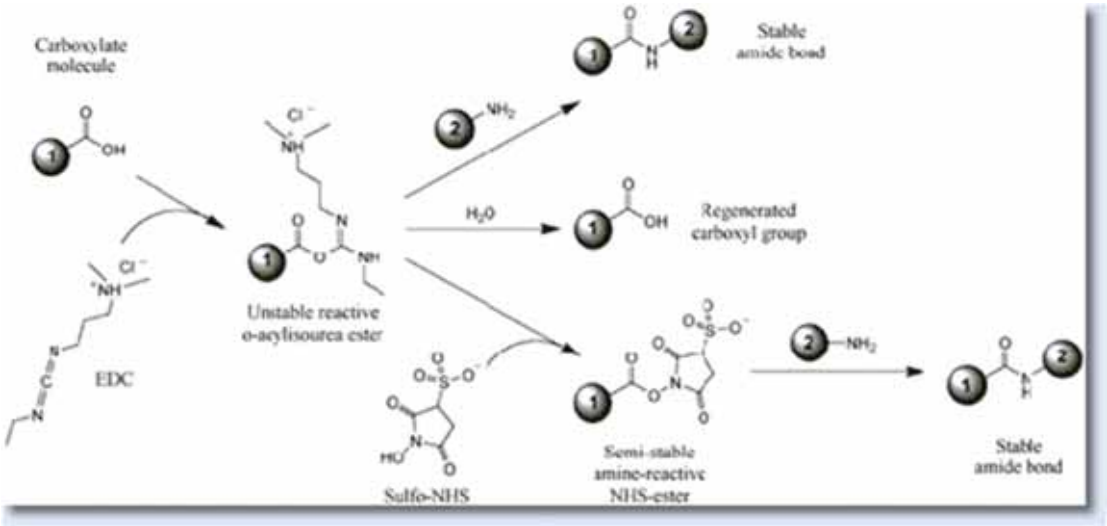

N-hydroxysuccinimide (NHS)

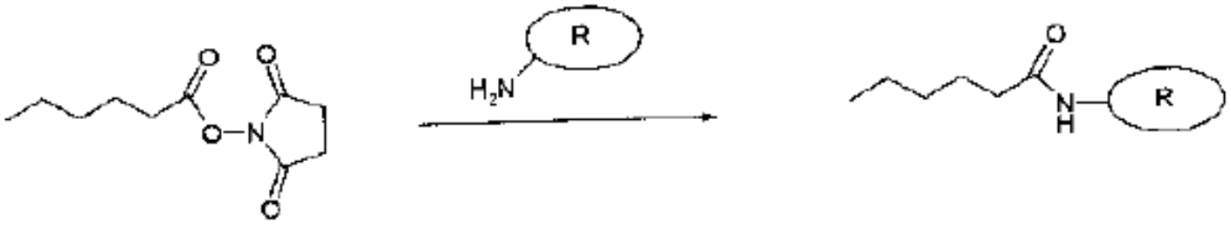

Scheme 2.6 Surface coupling reaction of NHS-esters with the amino residues of the side-chains of polypeptides (lysine units). R, protein.

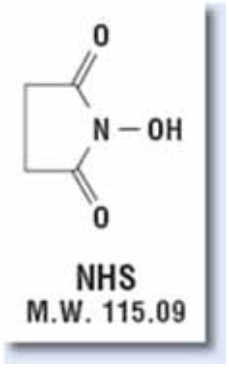

N-hydroxysuccinimide

His Tag

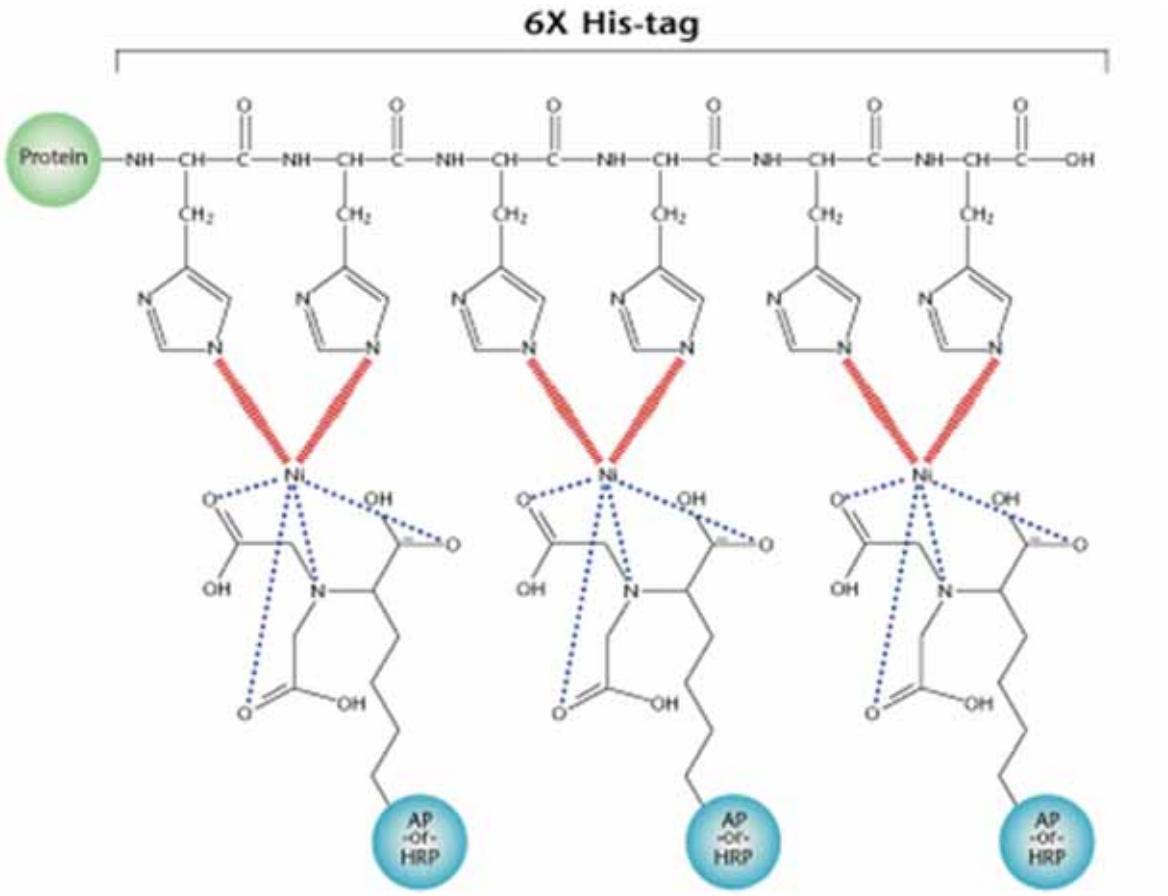

GeneChip

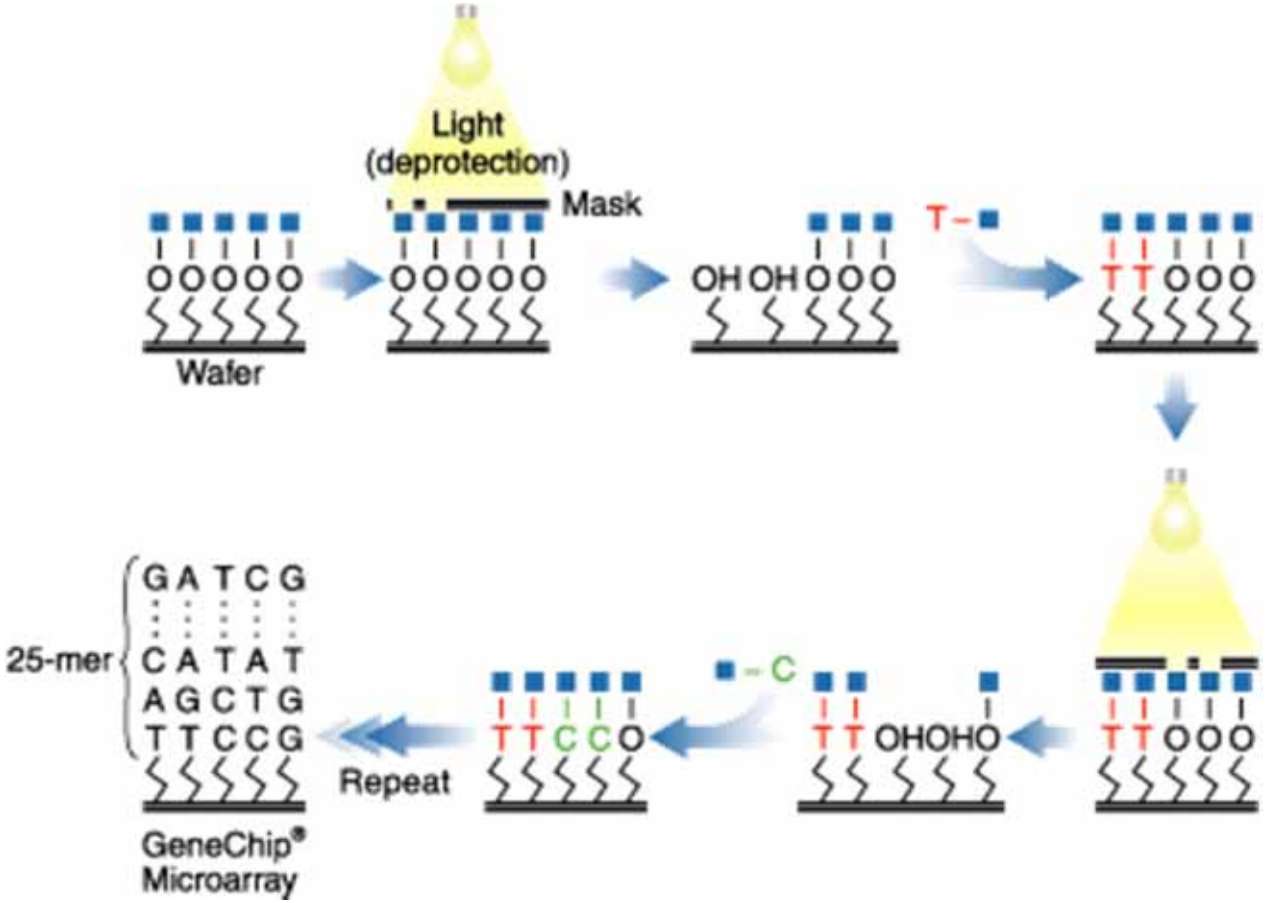
Light
(deprotection)
Mask
Wafer
T –
C –
Repeat
25-mer
GeneChip®
Microarray

Scheme

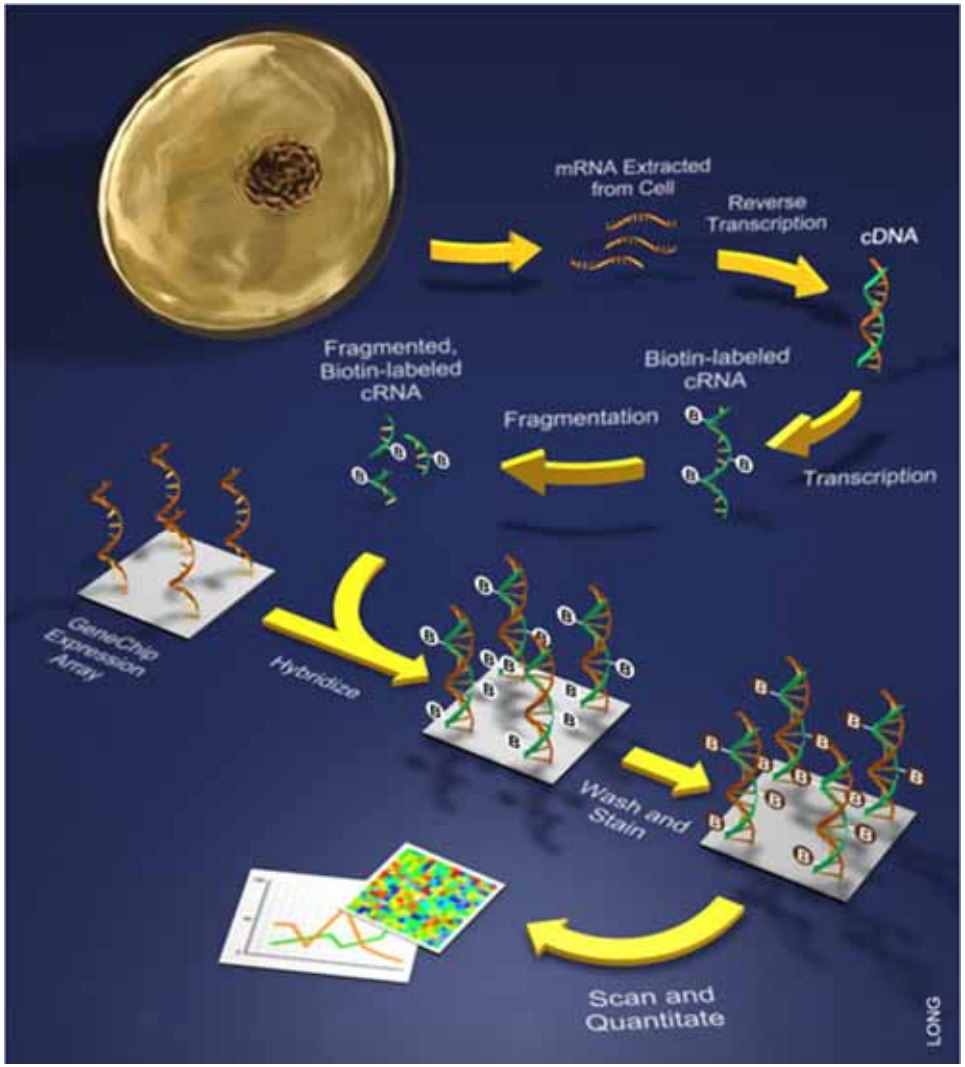
mRNA Extracted from Cell
Reverse Transcription
cDNA
Biotin-labeled cRNA
Transcription
Fragmentation
Fragmented, Biotin-labeled cRNA
GeneChip Expression Array
Hybridize
Wash and Stain
Scan and Quantitate
LONG

cDNA Microarray

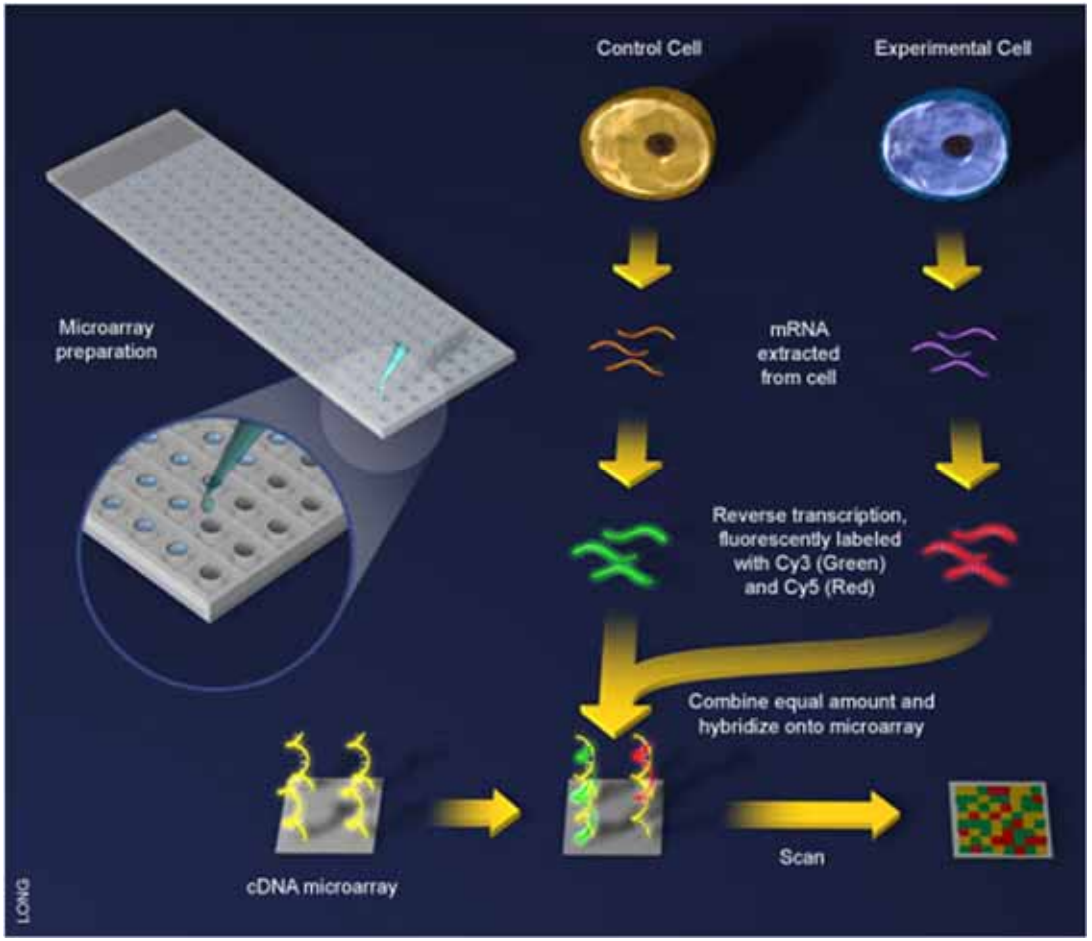

Protein Array

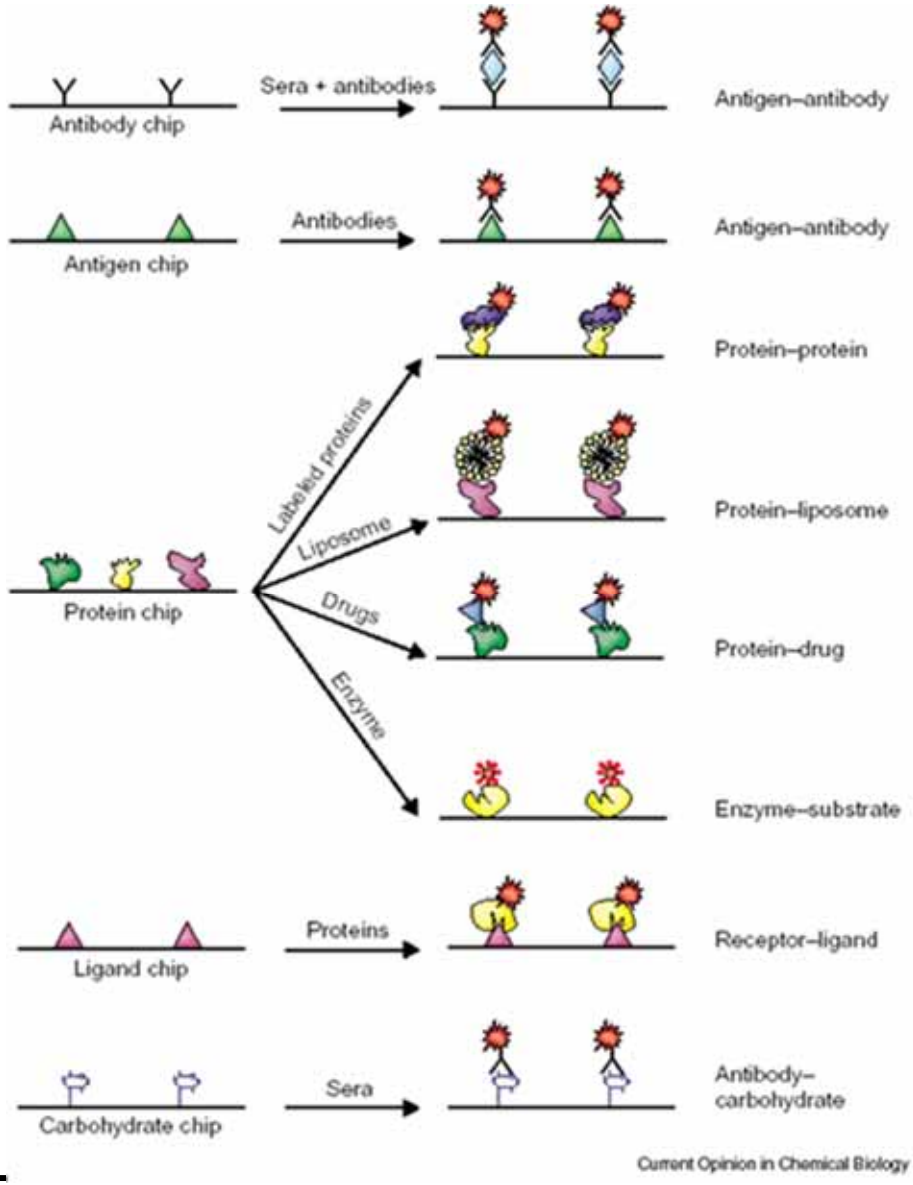

BSA Blocking

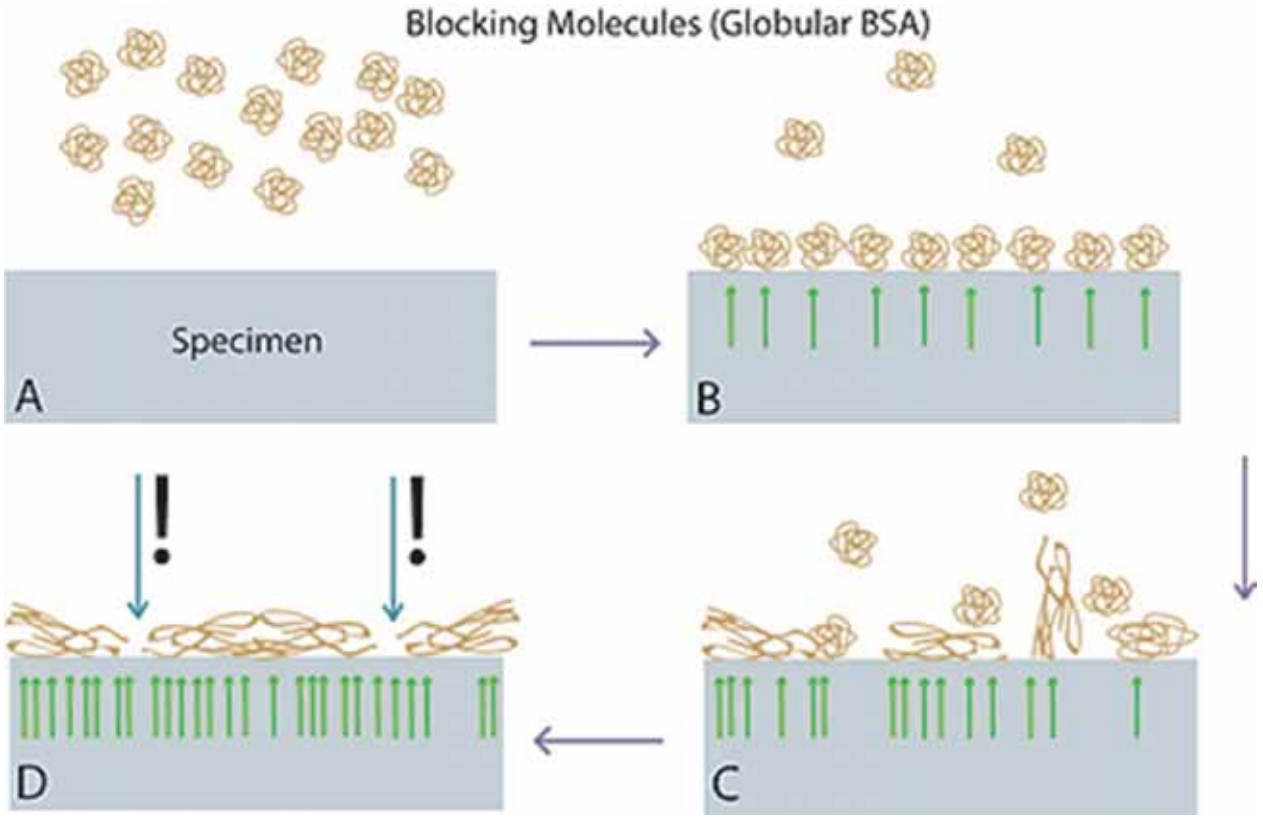

Cell Array

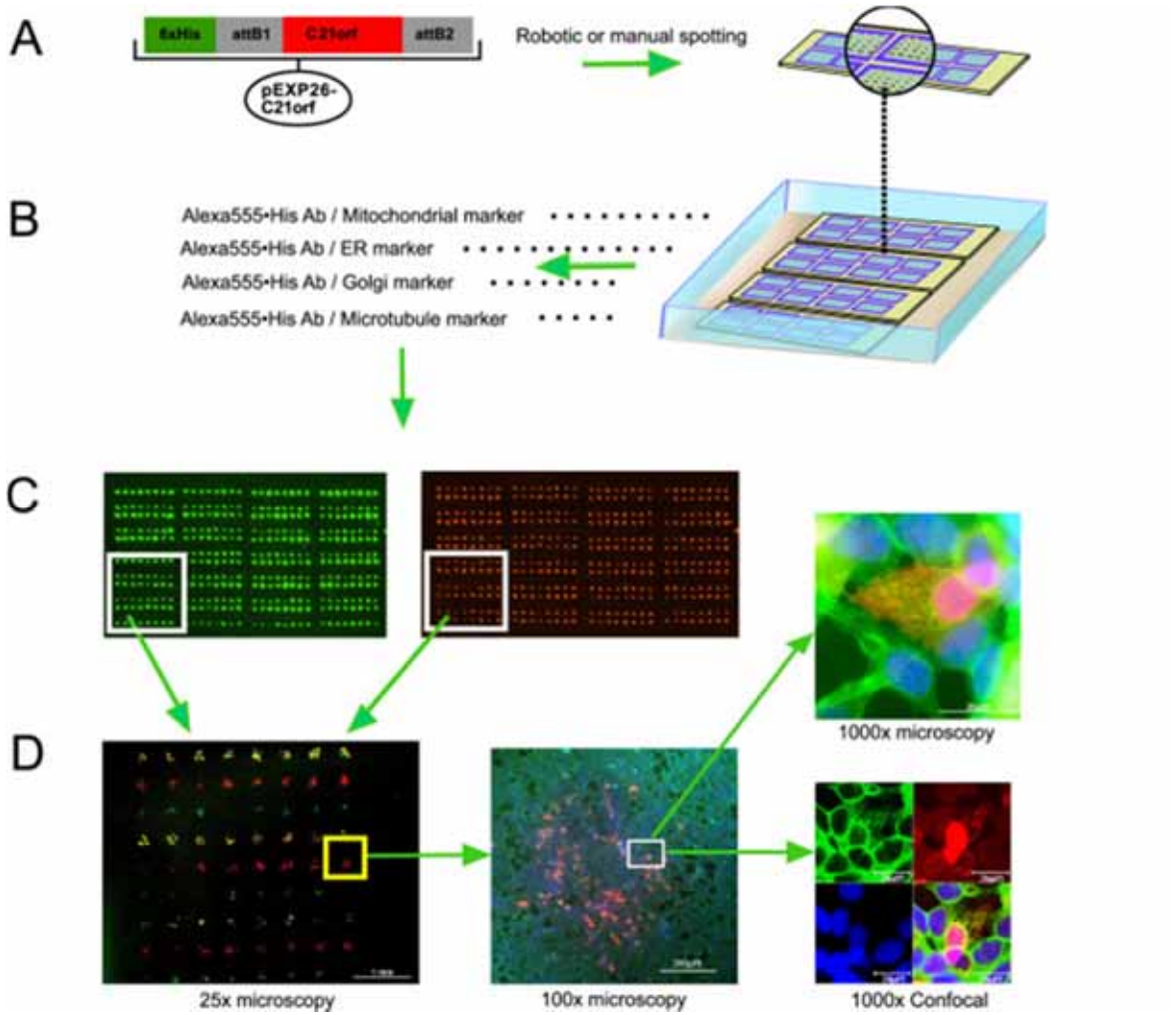
A
6xHis
attB1
C21orf
attB2
pEXP26-C21orf
Robotic or manual spotting
B
Alexa555•His Ab / Mitochondrial marker
Alexa555•His Ab / ER marker
Alexa555•His Ab / Golgi marker
Alexa555•His Ab / Microtubule marker
C
D
1000x microscopy
25x microscopy
100x microscopy
1000x Confocal

Surface Plasmon Resonance (SPR)

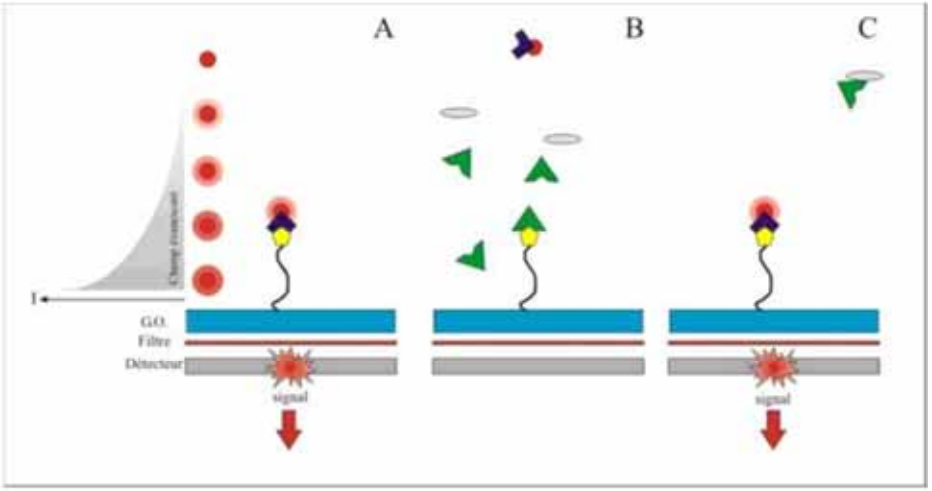

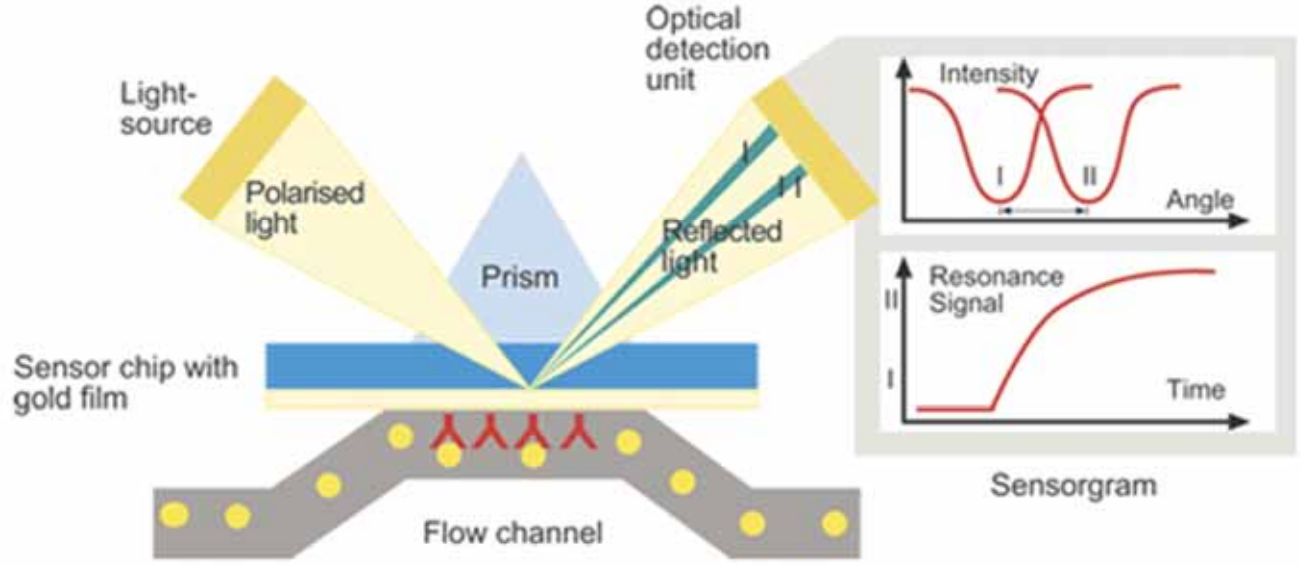

Glucose Sensor

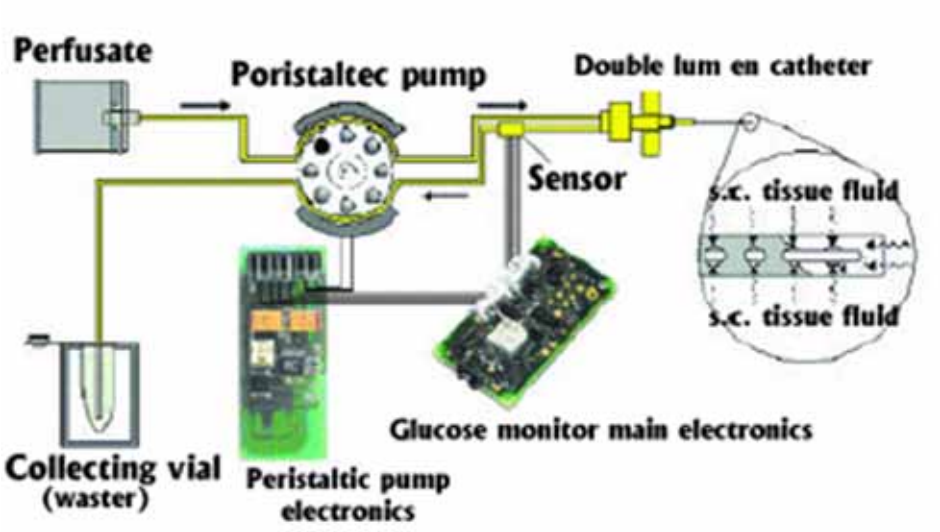

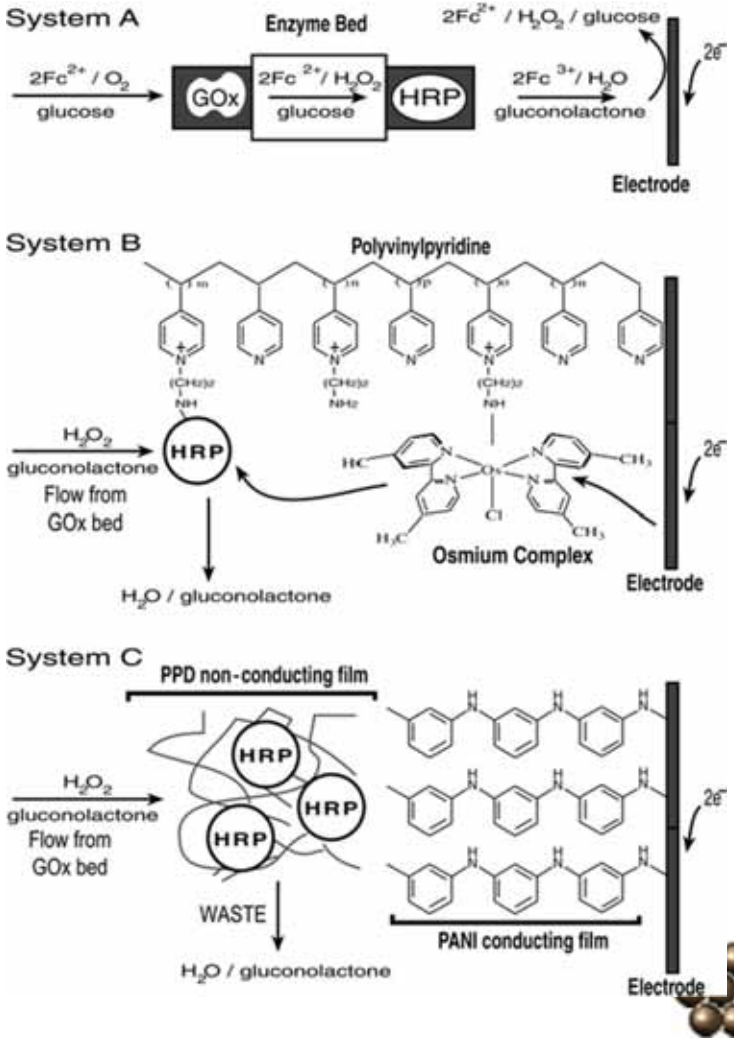

hCG immunoassay

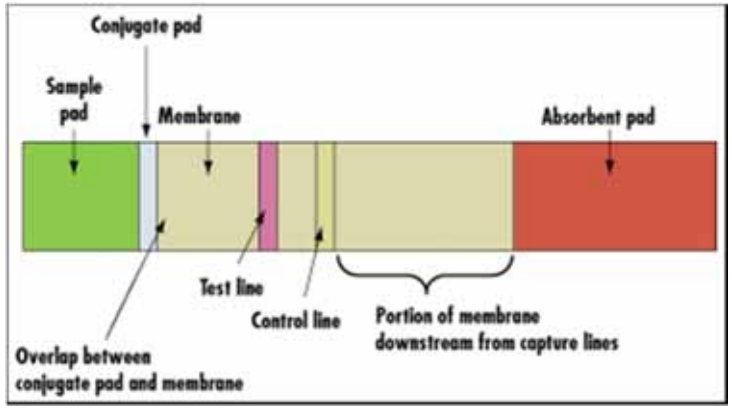

human chorionic gonadotropin (hCG)

Nucleotide Sensor

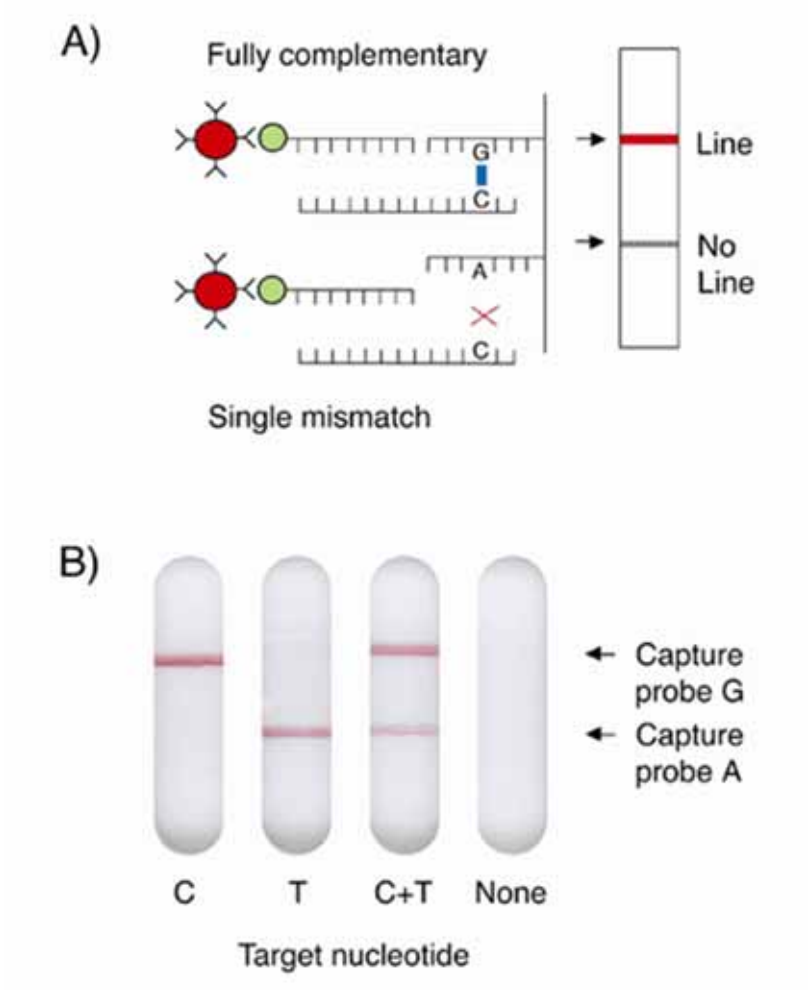

Microfluidic Immunoassay

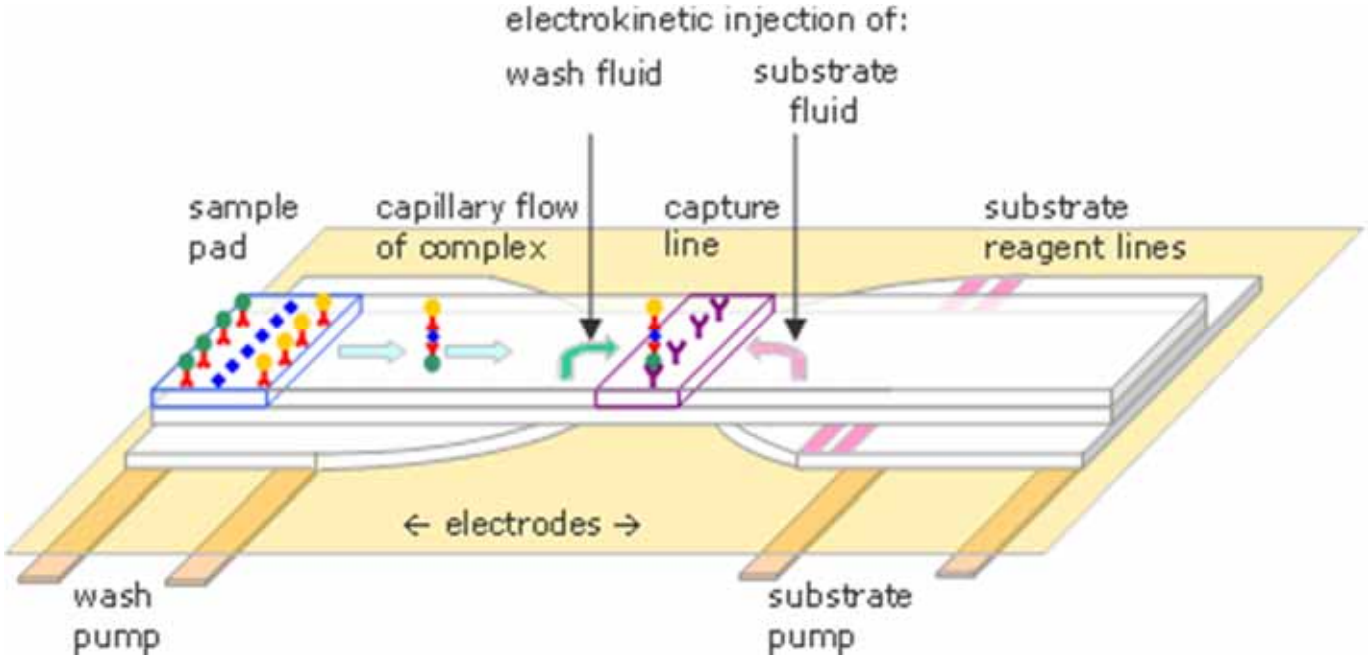

Chromatography

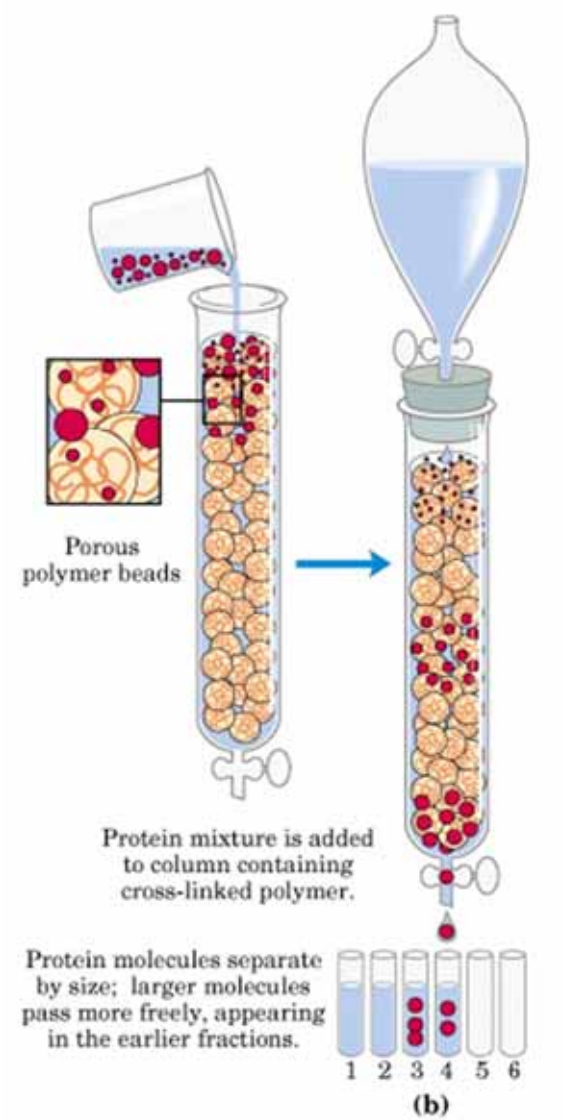

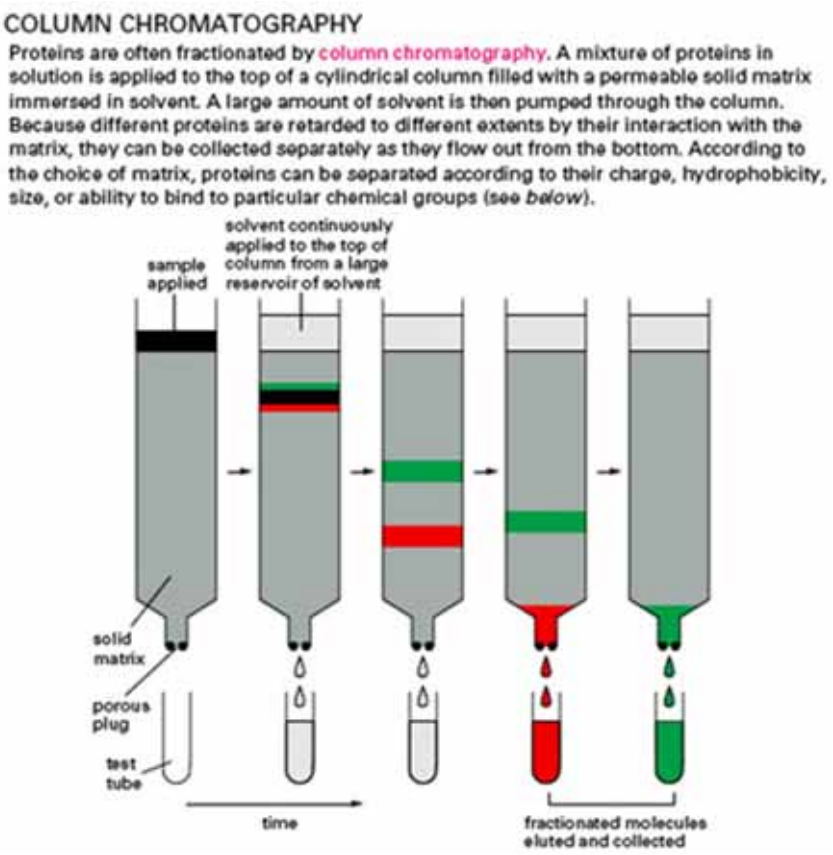

Reverse Phase

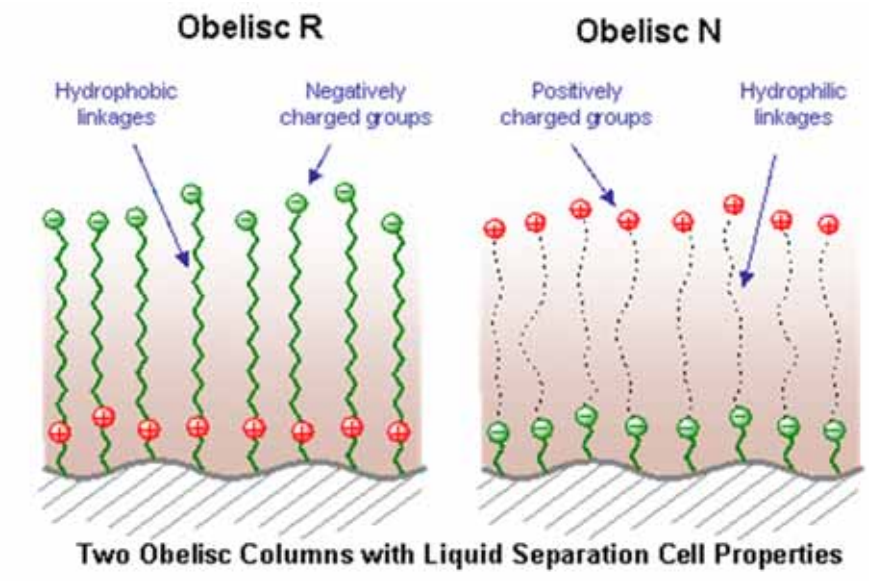

Two Obelisc Columns with Liquid Separation Cell Properties

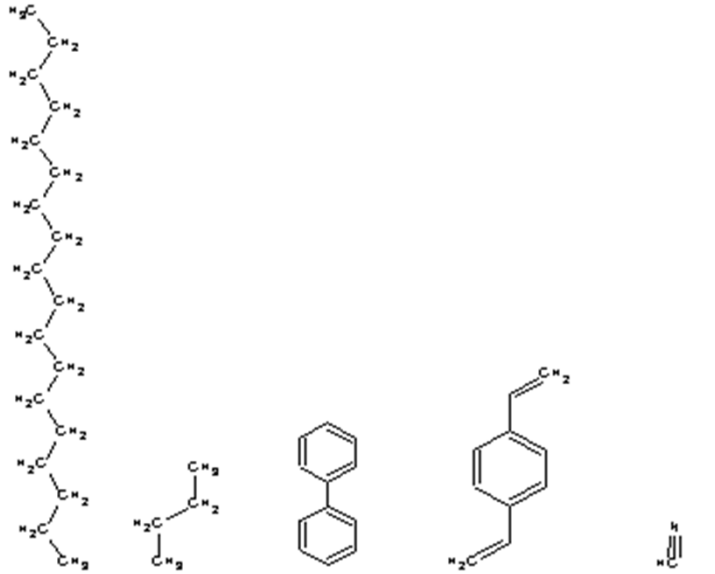

C-18 C-4 diphenyl divinylbenzene (DVB) cyano